Titre: Title:	Stretchable and Self-Healing Conducting Polymers for Organic Bioelectronics
Auteur: Author:	Yang Li
Date:	2020
Type:	Mémoire ou thèse / Dissertation or Thesis
Référence: Citation:	Li, Y. (2020). Stretchable and Self-Healing Conducting Polymers for Organic Bioelectronics [Ph.D. thesis, Polytechnique Montréal]. PolyPublie. https://publications.polymtl.ca/5570/

POLYTECHNIQUE MONTRÉAL

affiliée à l'Université de Montréal

Stretchable and self-healing conducting polymers for organic bioelectronics

YANG LI

Département de génie chimique

Thèse présentée en vue de l'obtention du diplôme de *Philosophiæ Doctor*

Génie chimique

Décembre 2020

POLYTECHNIQUE MONTRÉAL

affiliée à l'Université de Montréal

Cette thèse intitulée :

Stretchable and self-healing conducting polymers for organic bioelectronics

présentée par **Yang LI**

en vue de l'obtention du diplôme de *Philosophiæ Doctor*

a été dûment acceptée par le jury d'examen constitué de :

Gregory DE CRESCENZO, président
Fabio CICOIRA, membre et directeur de recherche
Stéphane KÉNA-COHEN, membre
Ingo SALZMANN, membre externe
Natalie STINGELIN, membre externe

DEDICATION

To my beloved family.

ACKNOWLEDGEMENTS

I am grateful for all the support, guidance and help that I have received over the last 4 years at Polytechnique Montreal.

First, I would like to express my deepest thanks to my research director, Prof. Fabio Cicoira, for giving me the opportunity to study a Ph.D. program in the field of organic bioelectronics. Thank you for guiding, supporting, and encouraging me to switch my research topic from inorganic materials to organic conducting polymers. Your passion for science and your personal involvement in my projects helped me to overcome many difficult moments in the past. The knowledge and skills I learned from you will also be highly valuable for me in my future career. Thank you for offering me freedom on the projects, for putting so much confidence in me, and for entrusting me. Thank you for always be passionate and helpful to discuss the projects with me. I am also grateful for your help for my stay in Montreal. No success will be there without your continuous care of me.

I am grateful to the jury members, Prof. Gregory De Crescenzo, Prof. Stéphane Kena Cohen, Prof. Ingo Salzmann, and Prof. Natalie Stingelin, for their time and interest in my work.

I am very grateful to Centre de Recherche sur les Systèmes Polymères et Composites à Haute Performance (CREPEC) and Polytechnique Montréal for partial financial support. I am also express my thanks to Fayolle Canada and Fondation et Alumni de Polytechnique Montréal for offering me Prestige États-Unis 2020 scholarship, which motivated me to set high standard for myself every single day.

Many thanks to all the collaborators, to Prof. Damiano Pasini of McGill University for his interpretation on the mechanical properties of conducting polymer films and his invaluable input in the kirigami project, and Prof. Thuc-Quyen Nguyen of the University of California Santa Barbara for AFM characterization on conducting polymer films. I am also grateful to Thomas Schmitt of Polytechnique Montreal for nano-indention and micro-scratch experiments, Prof. Noémie-Manuelle Dorval Courchesne of McGill University for synthesis and characterization on conducting polymer/protein composite project and Eric Quenneville from Biomomentum Inc. for tensile tester measurements.

I am grateful to all my friends. Thank Dr. Shiming Zhang (University of California, Los Angeles) for endless discussion in conducting polymers and stretchable electronics, Dr. Zongliang Zhang (University of Utah) for assistance in electrochemistry, Feng Liu (University of Toronto) for graph drawing, Dr. Wei Huang (Wuhan University) for fabrication of stretchable devices and Dr. Zhiwei Liu (Beijing University of Technology) for help in energy storage devices.

I also want to thank some distinguished scientists for individual discussions at the conference which greatly inspired me. These thanks go to Prof. John Rogers (Northwest University), Prof. Zhenan Bao (Stanford University), Prof. Jeff Karp (Harvard), Prof. Xuanhe Zhao (Massachusetts Institute of Technology), and many other scientists I met in the past years for invaluable discussions.

I am very grateful to technicians at Polytechnique: Daniel Pilon for his kind support on the Labview software for the device characterization, Christophe Clément for technical assistance in the clean room, and numerous discussions on my microfabrication issues, Chi Yuan Chang (training), Sébastien Chénard and Robert Delisle (instrument fixing), Matthieu Gauthier (DMA), Nicole MacDonald and Philippe Plamondon (SEM).

I have not yet thanked my colleagues at Polytechnique. I have to thank Arun, Michael, Xinda, Mona, Sanyasi, Jo'Elen, Natalie, Xin, Yiting, Ben, Michel, Nicolo, Mina, Catrina, Noémy, Pierre, Chithiravel, Nitin, Leslie, Floriane, John, Derek, Yasmin, Gaia, Prajwal, Irina, Yasmina, Michelle, Tom, Come, Elizabeth, Shalin, Fanny, Gabriel, Zhaojing, Tian, Xu, Martin, Manuel, and Abdelaziz. It was a pleasure to work with you all. I enjoyed the time I spent with you in Montreal. I should be very grateful to life and to the chance I had to meet you.

And many thanks to Polytechnique Montreal for academic and administrative services.

I want to thank my girlfriend Yingchao Yu. Without your support and help, I cannot make a lot of progress in this hard pandemic time.

Finally, I would like to thank my father Zengguang Li, and my mother Xiaoqin Liu, for their support and for always being with me. You are the most important persons in my life, and I wish my mother can recover from the illness soon. This is all for you and I hope this thesis can bring good luck for our family.

RÉSUMÉ

L'essor rapide de la bioélectronique organique, notamment dans la fabrication de dispositifs thérapeutiques, requiert le développement de nouveaux matériaux pour ce domaine. Les caractéristiques principalement recherchées pour ces nouveaux matériaux comprennent l'étirabilité, la propriété d'autoréparation, la capacité d'adhésion à la peau et la résistance aux contraintes mécaniques et interférences externes. Les polymères conducteurs sont des candidats idéaux pour la bioélectronique organique de par leur conductivité électronique et ionique et leur capacité d'auto-réparation. De plus, ces matériaux sont flexibles et simples à mettre en œuvre. Cependant, plusieurs aspects de ces matériaux ne sont pas encore élucidés. On compte parmi ceux-ci la compétition entre l'étirabilité et la performance des dispositifs électroniques, ainsi que la nécessité de comprendre plus en profondeur les mécanismes d'autoréparation de ces polymères conducteurs.

Cette thèse utilise des méthodes de mise en œuvre applicable au monde industriel pour affiner les propriétés d'étirabilité et d'autoréparation des polymères conducteurs et explore la fabrication de dispositifs bioélectroniques organiques avec des performances améliorées.

Nous avons tout d'abord étudié l'effet du poly(éthylène glycol) (PEG) de faible masse moléculaire sur les propriétés électromécaniques du polymère conducteur suivant : le poly(3,4-ethylenedioxythiophene) dopé avec du polystyrène sulfonate (PEDOT:PSS). Les résultats obtenus montrent que la présence du PEG en tant que plastifiant dans le PEDOT:PSS prévient la formation de fissures lorsque le film à base de ce mélange est soumis à une contrainte, tout en conservant une haute conductivité électrique, résultant donc à une amélioration des propriétés électromécaniques. De plus, l'addition de PEG provoque une augmentation de l'épaisseur des canaux et augmente ainsi la mobilité ionique dans les films de PEDOT:PSS. Ceci permet la fabrication d'OECT étirables avec une grande transconductance et un temps de réponse rapide. Les connaissances acquises dans le cadre de cette thèse peuvent servir de guide de référence pour fabriquer des dispositifs électroniques organiques étirables à haute performance.

Bien que le comportement d'autoréparation activée par l'eau du PEDOT:PSS ait été observé par notre groupe il y a de cela trois ans, aucun film de PEDOT:PSS autoréparant, biocompatible et facile à fabriquer n'a été rapporté. Nous avons observé qu'un comportement autoréparant

autonome répétitif, rapide et à haute efficacité des films est obtenu à partir d'un mélange du polymère conducteur PEDOT:PSS et de PEG. La présence du PEG dans les films de PEDOT:PSS diminue le module élastique et augmente l'élongation à la rupture, conduisant ainsi à un matériau plus mou et à des propriétés autoréparantes améliorées. Le mouvement de retour du matériau dans la zone endommagée, directement après une coupure est considéré comme étant à l'origine du mécanisme d'autoréparation. La confirmation des propriétés autoréparatrices, de la conductivité élevée, de la stabilité et de la biocompatibilité des films de PEDOT :PSS avec addition de PEG, établissent le composé polymère comme chef de file des matériaux conducteurs dans le domaine de la bioélectronique.

Dans le but d'accroître nos connaissances sur le fonctionnement de l'autoréparation activée par l'eau du PEDOT:PSS, nous avons étudié les effets de l'ajout d'additifs dans les mélanges ainsi que de post-traitements sur ses propriétés de réparation. Nous avons démontré que le comportement autoréparant activé par l'eau du PEDOT:PSS diminue en présence d'agents réticulant ou lorsqu'il est soumis à un post-traitement acide, ce qui limite la capacité à gonfler du dopant, le PSS. Nous avons par conséquent étudié ce dernier ainsi que le comportement autoréparant du polymère conducteur avec différents dopants ou synthétisé via différentes méthodes. Nous avons également réalisé une étude préliminaire sur la variation de la performance de l'autoréparation en fonction de la largeur de la coupure et de l'épaisseur du film.

La fabrication avancée de dispositifs bioélectroniques organiques étirables à hautes performances et les profondes connaissances au sujet du comportement autoréparant des polymères évoqués dans cette thèse ouvre une voie vers le développement d'une nouvelle génération de dispositifs bioélectroniques, et plus particulièrement dans le domaine des systèmes de santé portables personnels, des capteurs étirables, des peaux artificielles et des actionneurs thérapeutiques.

ABSTRACT

Rapid development of next-generation electronic materials is leading to the latest innovations in healthcare and therapeutic devices in the field of organic bioelectronics. Stretchability and healing ability are objectives for future organic bioelectronics, with the aim of conforming to human skin and becoming immune to mechanical stress or changes in environmental conditions, such as temperature or humidity. Conducting polymers are ideal candidates for organic bioelectronics due to their mixed electronic and ionic conductivity, inherent flexibility, easy processability, and healing ability. However, issues, such as the trade-off between stretchability and device performance, and an incomplete understanding of the healing performance of conducting polymers, necessitate further investigations to improve organic bioelectronics.

This thesis utilized different processing methods to tune the stretchability and healing properties of conducting polymers to fabricate organic electronic devices with enhanced performance.

First, we investigated the effect of low-molecular weight plasticizer, polyethylene glycol (PEG), on the electromechanical properties of the conducting polymer poly(3,4-ethylenedioxythiophene) doped with polystyrene sulfonate (PEDOT:PSS). The presence of PEG in the PEDOT:PSS films under strain prevents the formation of cracks and the loss of electrical conductivity, thus improving PEDOT:PSS film electromechanical properties. Furthermore, the addition of PEG leads to higher channel thickness and increased ion mobility in PEDOT:PSS films, resulting in stretchable organic electrochemical transistors (OECTs) with high transconductance and fast response time. The knowledge obtained in this thesis can be utilized to fabricate high-performance stretchable organic electronics.

Water-enabled healing behavior of PEDOT:PSS films was discovered by our group over three years ago. In this thesis we observed that repeatable, fast, and high-efficiency autonomic self-healing behavior of films is obtained from mixtures of PEDOT:PSS and PEG. The presence of PEG in PEDOT:PSS films decreases the elastic modulus and increases elongation at the break, leading to a softer material with self-healing characteristics. The healing mechanism of PEDOT:PSS and PEG films is hypothesized to be due to material flowing back to the separated area. The present work demonstrates highly conductive, autonomically healable, stable, and

biocompatible PEDOT:PSS films that meet the performance demands required for advanced flexible bioelectronics.

To gain a deeper knowledge about the water-enabled healing behavior of PEDOT:PSS, we studied both the effects of mixing additives and of post-treatment on its healing performance. The water-enabled healing behavior of PEDOT:PSS is decreased by crosslinkers and by acid post-treatment, due to decreased swelling of PSS. Furthermore, we investigated the swelling and healing behavior of PEDOT doped with varying ions or synthesized via different methods. We also established initial evidence on the relationship between healing performance, cut width and film thickness.

The fabrication of high-performance stretchable organic bioelectronics and the progress made in understanding the healing behavior of conducting polymers demonstrated in this thesis contributes valuable methods and knowledge necessary for developing next-generation organic bioelectronics for the growing market of personal wearable healthcare systems, stretchable sensors, artificial skins, and therapeutic actuators.

TABLE OF CONTENTS

LIST OF TABLES

LIST OF FIGURES

LIST OF SYMBOLS AND ABBREVIATIONS

AFM	Atomic force microscopy
Ag	Silver
AgCl	Silver chloride
Au	Gold
C	Carbon
C^*	Channel capacitance per unit volume
CBA	4-carbonxybenzaldehyde
$ClO4^-$	Perchlorate
CMOS	Complementary metal oxide semiconductor
CNT	Carbon nanotube
Cu	Copper
d	Thickness
D	Drain
DBSA	Dodecylbenzenesulfonic acid
DMA	Dynamic mechanical analysis
DMSO	Dimethyl sulfoxide
e^-	Electron
E’	Storage modulus
E’’	Loss modulus
ECG	Electrocardiography
EDOT	3,4-ethylenedioxythiophene
EEG	Electroencephalography,
EG	Ethylene glycol

EGaIn	Gallium-Indium eutectic
EIS	Electrochemical impedance spectroscopy
EMG	Electromyography
EMIM:TCB	1-ethyl-3-methylimidazolium:tetraacyanoborate
EOG	Electrooculography
f-BNNS	Functionalized boron nitrogen sheets
$FeCl_3$	Iron(III) chloride
FTIR	Fourier-transform infrared spectroscopy
G	Gate
g_m	Transconductance
GOPS	3-(glycidyloxypropyl)trimethoxysilane
H	Hydrogen
H^+	Hydron or proton
HSO_4^-	Hydrogen sulfate
H_2SO_4	Sulfuric acid
I_{ds}	Source-drain current
Ir	Iridium
ITO	Indium tin oxide
KCl	Potassium chloride
L	Length
M^+	Cations
MEAs	Microelectrode arrays
N	Nitrogen
η	Healing efficiency

NaCl	Sodium chloride
NIPAM	N-isopropylacrylamide
O	Oxygen
OECT	Organic electrochemical transistor
OFET	Organic field-effect transistor
OLED	Organic light-emitting diode
OPV	Organic photovoltaic cell
OSC	Organic solar cell
OTf	Trifluoromethanesulfonate
PAA	Poly (acrylic acid)
PBS	Phosphate buffer saline
PDMS	Poly(dimethylsiloxane)
PEDOT	Poly(3,4-ethylenedioxythiophene)
PEDOT:PSS	Poly(3,4-ethylenedioxythiophene) doped with polystyrene sulfonate
PEG	Polyethylene glycol
PEGDA	Poly(ethylene glycol) diacrylate
PEO	Polyethylene oxide
PET	Polyethylene terephthalate
PLGA	Poly (L-lactide-co-glycolide)
PNIPAM	Poly(N-isopropylacrylamide)
PPD	Paired pulsed depression
PPEGMEA	Poly(poly(ethylene glycol) methyl ether acrylate)
PSS	Polystyrene sulfonate
PSSNa	Poly(sodium 4-styrenesulfonate)

Pt	Platinum
PTHF	Poly(tetrahydrofuran)
PU	Polyurethane
PVA	Polyvinyl alcohol
rGO	Reduced graphene oxide
RH	Relative humidity
S	Sulfur
S	Source
Si	Silicon
SA	Sulfosuccinic acid
SDS	Sodium dodecyl sulfonate
SEBS	Styrene ethylene butylene styrene
SEM	Scanning electron microscopy
SNR	Signal-to-noise ratio
STEC	Stretchability and electrical conductivity
T	Temperature
t	Time
TGA	Thermogravimetric analysis
Ti	Titanium
Tos	Para-toluene sulfonate
Triton X-100	Polyethylene glycol tert-octylphenyl ether
μ	Charge carrier mobility
UV/O_3	Ultraviolet/ozone
V	Voltage

V_{ds}	Drain-source voltage
V_g	Gate-source voltage
V_{gs}	Gate-source voltage
V_{Th}	Threshold voltage
W	Width
XPS	X-ray photoelectron spectroscopy
Zonyl	Capstone FS-300 fluorosurfactant

LIST OF APPENDICES

CHAPTER 1 INTRODUCTION

1.1 Organic bioelectronics

Organic bioelectronics is a field that takes advantage of the unique features of π-conjugated organic (semi)conductors and applies them at the interface with biological systems[1]. After establishing connection with living organisms at various levels (*e.g.*, organs, tissues, cells, membranes, proteins), organic bioelectronic devices can either detect and read-out the biological signals, or apply a stimulus in the form of electrical charges and/or biochemical molecules to intervene in a biological event[2]. Over the past three decades, the tremendous growth in this exciting field occurred mainly because of the significant advances of organic electronic materials, the deeper understanding of the transport properties of existing materials and the communication between biological systems and bioelectronics, and the improved device fabrication technologies[3].

Conducting polymers are key component in organic bioelectronics. Unlike conventional electronic materials, conducting polymers can present mixed electronic and ionic conductivity, which can provide successful communication with biological systems. Moreover, the versatility of synthetic organic chemistry and processing methods allows for the conducting polymer to exhibit tissue-like softness, flexibility, and stretchability with the assistance of functional materials. As one important aspect of next-generation electronic materials, the self-healing feature can also be introduced to conducting polymers via the functionalization of certain side chains or mixing with other materials[4]. More importantly, the relative biocompatibility of conducting polymers set them apart from inorganic electronic materials, especially when bioelectronics need to be implanted and operated in vivo over long periods[5].

The most successful conducting polymer, poly(3,4-ethylenedioxythiophene) doped with polystyrene sulfonate (PEDOT:PSS) was invented together by Friedrich Jonas in the Central Research Department of Bayer AG and his colleague Werner Krafft from Agfa-Gevaert in 1989[6]. Later, the rise of PEDOT:PSS aroused considerable progress in the following fields: organic solar cells (OSCs), organic light-emitting diode (OLEDs), organic field-effect transistors (OFETs), and organic electrochemical transistors (OECTs), thermoelectric devices, wearable sensors, health monitor applications and artificial intelligent robotics[7]. Among the applications of PEDOT:PSS, one of the most exciting examples is the OECT. The deep understanding about the operation

mechanisms of PEDOT:PSS based OECTs is still incomplete, and the new functionalities of PEDOT:PSS and OECTs remain unexploited, especially in the field of organic bioelectronics.

1.2 Motivations

The human body is soft, while conventional electronics are rigid and susceptible to mechanical deformation. One of the main targets in the wearable bioelectronics for continuous health signals monitoring is to conform to skin and endure motion-induced strain while maintaining stable electrical performance. In the terms of wearable electronics, several terms need to be defined as they are sometimes confusing for readers. Stretchability defines the tendency of a material to return to its original shape after being stretched or compressed, and the strain is the change or deformation in length per unit length. Elongation at break or fracture strain is the ratio between deformed length and initial length after breakage. Toughness is the ability of a material to absorb energy and deform plastically without fracturing, while stiffness is the extent to which an object resists deformation in response to an applied force. The fundamental goal of wearable electronics is to enhance the device stretchability, or to achieve the stable electrical performance even under large deformation or strain. To fabricate wearable bioelectronics, intrinsic stretchable electronic materials or composites are always favorable due to the simple manufacturing process, and ease of encapsulation for integrated devices.

Self-healing defines the ability of a material to repair damage and restore the lost or degraded properties or performance. Self-healing is an attractive feature for bioelectronic devices, rendering the electronics robust and prolonging the lifetime. There are still few reports about the self-healable conducting polymer-based composites and bioelectronics, and the healing mechanism of conducting polymer-based materials is not well understood. To satisfy the need for next-generation bioelectronics, the research work on tuning the stretchability and self-healing properties is quite essential.

1.3 Hypotheses and Objectives

In the field of polymer science, a plasticizer is added to a polymer to increase the softness of this polymer via reducing the crystallinity and also increasing the segmental mobility of the polymer. The stretchability of PEDOT:PSS has been proved to be enhanced by the addition of plasticizers,

and we further hypothesize that the stretchability of PEDOT:PSS on elastomer substrate can be enhanced by addition of strong plasticizers or changing the processing conditions of films, especially film thickness and baking temperature. If the plasticizer can also improve the conductivity and ion transport of PEDOT:PSS, the transistor performance of the stretchable OECTs may also be improved. As the water enabled healing behavior of PEDOT:PSS is hypothesized mainly to be related with the swelling of PSS, we believe that any change of PSS concentration in the films would lead to a change in self-healing properties. Polymer chain diffusion plays an important role in the healing ability of polymers, we also hypothesize that change of flow ability of PEDOT:PSS after plasticizer addition may lead to the variation of healing property.

Hence, the primary objective of this thesis is to tune the stretchability and self-healing properties of conducting polymers for organic bioelectronics, *e.g.*, OECTs. In working towards this goal, it is of paramount importance to investigate the effect of the processing conditions on the stretchability and healability of conducting polymers and provide facile solutions to enhance the performance of conducting polymer based conductors and OECTs for bioelectronics.

Therefore, the main specific objectives of this thesis are:

(1) To enhance the stretchability of PEDOT:PSS via material based method (additive methods, without the need for pre-stretching the elastomer) and fabricate stretchable OECTs on elastomer poly(dimethylsiloxane) (PDMS). Furthermore, the performance of stretchable OECTs needs to be improved without the loss of stretchability.

(2) To gain deeper knowledge about the water-enabled behavior of PEDOT:PSS, tailor the healing performance of conducting polymers through the processing methods, and develop an autonomically healable, stable, and biocompatible conductor based on PEDOT:PSS.

1.4 Organization of the work

In Chapter 2, the introduction to conducting polymers as well as doping process, and PEDOT:PSS processing, with special attention paid to electrical and mechanical properties are presented. Chapter 2 deals with the operation mechanism, the figures of merit of OECTs, as well as the development of bioelectronics based on PEDOT. Finally, the existing technologies for the fabrication of stretchable electronics and research progress in PEDOT based healable materials and

electronics are reviewed. In Chapter 3, the material processing and synthesis, as well as the approaches of whole research work is briefly introduced.

Chapter 4 contains excerpts of an article where one of my colleagues and I contributed equally as the first author. Chapters 5 to 7 are reprints of three articles of which I was the first author.

-Excerpts of **Article**: Shiming Zhang, Yang Li, Gaia Tomasello, Madeleine Anthonisen, Xinda Li, Marco Mazzeo, Armando Genco, Peter Grutter, Fabio Cicoira. Tuning the electromechanical properties of PEDOT:PSS films for stretchable transistors and pressure sensors. Advanced Electronic Materials, 2019, 5(6), 1900191. (co-first author, contributed ~ 45% of total work)

-**Article 1**: Yang Li, Shiming Zhang, Xinda Li, Venkata Ramana Nitin Unnava, Fabio Cicoira, Highly stretchable PEDOT:PSS organic electrochemical transistors achieved via polyethylene glycol addition. Flexible and Printed Electronics, 2019, 4(4), 044004. (contributed ~ 85% of total work)

-**Article 2**: Yang Li, Xinda Li, Shiming Zhang, Leslie Liu, Natalie Hamad, Sanyasi Rao Bobbara, Damiano Pasini, Fabio Cicoira, Autonomic self-healing of PEDOT:PSS achieved via polyethylene glycol addition. Advanced Functional Materials, 2020, 30, 2002853. (contributed ~ 80% of total work)

-**Article 3**: Yang Li, Shiming Zhang, Natalie Hamad, Kyoungoh Kim, Leslie Liu, Michael Lerond, Fabio Cicoira, Tailoring the self-Healing properties of conducting polymer films. Macromolecular bioscience, 2020, 2000146. (contributed ~ 85% of total work)

In the excerpts of **Article** which I contributed equally as the first author, we tuned the electromechanical properties of PEDOT:PSS via changing processing conditions and fabricated stretchable OECTs on elastomer substrate without buckling. The stretchable OECTs can maintain stable performance up to 30% strain. The deposition of an ultrathin Parylene layer can further enhance the transistor performance of stretchable OECTs. In **Article 1**, we enhanced both stretchability and conductivity of PEDOT:PSS films via the addition of polyethylene glycol (PEG) and fabricated stretchable OECTs on elastomer substrate without pre-stretching the substrate. It is worthwhile to mention that the stretchable OECTs we fabricated are generally large (channel length, L, of 8 mm and a width, W, of 2 mm) compared to the deformation. The stretchable OECTs based on PEDOT:PSS/PEG films show superior performance in terms of both stretchability (stable

performance up to 45% strain) and transistor characteristics (enhanced transconductance, response time and ON/OFF ratio). In **Article 2**, we reported that fast, repeatable and autonomic electrical healing PEDOT:PSS is achieved by blending it with the bio-compatible polymer PEG. The PEG incorporation also improves the conductivity, softness and stability of the conducting polymer film. In **Article 3**, we demonstrated that the healing property of PEDOT:PSS films can be tailored via diverse processing methods. The preliminary investigation on the effect of cut width on both thin and thick PEDOT:PSS has also been done. Following these three articles, supplementary methods and results for this thesis are presented in the appendices.

In Chapter 8, the results of this thesis are discussed as a whole, supported by the literature review and the published articles. In Chapter 9, conclusions are drawn and perspectives on future work are also given here.

CHAPTER 2 LITERATURE REVIEW

The development of bioelectronics and wearable electronics relies on the advance of electronic materials. Most of current electronic materials are inorganic and normally conduct only electronic charge carriers. However, many biological systems transmit signals via ionic currents, which is the reason why inorganic materials-based electronics suffer some limitations when interfacing tissues or organs. Conducting polymers possess mixed electronic and ionic conductivity as well as ionic/electronic coupling ability, which makes them perfect candidates to deal with the interfaces between human-made electronics and biological systems[8].

Polymers are in general insulators. However, the discovery of doped polyacetylene, whose electrical conductivity can be increased by seven orders of magnitude via doping by iodine, resulted in the new era of research in conducting polymers. This decisive breakthrough in 1977 made Alan J. Heeger, Alan G. MacDiarmid and Hideki Shirakawa receivers of the Nobel Prize in Chemistry in 2000. Since 1977, a number of conducting polymers, like polythiophene, polyaniline, and polypyrrole are widely investigated to fabricate organic electronics[9-11]. Figure 2.1 shows the chemical structure of these conducting polymers.

In addition, conducting polymers have other advantages: (i) the biocompatibility is the supreme advantage of conducting polymers compared to inorganic electronic materials, which enabled them to be operated in-vivo without causing significant foreign body reaction[12]; (ii) the electrical conductivity is comparable with metallic conductors, and it can be tuned via chemical additives, electrochemical or organic synthesis[13]; (iii) the processing method of conducting polymers is mainly based on the solution, which makes them quite easy to process[14]. Moreover, the processed conducting polymers can also show similar mechanical properties to other commercial polymers, like flexibility or stretchability.

Up to now, different types of organic electronic devices have been developed based on conducting polymers, including organic light-emitting diodes (OLED), organic field-effect transistors (OFETs), organic photovoltaic cell (OPVs), and organic electrochemical transistor (OECTs)[15]. Due to high electrical conductivity by doping, and mechanical flexibility, conducting polymers play a more important role in the fields of implantable bioelectronics, artificial skin and muscles, wearable electronics, energy storage, and display devices.

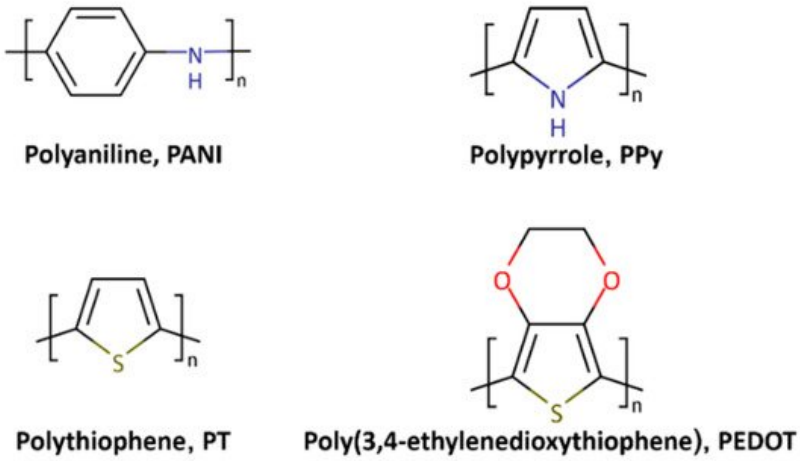

Figure 2.1 Chemical structures of representative conducting polymers[16]. Reprinted with permission.

2.1 Conducting polymers

Organic semiconductors are conjugated systems, where atoms are covalently bonded in a molecule with alternating single and double bonds. The simplest example of conjugated polymers is polyacetylene. Conjugated polymers can be intrinsically conductive, but their conductivity is typically very low (less than 10^{-5} S cm^{-1})[17]. Chemical doping is needed to increase the carrier density and electrical conductivity of the polymer. For instance, a seven orders of magnitude enhanced conductivity for polyacetylene can be achieved when doping with iodine [18].

2.1.1 Doping

The process of doping conjugated polymers is substantially a redox reaction, which removes an electron from the valence band or adds an electron to the conduction band and forms the polymeric cations (or anions) with counterions. A polaron, which is a radical ion associated with a lattice distortion and the presence of localized electronic states in the gap referred as polaron states, is formed after doping[19]. The polaron and bi-polaron (pair of charges after a second electron is removed) are the charge carriers inside the conjugated polymer, but they are localized in the polymer lattice with the counterion. With increasing the doping level, more free mobile charge carriers are introduced to the polymer chain, thus resulting in the increase of conductivity. In the

case of polyacetylene, the conductivity is increased by several orders of magnitude after being doped by iodine[20].

2.1.2 PEDOT and PEDOT:PSS

Although the iodine doped acetylene is the "prototype" of the conducting polymer, it has two main drawbacks: (i) instability in air and (ii) poor processability due to the insolubility in solvents. The introduction of heteroatoms (such as N or S) into polymer chains can stabilize the conjugated system due to the electron-donating property of heteroatoms. Polythiophene was firstly found to be electronically conductive in 1982, with a conductivity value of 10-100 S cm^{-1}[21]. However, when exposed to air and humidity for a long time, the doped polythiophene cannot keep the bi-polaron state, which is a prerequisite for high-conductivity. Owing to the electron donating properties, oxygen substituents at 3- and 4- position of thiophene can further stabilize the conjugated system. With the closed ring of two oxygen atoms and the ethylene group, high conductivity and stability are achieved in poly 3,4-ethylenedioxythiophene (PEDOT).

After the problem of water-stability of doped polythiophene was solved by the invention of PEDOT, scientists worked on improving the processability of PEDOT, as it is insoluble in most solvents. The water soluble polystyrene sulfonate (PSS) polyanion can function as counterion for PEDOT, forming the complex PEDOT:PSS (Figure 2.2). This was an amazing breakthrough, since this complex is easily processable and this dispersion is soluble and stable in water. In the PEDOT:PSS complex, short PEDOT chains are attached to the long PSS chain by the coulombic force. The repulsion between PSS chains leads to the coiled like structure of PSS segment with PEDOT inside, preventing the exposure of PEDOT to water (Figure 2.2)[22]. The PSS is always used in excess in PEDOT:PSS complex, working as host polyelectrolyte. PSS shows almost no absorption in the visible light range, which makes thin films of PEDOT:PSS transparent. The PEDOT:PSS dispersions are commercialized as the trade name Clevios™ from H.C. Stark Clevios GmbH with a wide range of conductivity (from 10^{-5} S cm^{-1} to 1000 S cm^{-1}) and viscosity for different usages and also the trade name Agfa, Orgacon S315 as transparent conductive ink [23]. PEDOT or PEDOT:PSS is now widely used in wearable electronics, organic energy storage devices and bio-electronics, and will continue its successful story as electronic material in the future [24].

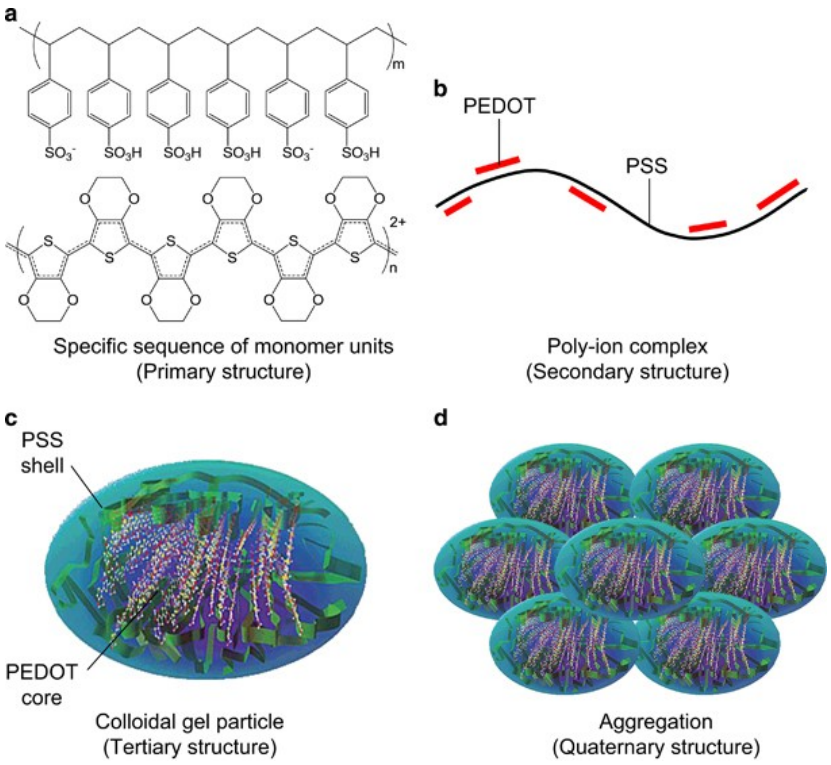

Figure 2.2 Chemical structure of PEDOT:PSS. (a) specific sequence of monomer units (primary structure), (b) poly-ion complex (secondary structure), (c) colloidal gel particle (tertiary structure) and (d) aggregation (quaternary structure)[22]. Reprinted with permission.

2.2 PEDOT:PSS processing

The commercial PEDOT:PSS product used in our experiments is the Clevios PH1000 suspension, a typical micellar system with a PEDOT:PSS weight ratio of 1:2.5. The micelle of PEDOT:PSS contains a PEDOT core and a PSS shell, and the PEDOT-rich domains are usually separated by the excess PSS-rich domains, leading to a relatively low conductivity. To achieve the requirement of electronic materials used in stretchable electronics or bioelectronics (*e.g.*, high conductivity, stretchability), certain processing is necessary for the PH1000.

2.2.1 Electrical conductivity

PEDOT:PSS is a conductive polymer, which can be is considered as a mixed conductor where cations are transported in PSS segments and electrons are moving in PEDOT rich areas. The films obtained from baking the as-received PEDOT:PSS suspensions have electrical conductivities

ranging from 10^{-4} to 1 S cm^{-1}, depending on the PEDOT/PSS ratio[25]. A "conductivity enhancer" is needed to further increase the conductivity of already doped commercial PEDOT:PSS by several orders of magnitude. The conductivity enhancers for PEDOT:PSS should satisfy the following characteristics: (i) good solubility in water and (ii) possession of highly polar groups or highly acid anions which can act as effective dopants. Up to now, many organic solvents, polyols, ionic liquids, surfactants and salts are used as conductivity enhancers[26]. However, the mechanism of the enhanced conductivity is still under debate.

Kim et al. attributed the conductivity enhancement to the separation of the PEDOT and PSS phase when adding conductivity enhancers[27]. When the highly polar organic solvents are added to the PEDOT:PSS suspension, the coulombic attraction between PEDOT and PSS segments is reduced by the screening effect of high-polarity groups. During the drying process, as the water is evaporated from the film, these polar solvents induced PEDOT-rich domains forms the conducting network. This explanation applies to the conductivity enhancement due to the addition of ethylene glycol (EG), glycerol, dimethyl sulfoxide (DMSO), sorbitol, and polyethylene glycol (PEG)[28-30]. Bao et al. also suggested that the charge screening effect of the ionic liquid additives can lead to the formation of more crystalline and more interconnected PEDOT aggregations[31]. Besides, post-treatment with alcohols can also significantly increase the conductivity of PEDOT:PSS films also due to the separation of PEDOT and PSS. Chu et al. found that the enhancement depends on the chemical structure of alcohols. With the rinsing of methanol, 1015 S cm^{-1} can be reached while it is only 286 S/cm when treated with i-butanol[32]. Jeong et al. also argued that methanol is the most suitable solvent because it can dissolve the excess PSS without changing the morphology of PEDOT and the solubility of PSS decreases with the increase of the carbon number in the alcohol[33].

Ouyang et al. argued that the conductivity enhancement was attributed to the effect of the conductivity enhancer on the conformation of the conductive $PEDOT^+$ chains, and the protonation of PSS ($PSS^- + H^+ \rightarrow PSSH$) resulted in phase segregation[34]. The conformational change of PEDOT and significant removal of PSS will lead to the formation of PEDOT nanofibrils (Figure 2.3). This explanation is proved by the significant conductivity increase by the treatment by the acids, especially sulfuric acid[35, 36]. The conductivity of PEDOT:PSS films can reach around 2400 S cm^{-1} after the treatment with 1.5 M H_2SO_4 and 3065 S cm^{-1} after being treated with 1 M

H_2SO_4 three times at 160 °C, which are comparable values to ITO on glass (around 13000 S cm^{-1}). But the highly corrosive property of the acid limits the application of this method[37]. Ouyang et al. discovered that similar conductivity (higher than 3300 S cm^{-1}) can be reached after the treatment of methanesulfonic acid (not corrosive), which might be more useful for bioelectronics[38].

Besides, surfactants are reported to improve the film conductivity of PEDOT:PSS due to their ability to induce the conformational change of PEDOT:PSS structure or remove excess PSS domains. The addition of non-ionic surfactants, including Capstone FS-300 fluorosurfactant (Zonyl) and Triton X-100 results in the formation of PEDOT nanofibrils, improving the film conductivity[39, 40]. Anionic surfactants, such as sodium dodecyl sulfonate (SDS), can enhance the conductivity of PEDOT:PSS film by a factor of several orders of magnitude regardless of the blending or post-dipping methods[41]. These anionic surfactants can replace PSS as the counterions to PEDOT and change the distortion structure of PEDOT chains to linear, after the anionic surfactants are introduced. However, cationic surfactant tetraoctylammonium bromide doesn't change the conductivity of PEDOT:PSS[42].

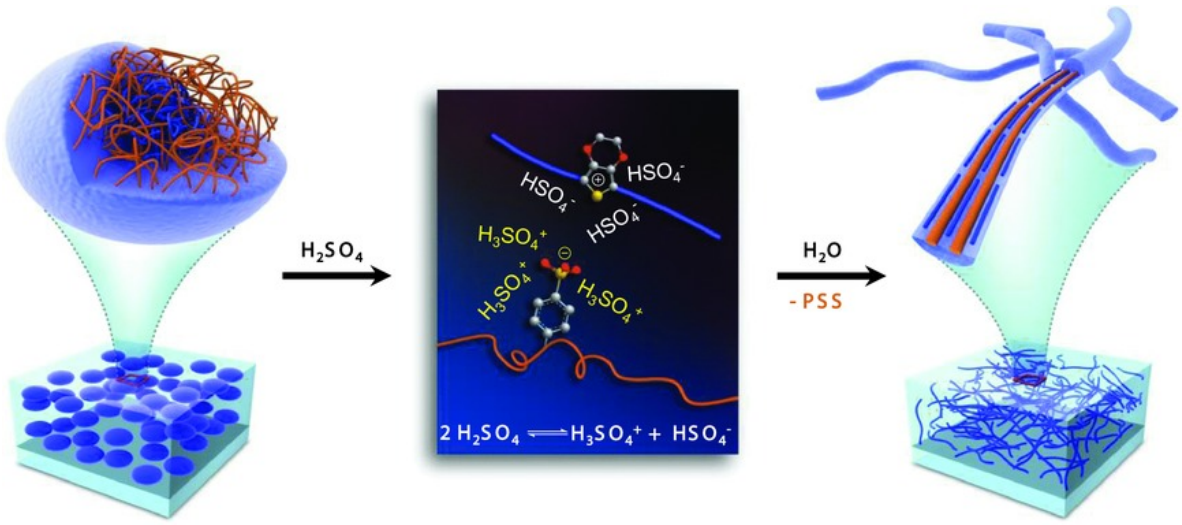

Figure 2.3 Diagram of the structural rearrangement of PEDOT:PSS. The amorphous PEDOT:PSS grains (left) are reformed into crystalline PEDOT:PSS nanofibrils (right) via a charge-separated transition mechanism (middle) via a concentrated H_2SO_4 treatment[35]. Reprinted with permission.

2.2.2 Flexibility and stretchability

Compared with rigid materials, e.g., silicon, metal oxides or ITO, PEDOT:PSS has intrinsic advantages since polymers do not crack easily during bending. The "flexible" nature of PEDOT:PSS comes from the weak van der Waals or electrostatic interactions inside the polymer domains, which can dissipate certain energy during deformation. A lot of effort has been put into replacing ITO with flexible or stretchable and transparent PEDOT electrodes or to develop flexible or stretchable devices. Di Carlo et al. fabricated a flexible sensor by depositing the PEDOT:PSS film on a flexible polyimide substrate by electrochemical polymerization and peeling technique[43]. In our group, Zhang et al. reported that the robust adhesion and excellent flexibility of PEDOT:PSS films when coating on polyethylene terephthalate (PET) substrate, since the current loss is only 4% after 500 bending cycles[44].

The PEDOT:PSS film usually exhibits failure upon 5% strain, which limits the use of PEDOT:PSS in stretchable devices. Lang et al. investigated the mechanical properties of PEDOT:PSS free-standing films by tensile tester[45]. They found that the Young's modulus of PEDOT:PSS film strongly depends on the relative humidity (RH). The strain at break increases from 2.3% at 23% RH to 5.8% at 55% RH. The addition of small molecule surfactant or plasticizer is often utilized to provide soft domains between PEDOT and PSS domains, which makes the film compliant to tensile strain or mechanical deformation. With the addition of a fluorosurfactant Zonyl and DMSO to the processing mixture, Bao et al. developed highly stretchable and transparent PEDOT:PSS electrodes[46]. The sheet resistance is 46 Ω sq^{-1} at 82% transmittance and 240 Ω sq^{-1} at 97% transmittance. Besides, the Zonyl can increase the wettability of PEDOT:PSS on various hydrophobic substrate. When depositing on the pre-strained polydimethylsiloxane (PDMS) substrate, the stretchable PEDOT:PSS electrodes can withstand 5000 cycles of 10% strain without losing any conductivity. Lipomi et al. fabricated the PEDOT:PSS film on PDMS substrate by the addition of 1% fluorosurfactant Zonyl to PEDOT:PSS solution and a mild treatment of the PDMS surface with ultraviolet/ozone (UV/O_3)[47]. The samples are stretchable and retain conductivity up to 188% strain (due to the failure of PDMS substrate). The addition of Zonyl and UV/O_3 treatment on PDMS can have a synergistic effect on the morphology of PEDOT:PSS. Grains are able to reorient in the strain direction and accommodate tensile deformation, which leads to good stretchability.

As discussed in the last section, ionic liquids can act as conductivity enhancers to enhance the conductivity of PEDOT:PSS, but it can also serve as plasticizer to prolong the film elongation. Bao et al. reported a highly stretchable conducting polymer by adding stretchability and electrical conductivity (STEC) enhancers to PEDOT:PSS[31]. The change of PEDOT:PSS morphology (nanofibrils) and the formation of more interconnected PEDOT rich crystalline structures lead to very high values for both conductivity and stretchability of PEDOT:PSS. The resultant films show over 3100 S cm^{-1} under 0% strain, 4100 S cm^{-1} under 100% strain, above 100 S cm^{-1} under 600% strain and a fracture strain of 800%. The conductivity even remains 3600 S cm^{-1} after 1000 cycles of 100% strain. The ionic liquid 1-ethyl-3-methylimidazolium:tetraacyanoborate (EMIM:TCB) incorporation also can transform the PEDOT:PSS into a stretchable and conductive film, with an enhanced stretchability of 50% strain along with a high conductivity of ~ 1280 cm^{-1}[48]. The films can maintain their electric performance even up to 180% strain on a pre-strained substrate, with only a 2-fold increase in resistance.

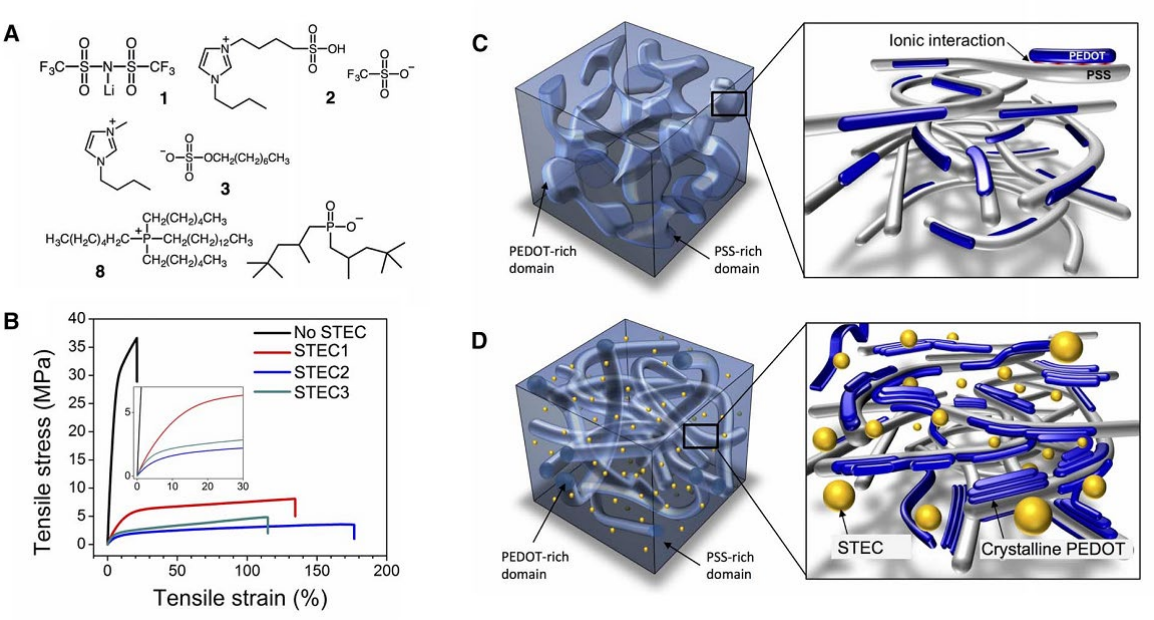

Figure 2.4 Chemical structures and schematic representation. (A) Representative stretchability and electrical conductivity enhancers. (B) Strain-stress curves of PEDOT:PSS with and without stretchability and electrical conductivity (STEC) enhancers. (C and D) Schematic diagram representing the morphology of (C) a typical PEDOT:PSS film versus that of (D) a stretchable PEDOT film with STEC enhancers[31]. Reprinted with permission.

The blending with soft polymers, such as PEG, polyethylene oxide (PEO) and polyvinyl alcohol (PVA) can also significantly increase the elongation at break of PEDOT:PSS films due to their role in softening the film[49]. After 66.7 wt% PVA blending, the elongation at break of PEDOT:PSS free-standing films increases to ~50% strain, and an enhanced conductivity of ~ 75 S cm^{-1} is also achieved at same time. However, excess weight fraction of these soft polymer will lead to the formation of a gel, which is not favorable for film processing.

2.3 Organic electrochemical transistors (OECTs)

Among of the applications of conducting polymers, the organic conducting polymer-based transistors attract great attention due to their wide range of utilization in biological systems. OFETs always adopt conjugated molecules as semiconductor and modulate the channel current via the field-effect doping between the semiconductor and dielectric layer after the gate voltage is applied. Instead of using dielectric, an electrolyte is used between the gate and channel in OECTs. Taking advantage of ionic/electronic coupling property of conducting polymers, the channel current in OECTs is modulated by the electrochemical doping and dedoping process with the injection of ions from the electrolyte. OECTs always work at low voltages (below 1 V) and the similar aqueous electrolyte medium as biological reactions or species makes OECTs quite promising in bioelectronics[50].

2.3.1 Introduction of OECT and working principle

The first demonstration of OECT was done in 1984, with polypyrrole functioning as the channel material[51]. Due to the enhanced water stability, PEDOT, especially PEDOT:PSS, has been receiving renewed attention in the field of organic bioelectronics. A typical PEDOT:PSS based OECT consists of a PEDOT:PSS channel in contact with an electrolyte where a gate electrode dips inside, and source and drain electrodes define the path for charge carriers (Figure 2.5a). The drain-source voltage induces a drain current (I_{ds}), which is determined by the mobile holes or electrons inside the channel material, while the gate voltage controls the injection of ions to dope or dedope into channel material, thus modulating the current (or redox reaction in the electrochemistry term, equation 1). When the gate voltage is removed, ions go back to the electrolyte and drain current returns to the initial value.

$PEDOT^+PSS^- + M^+ + e^- = PEDOT^0 + M^+ PSS^-$ (Equation 1)

Most channel materials used in OECT are conjugated polymers. As the most common one, PEDOT:PSS is p-type doped, so holes can hop to nearby chains when the drain voltage is applied (ON state). Once the positive bias is applied, cations from the electrolyte go inside and compensate $PEDOT^+$. As a result, the number of mobile holes decreases, leading to the drop of drain current (OFF state). This is called depletion mode OECT (Figure 2.5b). On the contrary, the accumulation mode is where the drain current increases when negative bias is applied, and injected anions dope the channel polymer (Figure 2.5c). The common examples of channel materials working in accumulation mode are polypyrrole and several glycolated thiophene copolymers[52-54].

The physics of an OECT is described by the Bernards model[55]. In this model, the device is separated into two circuits: the electronic circuit, which describes the charge carrier flow in the source-channel-drain path according to the Ohm's law, and the ionic circuit, which describes the ion injection in gate-electrolyte-channel path (Figure 2.5d). The electronic circuit is considered as the resistor, whose conductivity varies during gating. The ionic circuit is considered as the combination of a resistor (electrolyte), and two capacitors at the boundary of gate-electrolyte and channel material. The solid line in Figure 2.5d shows the case of efficient gating, where most of the gate voltage drops at the electrolyte-channel material interface, producing the strong injection of the ions. In this model, the ions just compensate the presence of opposite charges of organic film. At steady state, the capacitor is charged and the gate current becomes zero[56]. At saturation of depletion mode devices, it gives the equation of transconductance g_m.

$$g_m = \left(\frac{W}{L}\right) \times d \times \mu \times C^* \times (V_{Th} - V_G) \quad \text{(Equation 2)}$$

Where W, L and d are the channel width, length and thickness, respectively; μ is the charge carrier mobility; C^* is the capacitance of channel per unit volume and V_{Th} is the threshold voltage.

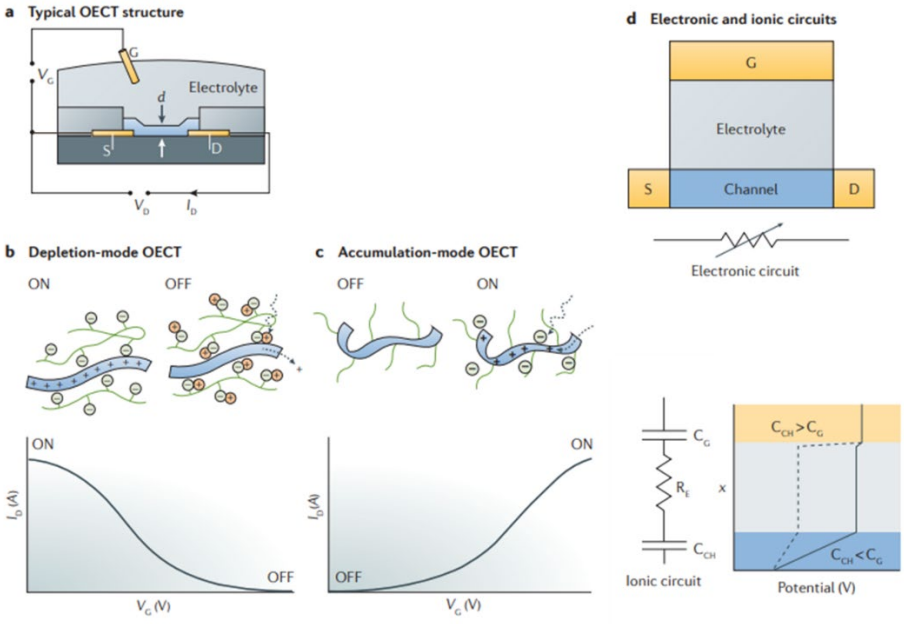

Figure 2.5 The device physics of organic electrochemical transistors. (a) The typical structure of an organic electrochemical transistor (OECT), showing the source (S), drain (D), electrolyte and gate (G). (b) Transfer curve showing depletion-mode operation of an OECT with a conducting polymer channel. At zero gate voltage, holes on the conducting polymer contribute to a high drain current and the transistor is ON. When a gate voltage is applied, the holes are replaced by cations and the transistor is OFF. (c) Transfer curve showing accumulation-mode operation of an OECT with a semiconducting polymer channel. At zero gate voltage, the channel has few mobile holes and the transistor is OFF. When a gate voltage is applied, holes accumulate and compensate injected anions, and the transistor is OFF. (d) Ionic and electronic circuits used to model OECTs. The electronic circuit, shown below the device layout on the left, is modelled as a resistor with a resistance that varies upon gating. The ionic circuit, shown in the middle, consists of capacitors corresponding to the channel, C_{CH}, and gate, C_G, respectively, and a resistor corresponding to the electrolyte, R_E. The panel on the right shows the distribution of potential in the ionic circuit. The solid line corresponds to the case of efficient gating, in which most of the applied gate voltage drops at the electrolyte-channel interface, driving ions inside the channel. The dashed line corresponds to the case of poor gating, where most of the applied gate voltage drops at the gate-electrolyte interface. d, channel thickness; I_D, drain current; V_G, gate voltage; V_D, drain voltage; x, distance[57]. Reprinted with permission.

2.3.2 Figures of merit of OECTs

2.3.2.1 Transfer and output characteristics

The figure of drain current (I_{ds}) against drain voltage (V_{ds}) with constant gate voltage is called the output curve, and the figure of drain current against the gate voltage (V_{gs}) with a constant drain voltage is the called transfer curve (Figure 2.5b). Most characteristics of the transistors are obtained from these two curves.

2.3.2.2 ON/OFF ratio

The ON/OFF ratio is the ratio of the drain current in "ON" state and "OFF" state within a given voltage range. Typically, for PEDOT:PSS based OECT working in depletion mode, the I_{ds} (ON) is the drain current when no gate voltage is applied and the I_{ds} (OFF) is the drain current when positive gate voltage is applied. This value varies depend on the different selected "OFF states" and drain voltages.

2.3.2.3 Transconductance

The transconductance of OECT describes the modulation of V_{gs} to I_{ds}, whose definition is $g_m = \Delta I_{ds}/\Delta V_{gs}$. This figure of merit leads to the success of OECT applications. PEDOT:PSS based OECTs can reach transconductance as high as 250 mS, which is significantly higher than that of solid-state silicon transistors[58]. The difference arises because the electronic charge transport in OECT can be greatly modulated via the injection of ions into whole channel material, whereas field-effect doping only regulates the charge carrier at the semiconductor/dielectric interface. Owing to the bulk doping effect, the transconductance can be increased by increasing the ratio of width to length, but also by increasing the thickness. Besides these geometric parameters, the transconductance is also affected by charge carrier mobility μ and volumetric capacitance C^*, which are materials parameter related to electronic and ionic properties, respectively[59].

2.3.2.4 Response time

The response time of OECT is defined as the time elapsed between the application of a gate voltage and the time when the corresponding I_{ds} variation achieves the final stable state. It depends on both the transport of ions from the electrolyte solution to the channel and electronic charge carriers along

the channel (between source and drain). It has been revealed that in most cases, the ionic transport is the limiting process since the hole transport (~10^{-1} cm^2 V^{-1} s^{-1}) in the OECTs is 10-100 times faster than the ionic transport (~10^{-3} cm^2 V^{-1} s^{-1})[60]. A reduction in response time can be achieved by decreasing the thickness of channel material and controlling the dimensions of the transistor. Therefore, OECTs designed for monitoring the neuron actions need measurement in higher frequency, and response time should be decreased[61]. The microfabricated OECTs with liquid electrolyte can achieve response times of few tens of microseconds, and the use of a gel or solid electrolyte may lead to slower response time[62].

2.4 Applications of PEDOT in bioelectronics

2.4.1 Electrophysiology recording

Electrophysiological signals are often recorded clinically to monitor the specific pathological state of a biological system, such as an organ or tissue. Depending on which part of the body the recording devices are mounted, different electrophysiological signals, such as neurological rhythms (electroencephalography, EEG), muscle activity (electromyography, EMG), cardiac cycle (electrocardiography, ECG), and eye movement (electrooculography, EOG), can be obtained. Due to the mixed ionic/electronic conductivity, PEDOT has inherent advantage to record electrophysiological signals in high-quality by lowering the impedance at electronic/skin interface. Malliaras et al. prepared the flexible and dry PEDOT:PSS electrodes on polyimide substrate and used them for EEG recordings (Figure. 2.6)[63]. Compared to Au electrodes of same geometry, PEDOT:PSS electrodes can record low-amplitude brain activities with higher precision and signal-to-noise ratio (SNR). In order to further increase the SNR, Biscarini et al. replaced the counterion PSS with the fluorinated polymer Nafion for PEDOT, and fabricated a flexible neural micro-electrode array using the PEDOT:Nafion composite[64]. PEDOT:Nafion coated electrodes exhibits slightly lower impedance and higher SNR compared to reference PEDOT:PSS due to the excellent ionic transport ability of Nafion and PEDOT:Nafion shows a charge injection two times larger than that of PEDOT:PSS when used for stimulation.

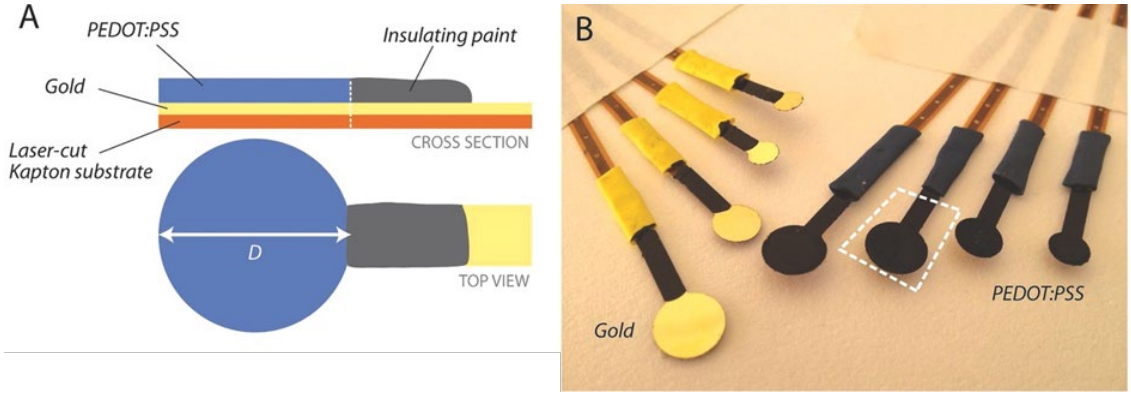

Figure 2.6 (A) Schematic of the PEDOT:PSS electrode indicating the cross section and the top view (not to scale). (B) Photograph of dry electrodes with different diameters[63]. Reprinted with permission.

The electrophysiology recording relies on the precise detection of variation of cell membrane potential induced by the ionic current flux, so electrodes with higher ionic conductivity and lower contact impedance can provide better recording performance. Though dry PEDOT:PSS electrodes can function as both ionic and electronic conductors, it is found that the dry electrodes cannot achieve stable contact with skin and the signal amplification becomes higher when the electrodes are wetted[65]. Similarly, an organohydrogel consisting of PEDOT and poly (acrylic acid) (PAA) skeleton shows excellent recording performance in ECG and EMG due to the lower impedance and better conformability[66]. Moreover, the drying of wetted PEDOT electrodes or gels will cause increased impedance. Malliaras et al. incorporated the ionic liquid 1-ethyl-3-methylimidazolium ethyl sulfate into the PEDOT/poly(ethylene glycol) diacrylate (PEGDA) gel electrodes[67]. The addition of ionic liquid not only lowers the impedance at the interface with human skin to levels that are similar than those of commercial Ag/AgCl gel electrodes, but also assist electrodes to record with a low impedance over 3 days, while commercial electrodes lose the functionality only after 20 h. These results prove that the addition of stable and non-volatile components in PEDOT gel electrodes enables the long-term cutaneous recording of electrophysiological data.

OECTs can transduce the fluctuation of ionic fluxes in biological systems to electrical signals and amplify it as the change in the transistor drain current. In the case of electrophysiology recordings, via direct contact with skin, OECTs has the ability to achieve higher resolution recording due to the improved SNR[68]. Biscarini et al. patterned PEDOT:PSS based OECTs on a fully resorbable

bio-scaffold poly (L-lactide-co-glycolide) (PLGA)[69]. The exposed PEDOT:PSS channel is directly attached to the skin of the forearm, and the ground contact is placed on the chest. Skin replaces the role of the gate and the source-drain current changes due to the fluctuations of potential at skin with respect to the ground. The OECT shows a comparable SNR to one of standard Faradaic electrodes when applied in ECG recording (Figure 2.7). Someya et al. also fabricated an ultrathin OECT with a nonvolatile glycerol-based electrolyte[70]. The OECT can be conformably placed on the skin and effectively monitor the cardiac signals from skin with an SNR of 24 dB. Thanks to the non-volatile gel electrolyte, this OECTs can achieve multiple reuses in a test that lasts more than one week. Unlike the PEDOT:PSS electrodes, the electrophysiological signal collected from PEDOT based OECT is the current data, which might need further procession in analyzing.

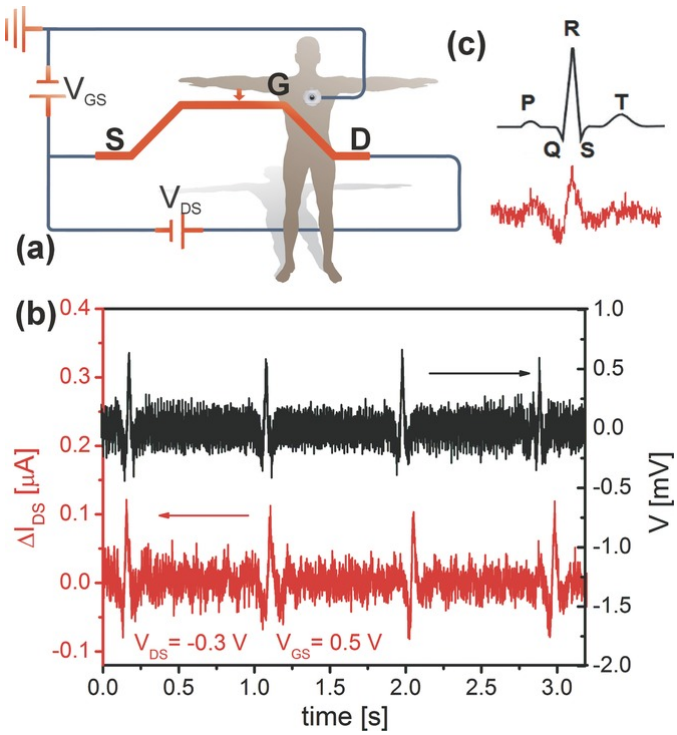

Figure 2.7 ECG recording with a bioresorbable OECT operated in direct contact with the skin. (a) Wiring diagram of the experiment. (b) Measured drain current trace (red) as obtained during ECG recordings (V_{gs} = 0.5 V, V_{ds} = -0.3 V) and comparison to a normal potentiometric recording with standard disposable leads (black). (c) Enlarged transistor ECG trace of a single cardiac cycle and comparison to a schematic textbook example[69]. Reprinted with permission.

2.4.2 Neuromorphic devices

In order to mimic the information processing in the human brain, scientists have developed biologically inspired artificial synapses via using complementary metal oxide semiconductor (CMOS)[71]. Generally, two types of functionalities in the signal processing of the synapses need to be realized: short-time plasticity (ms to min, refer to the computation tasks of the brain) and long-time plasticity (> min, days, or even longer, refers to memory and learning)[72]. PEDOT based OECTs are also able to simulate the synaptic behavior due to its similar ion flux transmission to biological systems. In 2015, Malliaras et al. first demonstrated the realization of neuromorphic functions in the simple PEDOT:PSS OECTs by applying a short pulse to its presynaptic terminal[73]. The device is laterally gated by the Au electrode in the KCl electrolyte confined in a PDMS well (Figure 2.8a). Via applying various V_g pulses with different amplitudes and time interval, they find that short-term depressive or paired-pulsed-depression (PPD) behavior is achieved when the time interval is insufficient to obtain charge equilibrium before the application of the second pulse. In this case, after removing the pulse, the injected cations cannot all return to the electrolyte and PEDOT:PSS channel is not doped to the initial state reversibly, leading to accumulated cations to channel and cumulatively dedoped PEDOT:PSS channel. Besides, some other basic neuromorphic functions (*e.g.*, adaptation, dynamic filtering) were also reported. Furthermore, they realized the long-term plasticity behavior with PEDOT based OECTs, due to the conformational change of poly(tetrahydrofuran) based PEDOT (PEDOT:PTHF) film when high gate spike bias is applied[73]. Short-term plasticity, short-to long-term memory transition, and other neuromorphic functions similar to biological storage were obtained.

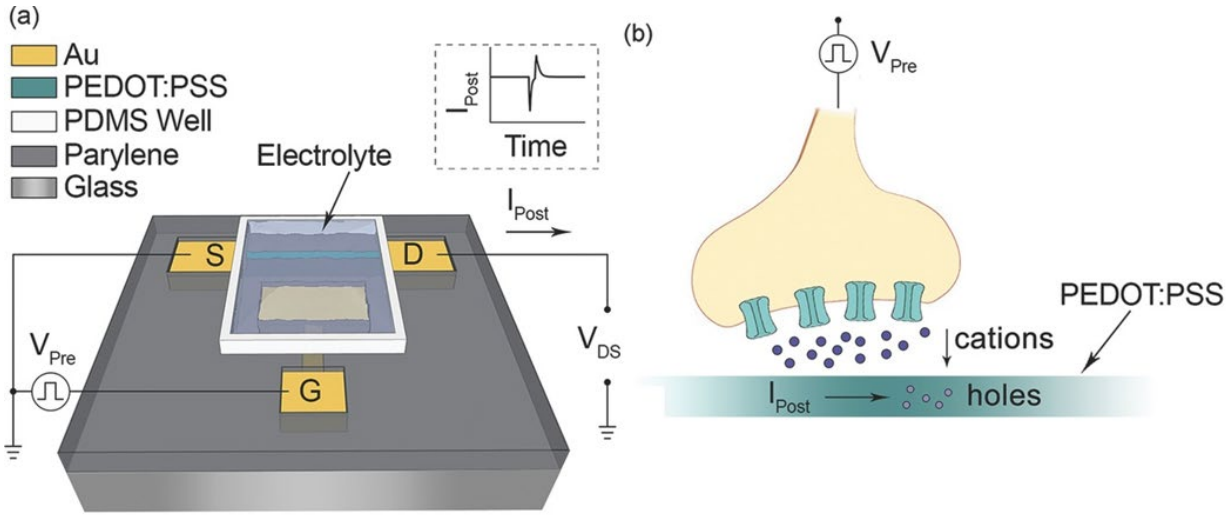

Figure 2.8 (a) OECT schematic and wiring diagram. (b) Schematic representation of the synaptic OECT in analogy to a biological synapse[73]. Reprinted with permission.

The synaptic response time in human brains is generally in milliseconds[74]. However, OECTs exhibit relatively long response time because ionic transport in the whole bulk dedoping of PEDOT:PSS consumes a lot of time. In order to achieve neuromorphic devices in higher frequency, scientists are improving the ionic transport in the PEDOT channel of OECTs. Biscarini et al. fabricated PEDOT:Nafion composite via the oxidative polymerization of EDOT in the presence of Nafion and $FeCl_3$[75]. In the electrochemical impedance spectroscopy (EIS) test, PEDOT:Nafion exhibit similar charge transfer but lower diffusion time constant than PH1000, demonstrating the faster ion transport. The PEDOT:Nafion based artificial synapses can achieve 10% short-time depression at 625 Hz with a characteristic depression time scale of 1 ms. In order to tune the neuromorphic functions in OECTs, Malliaras et al. blended an ionic conductor (PSSNa) with PEDOT:PSS[76]. The increase ratio of PSS to PEDOT in the channel material of OECTs decreases the electric conductivity and current, but speeds up the response time, enabling the dynamic filtering of neuromorphic devices when subjected to a 100 kHz gate pulse train.

2.4.3 Implantable electronics

Implantable electronics, which require a surgical operation before implantation, are more in need of the biocompatibility, stability, and long-term operation of the devices[77]. Though electrophysiological signals can be recorded with on-skin electrodes or devices based PEDOT, an

intimate contact with tissue or neurons improves the quality of recording and stimulating. Besides PEDOT possess the possibility to gain softer mechanical properties via various processing methods and its believed biocompatibility enables to reduce the foreign body reaction of biological tissues to implants. As a result, PEDOT based materials, coatings and devices have received great attention in implantable electronics.

To facilitate a better record quality of implantable Au electrodes, Kipke et al. electropolymerized the PEDOT coatings on the recording electrodes to lower the impedance without changing the surface area of electrodes[78]. Prior to implantation, it is found that the impedance of electrodes decreases from 9.1 MΩ to 0.37 MΩ after the introduction of PEDOT coating. Upon implantation, unmodified electrodes fail in the recording of isolated unit brain activity due to the increased impedance and noises, whereas PEDOT coated electrodes can consistently record high-quality neural activity with a remarkably lower noise. Fang et al. developed the transparent 32-channel Au/PEDOT:PSS nanomesh microelectrode arrays (MEAs) on a flexible parylene C film, with over 70% transmittance at 550 nm (Figure 2.9)[79]. The PEDOT:PSS coatings are also electropolymerized on the Au nanomesh template in presence of the mixture of EDOT and PSSNa. These electrodes are highly scalable and show comparable impedance at 1 kHz to non-transparent Michigan electrodes. After implanted on visual cortex of mice, the MEAs exhibit a high SNR of 33 dB, and allows for the long-term electrophysiology recording with simultaneous two-photon imaging. Moreover, due to the excellent biocompatibility, no significant inflammation due to the implantation is observed after 20 days.

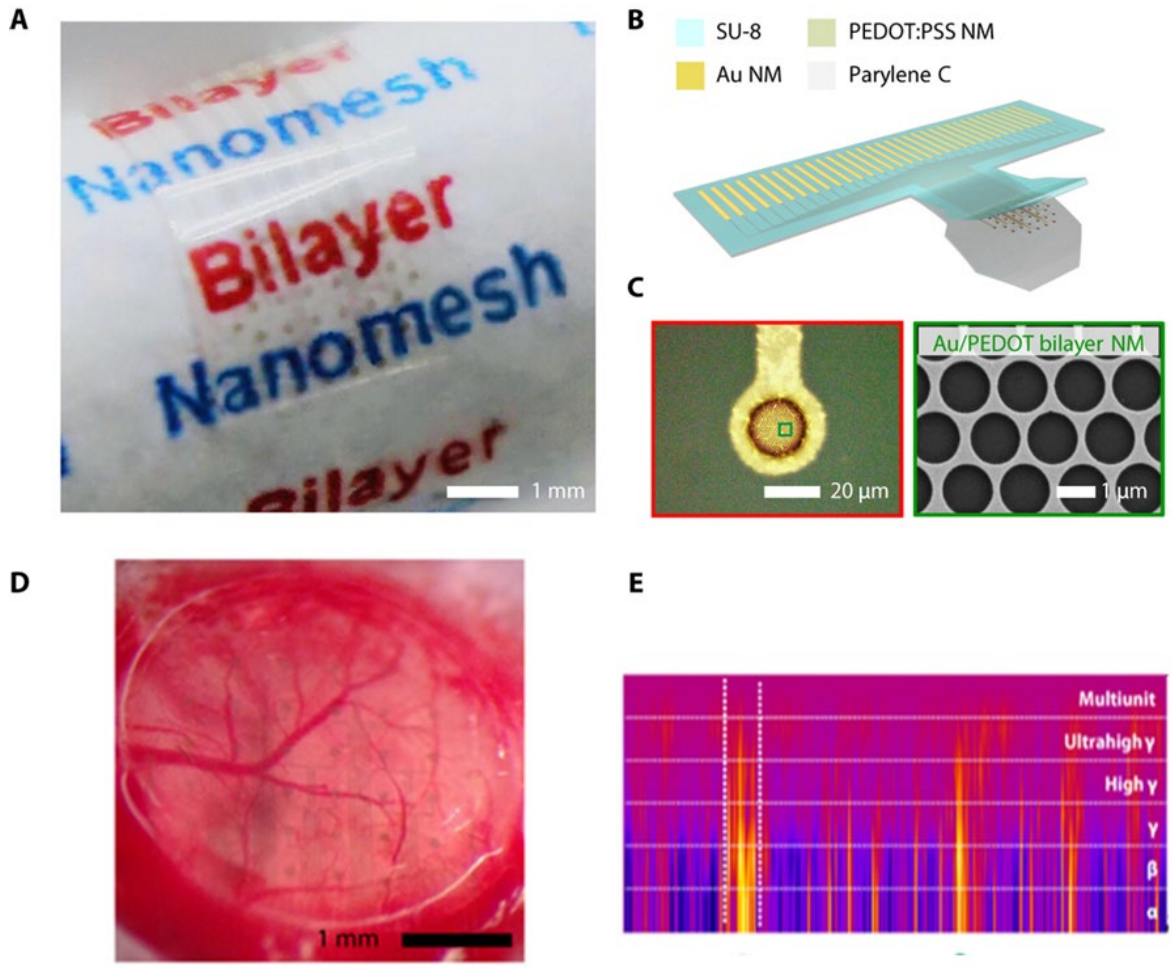

Figure 2.9 (A) Photograph of a 32-channel Au/PEDOT:PSS nanomesh MEA wrapped on a paper rod. Scale bar, 1 mm. (B) Device schematic of the 32-channel Au/PEDOT:PSS nanomesh MEA in (A). (C) Left: Microscope image of a Au/PEDOT:PSS bilayer-nanomesh microelectrode (20 µm in diameter). Right: SEM image of a zoomed-in region of the microelectrode shown on the left. (D) Enclosure of the transparent MEA with the cranial window. (E) Simultaneous electrophysiology recording (spectrogram)[79]. Reprinted with permission.

In addition to recording, implantable electronics can function as stimulation devices, enabling the therapies for various disorders or diseases (*e.g.*, seizure, Parkinson's)[80]. Our group has coated PEDOT on PtIr microelectrodes via electropolymerization for deep-brain stimulation.[81] The coated electrodes exhibit increased capacitance, decreased impedance, and good electrochemical stability during sterilization as well as in vitro stimulation. After implantation, the coated electrodes are tested for stimulation purposes and proved to be stable in vivo for 15 days. Furthermore, our

group deposited PEDOT on stainless steel multistranded wire electrodes[82]. The bare and PEDOT-coated electrodes were implanted in the neck muscle of five mice for EMG activity recording over a period of 6 weeks. Compared to bare electrodes, the PEDOT coating lowers the impedance of electrodes, resulting in an enhanced SNR during in vivo EMG recording. Bao et al. developed a chronic and neurologically implantable morphing electronic device via adopting a viscoelastic PEDOT:PSS/glycerol composite material (Figure 2.10a)[83]. The viscoelasticity allows the device to adapt to the in vivo tissue growth via plastic deformation. Compared to commercial cuff electrodes, the morphing electronics exhibit lower impedance and higher charge storage capacity, due to the dual conductive nature of PEDOT:PSS, and high volumetric capacitance of nano-porous PEDOT:PSS. After the assembly with sciatic nerve, morphing electronics can evoke the compound action potential with stable neuromodulation performance for 8 weeks, while cuff electrodes fail in evoking a detectable compound action potential after week 2 (Figure 2.10b). It is found that implanted cuff electrodes partially detach from the nerve due to the incapability to accommodate nerve growth, but morphing electronics can maintain a robust interface for long-term neuromodulation (Figure 2.10c). Malliaras et al. also demonstrated the role of PEDOT based OECTs for local neural network stimulators[84]. OECTs are embedded in the 4 μm thick Parylene film on the SU-8 shuttle depth probes. After penetrating the cortex, the probes feature a mechanical delamination and leave only OECTs inside the brain, reducing the invasiveness. It is proved that OECTs can deliver targeted stimulation to a specific local population of neurons (nor more than 300 μm away from the device). Coupling with ability to provide high SNR recordings, OECTs can behave as high performance and minimally invasive devices for in vivo electrophysiology.

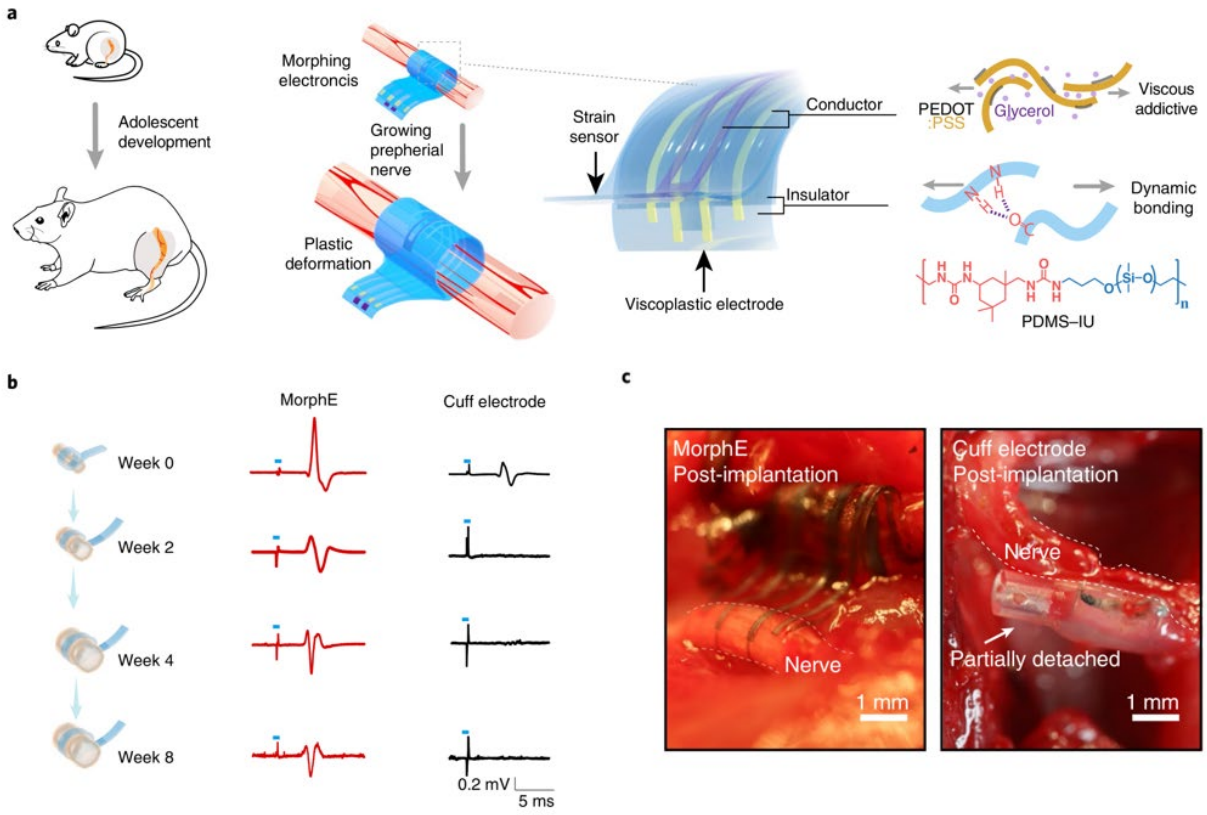

Figure 2.10 (a) Schematics showing adolescent development of the rat and the morphing electronics that conformally adapts to sciatic nerve growth. The Morphing electronics is composed of two materials: PEDOT:PSS plasticized by a viscous additive (glycerol) serving as a soft conductor and a polymer blend of PDMS-IU and PDMS-IU0.6-MPU0.4 as a viscoplastic insulator. Morphing electronics allows plastic deformation with little stress when stretched by a growing nerve. (b) Representative trace of elicited compound action potential stimulated by morphing electronics and cuff electrode for 8 weeks. Blue dash denotes the 200 μs electrical stimulation pulse with amplitude of 300 mV. (c) Image of cuff electrode and morphing electronics after 4-week implantation. The cuff electrode was outgrown and partially detached from the sciatic nerve. Scale bar, 1 mm[83]. Reprinted with permission.

2.5 Strategies to fabricate stretchable electronics

Compared with conventional electronics, stretchable electronics are more mechanically conformable with various objects, especially curvilinear soft epidermis of the human body. Stretchability demands that electronics have the capacity to absorb or accommodate mechanical

deformation without fracture or obvious degradation in the performance. Compared with the flexible devices that only offer bendability, it is more difficult to fabricate stretchable electronics, where circuits inside must be wrapped conformally around complex curvilinear shapes or integrated with biological tissues[85]. Extensive efforts have been devoted to the field of stretchable electronics, such as wearable smart displays, biosensors, artificial skin and personalized healthcare systems[86]. The methods to fabricate stretchable electronics are generally categorized by two strategies, namely “structure-based” and “material-based” approaches[87].

Structure-based method was developed for conventional non-stretchable electronic materials, including metal, metal oxides, and semiconductor thin films. Here, special interconnections, formation of buckled structure need to be designed to tolerate the strain. For instance, the periodic buckles that are formed by depositing conductive materials on a pre-stretched substrate can allow the material to accommodate the cycles of initial pre-stretched strain without significant degradation[88]. In the special interconnection design, the rigid electronic materials are patterned into “wavy” structures or open mesh geometries, where each single unit can provide its stretchability to the whole network when elongated. Fundamental stretchable patterns include serpentine, polygonous networks and other lattice shapes such as horseshoe, hexagon and hierarchical triangle[89]. The kirigami design can also form a network of notches and transform the two-dimensional strain to three-dimensional deformation, increasing the strain at break of the rigid nanocomposite from 4% to 370%[90]. Generally, this method makes it possible to transform every rigid material to be stretchable without losing its electrical performance. However, the fabrication process is complex, and the out-of-plane patterns make it difficult to be encapsulated, especially for the devices that require planar interfaces[91].

Material-based method starts with the synthesis, processing, and patterning of materials, in order to impart the stretchability to the whole electronic devices (Figure 2.11). Though intrinsically stretchable materials possess the solid-state structure or molecular structure that produces stretchability, they are quite rare in the field of electronic materials and substantially less developed due to the intricacy[92]. Alternatively, embedding the conductive materials into the elastomer matrix to form percolated networks is one well-established way to fabricate stretchable composites. The choice of conductive fillers determines the electrical property of stretchable composites. Conductive fillers with good conductivities, charge-transport properties and natural mechanical

deformability, such as carbon nanotubes (CNTs), silver nanowires and conducting polymers, are good candidates in this method[93]. The mechanical property of composites is largely governed by the elastomer, which acts as the buffer to dissipate the energy during mechanical stretch and protect the percolated conductive networks. Here, chemically crosslinked elastomers (*e.g.*, PDMS, Ecoflex), physically crosslinked elastomers (*e.g.*, styrene ethylene butylene styrene, SEBS) and dually crosslinked elastomers (*e.g.*, polyurethane, PU) are widely investigated[94]. Stretchable composites can be further subdivided on the basis of whether active materials are homogeneously dispersed or assembled as a bi-layered structure on the substrate[87]. A homogenously blended composite exhibits better strain endurance, while bi-layered structure is easy to be done and optimized without the concern about the miscibility between the fillers and elastomers.

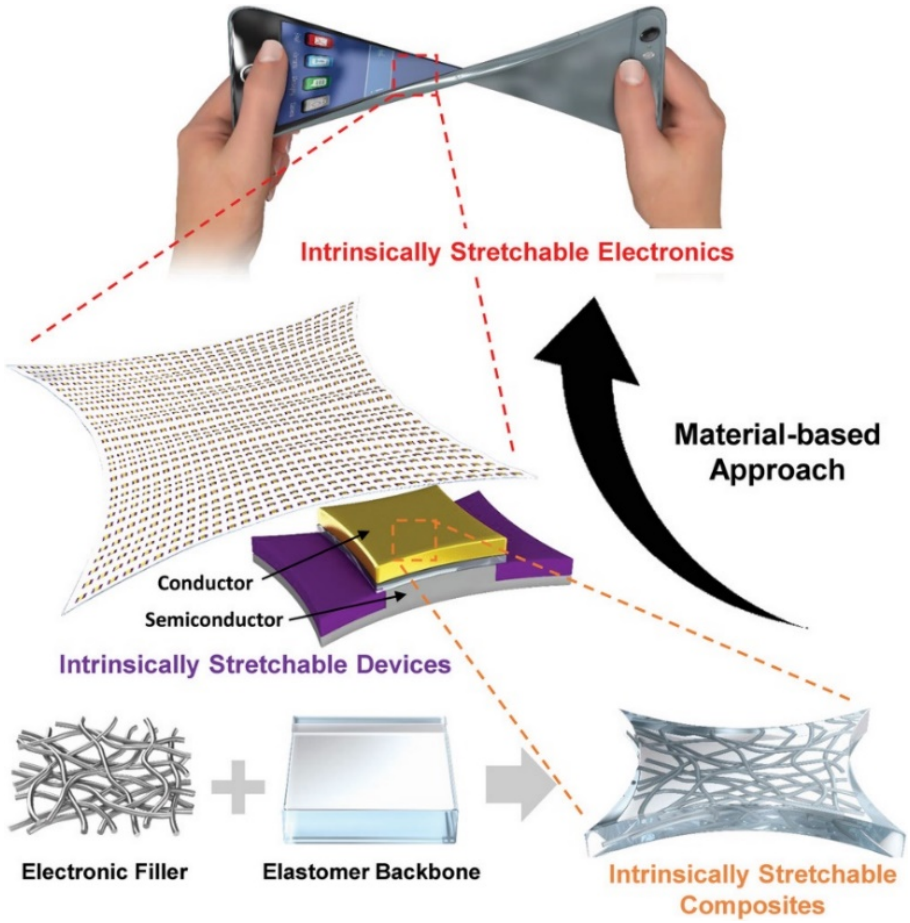

Figure 2.11 Schematic illustration depicting the material-based approach for the fabrication of stretchable electronics[87]. Reprinted with permission.

2.6 Healable materials and electronics based on PEDOT

2.6.1 Introduction to healable materials and electronics

Self-healing electronics are emerging as new technologies that push the boundaries and limitations of conventional devices that are susceptible to unexpected damage or breakage. The design and fabrication of self-healing electronics highly rely on healable electronic materials, a class of materials which possesses the ability to fully or partially reconstruct the electrical pathways and mechanical properties upon external damages. In consequence, self-healing electronics can retain electrical performance over time, upon fatigue, corrosion or damage, fundamentally prolonging the device's lifetime. To this date, a wide array of applications for self-healable electronics have newly been demonstrated. A few notable examples include electronic skin (E-skin) for health monitoring, wearable and stretchable sensors, actuators, transistors, solar cells for energy harvesting, and batteries and supercapacitors for energy storage (Figure 2.12)[95].

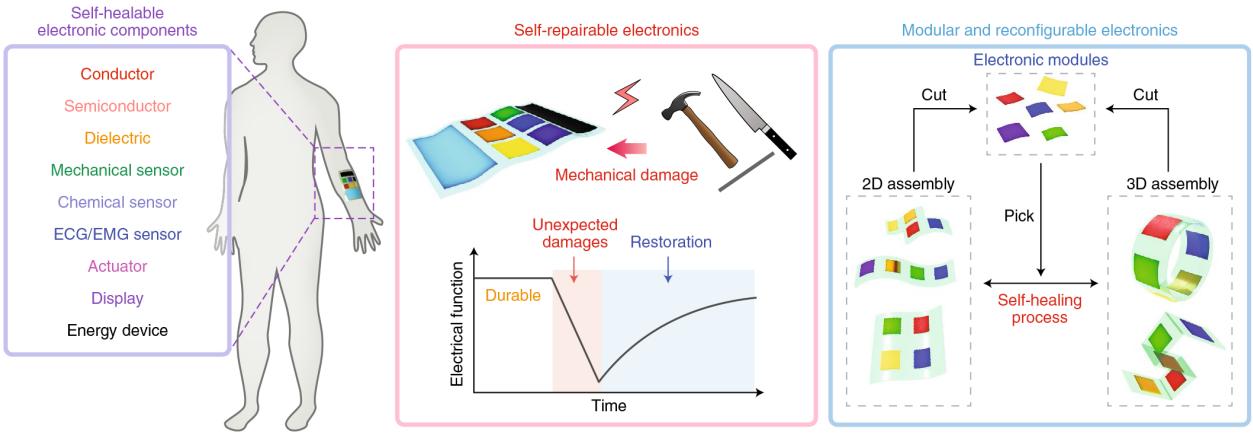

Figure 2.12 Schematic of a multifunctional self-healable soft electronic device on human skin. Self-healability of electronic systems uniquely enables the fabrication of self-repairable electronics and modular and reconfigurable electronics. Self-repairable electronics can autonomously restore their electrical and mechanical properties when they are mechanically damaged by scratching, poking, rubbing and tearing. Modular and reconfigurable electronics allow users to customize their own electronic devices with various two- or three-dimensional shapes and multiple functionalities by a simple mechanical cut and self-healing process[95]. Reprinted with permission.

For self-healing electronic materials, two parameters are generally denoted to evaluate the healing performance. The first and most important parameter, "healing efficiency η" is defined as the ratio of property change before and after healing: $\eta = (P_{healed}-P_{damaged})/(P_{pristine}-P_{damaged})$, where P is material property of interest[96]. Electronic properties including conductivity or current, and mechanical properties such as tensile stress or elongation at the break, are often involved in the calculation of healing efficiency. The other parameter is known as healing response time, which describes the recovery time of healing process. Due to the variation in the polymer chain mobility and healing mechanisms, healing response time can be varied from less than one second to few hours, or even several days[95].

2.6.2 Self-healing behavior of PEDOT

The conjugated system leads to intrinsic conductivity of conducting polymer. However, these π-conjugated polymer chain backbones are rigid and lack of motion. In addition, they mainly interact via weak Van der Waals interactions (bonding energy lower than 10 kcal mol^{-1})[97]. These characteristics of conducting polymer, such as the lack of polymer chain diffusion and the difficulty of achieving reversible dynamic bonding sites (*e.g.*, hydrogen bonds, metal-ligand bonds), are not ideal for healing[98-101]. Fortunately, tunable physical and chemical properties can be provided by the diverse choices of dopants despite the rigid backbone, and the high processability of conducting polymers further allows for easy modification to achieve self-healing[13]. The first method is to increase the viscoelasticity of the conducting polymer and promote the rapid diffusion of polymer chains, resulting in the healing behavior[95]. The second approach to achieve self-healing electronic materials is to incorporate CPs into a self-healing system, especially a hydrogel network[102]. The resultant conductive composite usually can recover both electrical performance and mechanical strength after being damaged. Yet another method is to introduce reversible bonds via grafting polymer chains or adding functional groups into the polymer network[103].

The self-healing performance of PEDOT films can be briefly classified into the water-enabled healing and the autonomic healing behavior, depending on if the external healing trigger water is needed. The first investigation of the healing behavior of pristine PEDOT:PSS was reported by our group in 2017. Thick PEDOT:PSS films were prepared by drop-casting commercial PEDOT:PSS suspension on a glass substrate, then baking it at gradually increasing temperature[104]. We

discovered that films of 1 μm thickness or more, cut by a razor blade, recover more than 90% of their initial electric currents within ~ 150 ms, after covering the damaged area with a drop of water (Figure 2.13). We hypothesize that this is related to the swelling of PSS chains in the film. After water is dropped on the damaged area, PSS chains can take up water rapidly, enlarge their volume, and propagate to the gap area[105]. PEDOT-PEDOT conducting paths are rebuilt due to the strong coulombic interaction between PEDOT and PSS. Based on water-enabled healing behavior of PEDOT:PSS, an ultra-sensitive and rapidly responsive water leak sensor has been demonstrated on both rigid and flexible substrates. In addition, current recovery can also occur within a few minutes at high relative humidity (80%-90%). The wet PEDOT:PSS film can function as an autonomically healable conductor and the current becomes almost non-interrupted despite the multiple cuts in different regions. Furthermore, via applying the wet PEDOT:PSS film as a channel material, we obtained a self-healable OECT, which can show similar identical transfer characteristics before and after blade cutting. Conductive composites or copolymers that contain PEDOT and PSS have also been reported to possess water or vapor induced healing behavior. A porous composite aerogel consisting of PEDOT:PSS and reduced graphene oxide (rGO), with a thickness of 200 μm, can heal the scratch made by a razor after the damaged region is treated with water vapor for 30 min[106]. The PEDOT:PSS/rGO aerogel electrodes retain similar cyclic voltammetry curves even after eight damaging/healing cycles, with a capacitance retention of ~ 95%. Similarly, a block copolymer, comprising PEDOT, soft segments of poly(poly(ethylene glycol) methyl ether acrylate) (PPEGMEA), and hard segments of PSS was synthesized using a reversible addition-fragmentation chain transfer polymerization[107]. Spin-coated films of this block copolymer (~ 300 nm thickness) show a conductivity of ~ 0.05 S cm^{-1} and can recover the conductivity from a ~ 50 μm cut immediately after water dropping, with an electrical healing efficiency of ~ 50%.

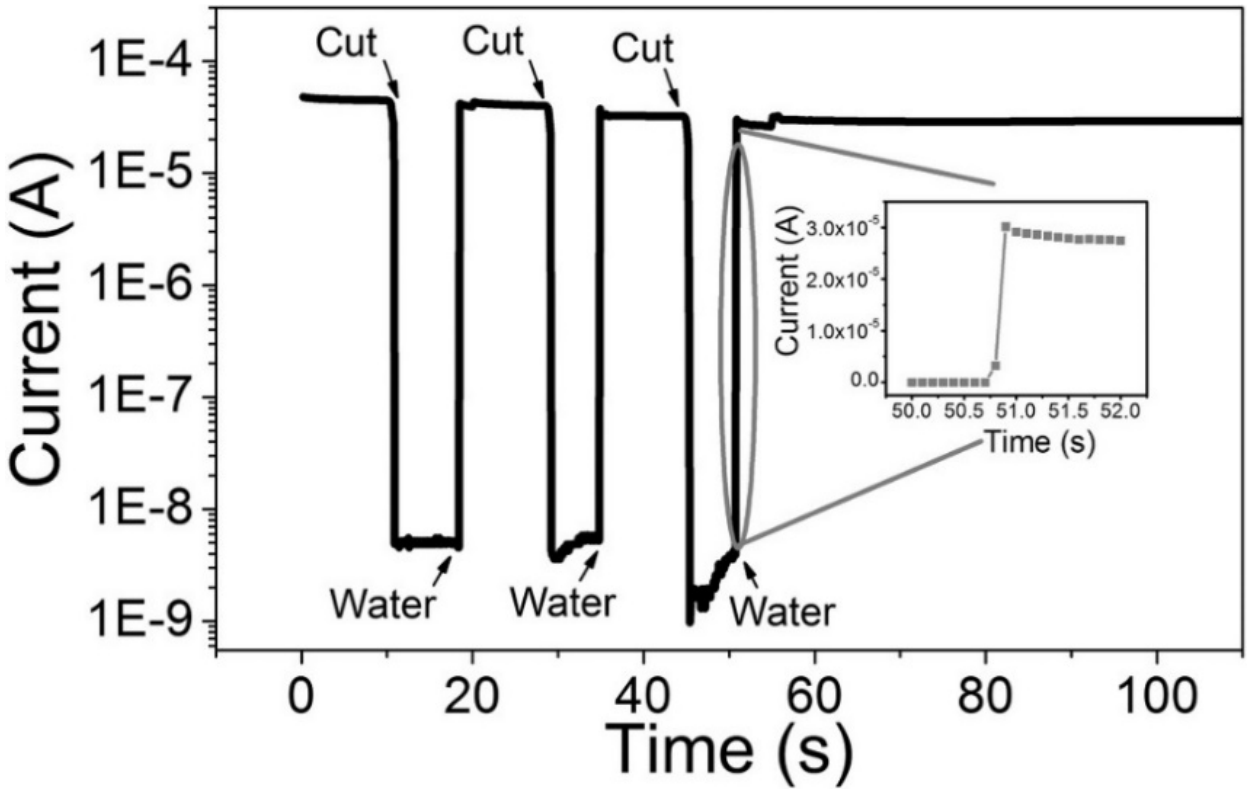

Figure 2.13 Current versus time measurements (applied voltage 0.2 V) for PEDOT:PSS film (thickness: 10 μm; width: 4 mm; length: 20 mm) showing the effect of damage (cutting with a razor blade) and healing (covering the damaged area with a drop of water). The damage/healing process was repeated three times on different regions of the film. The inset shows the magnified image of the current response time to highlight the rapidity of the healing process[104]. Reprinted with permission.

Autonomic healing of PEDOT:PSS could be achieved via wetting the films as described before. However wet films are very fragile and difficult to handle. To achieve a stable autonomic self-healable conductor, several additives, which can reduce the crystallinity of the polymer and also increases the polymer segmental mobility[108], are often blended to alter the mechanical property the PEDOT:PSS. By blending large amount of Triton X-100 with PEDOT:PSS, due to the non-volatile nature, Triton X-100 will remain inside the resultant film after baking, thus altering the nanostructure of PEDOT:PSS[109]. The formation of nanofibril physical network enhances the viscoelasticity, which enables the molecular rearrangement of polymer chains under a stress (or called creep). Thus, after being scratched, the viscoelastic polymer can flow back to the damaged

area quickly. Due to the high mobility of nanofibrils inside PEDOT:PSS film, the physical and conductive network in the damaged area will be restored (Figure 2.14). Generally, this healing process is fast (~ few seconds), repeatable, and stable. Using the viscoelastic PEDOT:PSS/Triton X-100 composite, a self-healing thermoelectric generator has been fabricated [110]. This device continues the function even after repetitive cuts, retaining >85% of its initial power output. Recently, self-healable and high-performing OECTs using PEDOT:PSS/Triton X-100 channel were reported[111]. These OECTs maintain high electrical performance after mechanical damage, retaining ~ 90% of initial transconductance and ON/OFF ratio. In terms of ion-sensing behavior, these OECTs exhibit a high ion sensitivity of ~85 mV dec^{-1} and recover ~95% of their ion sensitivity after healing.

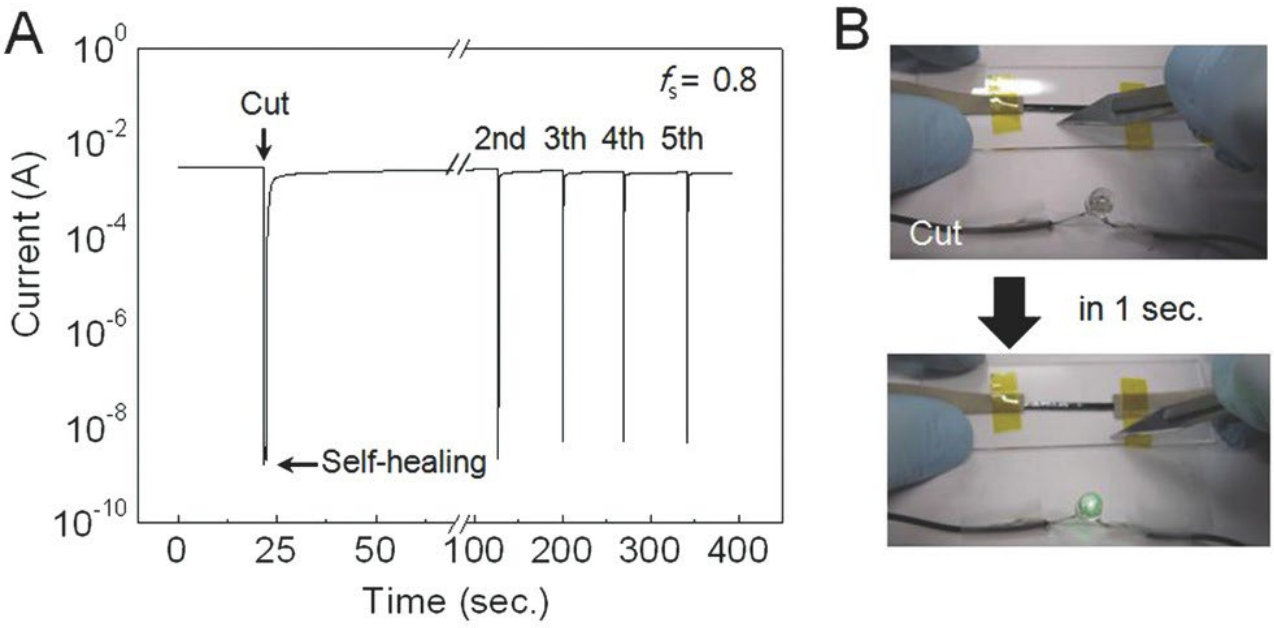

Figure 2.14 (A) Self-healing of the PEDOT:PSS. Current change of the PEDOT:PSS (fs = 0.8) during repeated cycles of cutting and healing. (B) Real images of the self-healed PEDOT:PSS[109]. Reprinted with permission.

2.6.3 Progress on self-healing composites and electronics based on PEDOT

Gelation of PEDOT:PSS aqueous suspensions with non-volatile additives (*e.g.*, agarose, lignin, alginates, guar gums or cellulose) can result in PEDOT:PSS hydrogels with low modulus, high electrical conductivity, and excellent electrochemical properties, which are desirable for

bioelectronics[112]. Most of these hydrogels are healable due to the existence of dynamic bonds (*e.g.*, hydrogen bonds) inside the scaffold[113-115]. A nanocomposite hydrogel which possesses porous structure and high swelling ability (~800% weight increase in water) has been fabricated via blending PEDOT:PSS with agarose [116]. The polymer agarose, made up of repeating units of agarobiose, functions as the backbone of this hydrogel, which can display reversible sol-gel transition upon heating and cooling. After the hydrogel is physically damaged, near-infrared light can locally melt the damaged site through photothermal conversion. The gap is then healed after cooling to room temperature due to gelation. In addition, acids are often used to protonate and remove PSS from PEDOT:PSS, leading to the conformational change and enhanced π-π stacking of PEDOT chains [117]. Zhang et al. obtained a PEDOT:PSS hydrogel formed at room temperature (RT-PEDOT:PSS hydrogel) via blending PEDOT:PSS with dodecylbenzenesulfonic acid (DBSA) due to its ability to separate PEDOT and PSS as well as to form gelated PEDOT micelles[118]. This hydrogel shows a moderate conductivity of ~ 0.1 S cm^{-1}, and a Young's modulus of ~ 1 kPa. Recovery of both electrical and mechanical properties is achieved by connecting two separated hydrogels parts due to the reformation of dynamic hydrogen bonds (Figure 2.15 a). This hydrogel also exhibits good injectability. The fibers formed by injecting it from a syringe can function as the channel material in OECT, exhibiting a typical transistor behavior in the depletion mode with a maximum transconductance value of ~ 1.4 mS (Figure 2.15 b-c).

However, the gelated PEDOT:PSS hydrogel is mechanically weak [119]. The limited mechanical strength of gelated hydrogels is attributed to high swelling, poor network organization, and inhomogeneous structure[120]. It still remains a great challenge to construct tough self-healing materials, balancing the conflicts between the adequate dynamic reversible interactions for healing and the strong interactions needed for robustness[121]. Self-healing functionality relies on mobility of polymer molecular chains, which is usually based on the relatively weak polymeric systems of dynamic covalent bonds and non-covalent bonds. In contrast, crosslinking sites are often embedded in the polymer network to increase the mechanical strength of hydrogels, which, however, hinders the diffusion rate of polymer molecular chains, and thus decreases the efficacy of self-healing[122]. The simplest method to generate both self-healable and mechanical tough hydrogel is the incorporation of PEDOT into tough healable host hydrogel network. Xu et al. synthesized a super-stretchable, tough and self-healable PEDOT:PSS hydrogel by polymerization of the N-

isopropylacrylamide (NIPAM) monomer inside the commercial aqueous suspension of PEDOT:PSS, and then the crosslinking by the functionalized boron nitrogen sheets (f-BNNS)[121]. The multiple dynamic hydrogen bonds between sulfonate groups of PSS and N-H group of f-BNNS, as well as between PSS and poly(N-isopropylacrylamide) (PNIPAM) chains not only provide the healing ability and adhesive ability, but also provide a large number of dynamic crosslinking sites to enhance the mechanical strength of the hydrogel. The f-BNNS/PEDOT:PSS/PNIPAM gel can endure an elongation of ~2600% at break, a tensile strength of 80 kPa, and a uniaxial compression up to 90% strain.

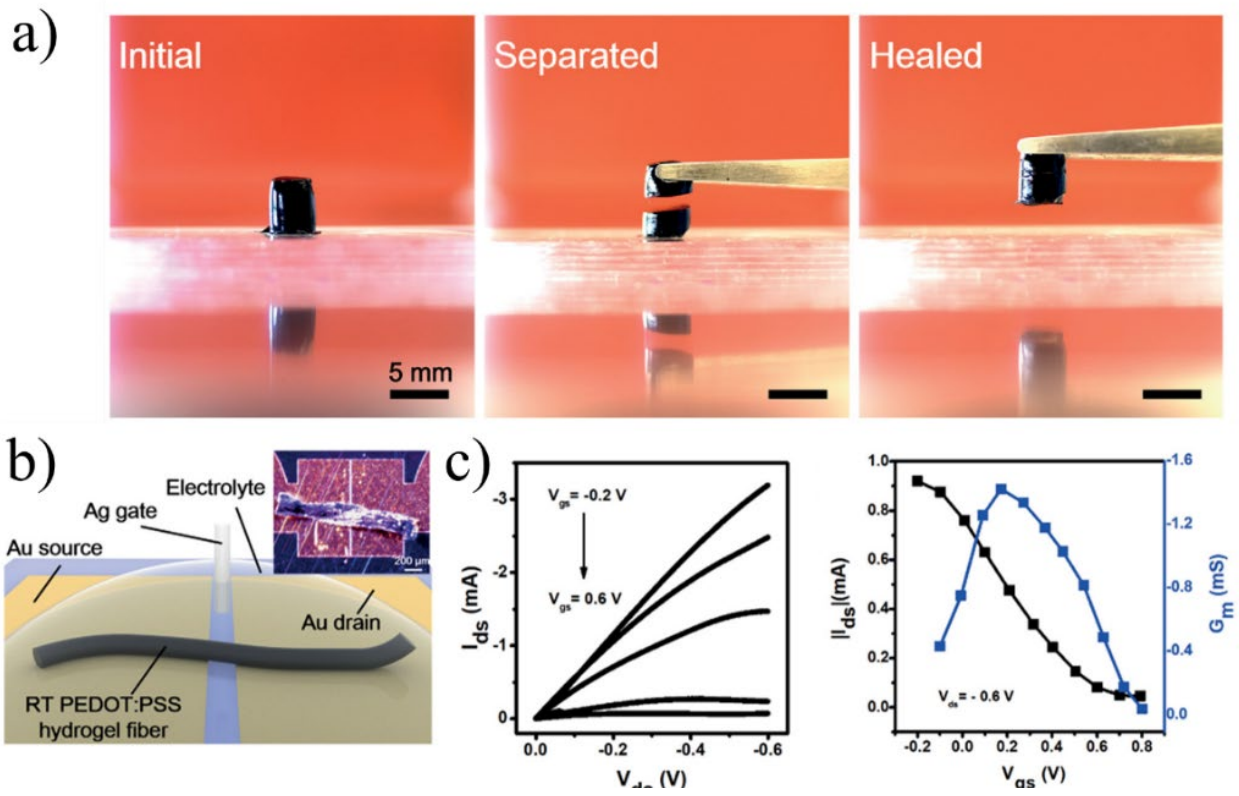

Figure 2.15 (a) Mechanical healing of the RT-PEDOT:PSS hydrogel by placing two separated RT-PEDOT:PSS hydrogels (mildly dehydrated) together for 5 min. (b) Schematic of the fabricated OECTs with injected PEDOT:PSS hydrogel fiber. The hydrogel fiber was freeze-dried after printing on the Au electrodes which have a gap of 10 μm; the inset shows the real optical image of the freeze-dried fiber on the source-drain electrodes. (c) Output and transfer curves of the OECTs with PEDOT:PSS hydrogel fibers as the channel[118]. Reprinted with permission.

However, mechanically tough host hydrogels usually have low conductivity due to the difficulty of forming percolation networks between PEDOT-rich domains[123]. More importantly, compared to soft hydrogel systems, the healing time in tough hydrogels is generally longer due to the impediment of the polymer chain diffusion in a more crosslinked network[124-126]. Thus, chemical modification or grafting of special functional groups can be used to reinforce the mechanical strength and healing property of the soft gel systems by promoting reversible internal interactions between the additives or grafted groups with the host gel. 4-carbonxybenzaldehyde (CBA), which can react with hydroxyl groups and form hydrogen bonds with the sulfonate groups of PSS, was added to tune the property of PEDOT:PSS/PVA hydrogel[127]. This conductive hydrogel provides self-healing, stretchability (up to 300% for elongation at break), conductivity (~ 600 S cm^{-1}), and strong adhesion. The reinforced hydrogel can also show fast electrical and mechanical self-healing ability at room temperature with high healing efficiency, mainly due to the robust electrostatic interactions and dynamically reversible hydrogen bonds between PEDOT:PSS and PVA chains. This stretchable and self-healing hydrogel was utilized as the binder for silicon anodes in lithium-ion batteries to minimize capacity loss due to the huge change of silicon volume during lithiation and de-lithiation cycles. The silicon/hydrogel composite electrodes can maintain superior cycling stability with a capacity retention of ~ 74% and remain at a high reversible capacity of ~ 1700 mA h g^{-1} after 200 cycles at current density of 2000 mA g^{-1} at 55 ºC. Post-treatment of soft PEDOT hydrogels is another method to enhance the toughness without sacrificing healing ability[128, 129]. For instance, soaking of hydrogels in organic solvents usually prompts a change in structure and composition of the gel network, enabling some active sites/groups that are originally occupied by water to form specific interactions with solvent molecules to strengthen the hydrogels[130]. Gao et al. improved the toughness and stretchability of PEDOT/PVA hydrogel greatly via soaking in sulfosuccinic acid (SA)[131]. The hydrogel shows a significant increase in toughness (from ~ 0.7 to ~ 7.8 MJ m^{-3}), tensile strength (from ~ 0.4 to ~ 2.5 MPa), and elongation at break (from ~ 270% to ~ 600%) after soaking. The enhancement of these mechanical properties is due to the formation of multiple noncovalent bonds induced by soaking, such as hydrogen bonding between the carboxylic groups of SA and hydroxyl groups of PVA, and electrostatic/dipole interaction between sulfonate groups of SA and positively charged PEDOT. These multiple noncovalent bonds allow the gels to be healed after being cut and pressed together

in hot water at 80 °C for 5 min, with a healing efficiency of 83% in fracture stress and 99% in conductivity (Figure 2.16).

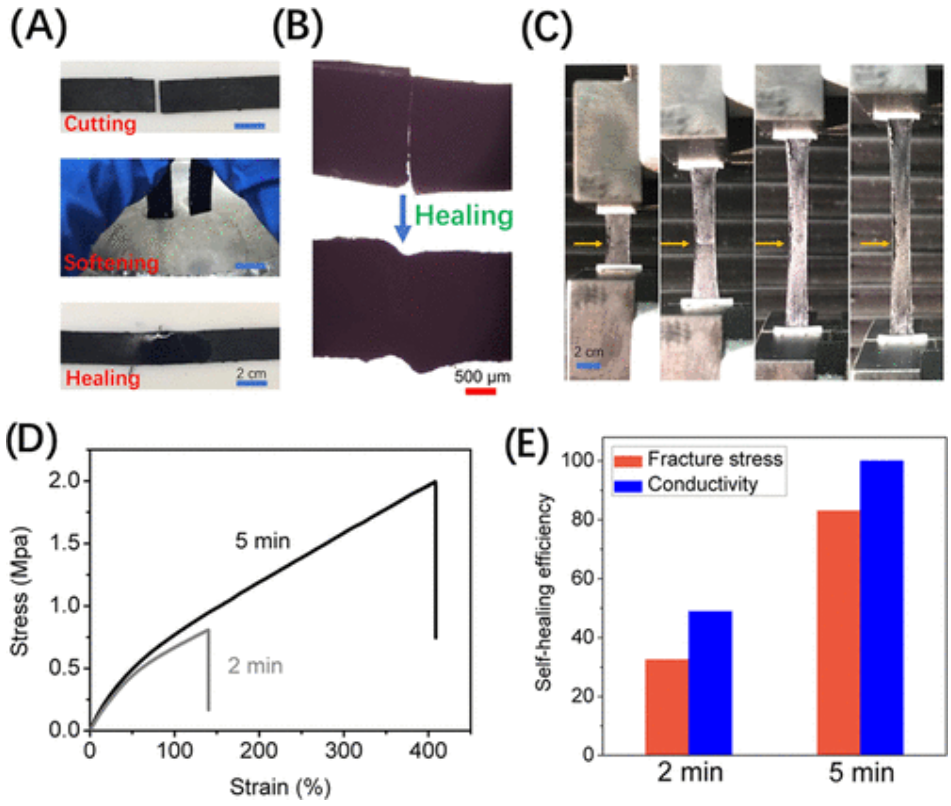

Figure 2.16 Study on the self-healing properties. (A) The self-healing process with the aid of hot water; (B) optical microscopic images of the self-healing process to show the disappearance of the boundary between the two gels; (C) mechanical stretching of the healed GEL-30 (yellow arrow indicates the wield interface); (D) stress-strain curves; (E) self-healing efficiency of healed GEL-30 upon dipping the cutting surface in hot water for 2 and 5 min. The self-healing efficiency is calculated by the formula $\eta = A_h/A_o \times 100$, where A_h and A_o are the fracture stress or conductivity of the healed and the original samples, respectively[131]. Reprinted with permission.

CHAPTER 3 MATERIALS AND APPROACHES

3.1 Preparation of conducting polymers

3.1.1 Processing of PEDOT:PSS

The PEDOT:PSS aqueous suspension (Clevios PH1000) from Heraeus Electronic Materials GmbH (Leverkusen, Germany) is used as the starting material for this project. Different additives are blended with as-received suspension to improve the property of PEDOT:PSS: glycerol, PEG and sulfuric acid soaking can improve the film conductivity; Capstone FS-300 flurosurfactant, PEG, and Triton X-100 are used as surfactant or plasticizer to enhance the stretchability or/and wettability of PEDOT:PSS film; GOPS is able to crosslink PEDOT:PSS and increase the film adhesion especially on glass substrate. The mixtures of PEDOT:PSS and additives are spin-coated or drop-cast depending on the requirement of the film thickness, and then baked on the hotplate.

3.1.2 Synthesis of other conducting polymers

Other conducting polymers are synthesized via oxidative polymerization or electropolymerization method. The synthesis details of PEDOT:ClO_4, PEDOT: para-toluene sulfonate (PEDOT:Tos), and PEDOT:trifluoromethanesulfonate (PEDOT:OTf) are described in section 6.6.

3.2 Conductivity measurement

The conductivity is calculated from the film thickness and sheet resistance. The resistivity of the PEDOT:PSS thin films is measured by using a source/measure unit and a point probe setup with four equally spaced tungsten metal tips (Figure 3.1). The thickness of the films is measured by a profilometer. For thin solid films with large surface area and thickness below 100 μm, the following equation can be used to extract the resistivity value:

$$\frac{\rho}{d} = 4.5324 * \frac{V}{I} \qquad \text{(Equation 3)}$$

Where ρ is the resistivity of the film, d is the film thickness, I is the supplied current and V is the measured voltage. The conductivity σ then can be extracted using the following relation:

$$\sigma = 1/\rho \qquad \text{(Equation 4)}$$

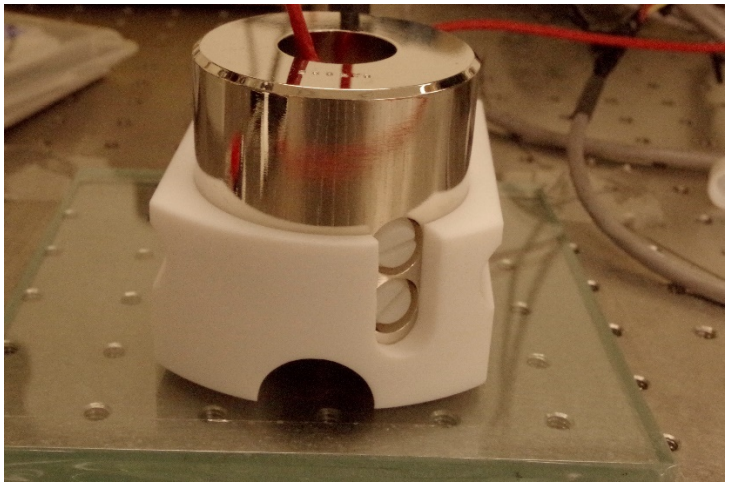

Figure 3.1 The image of four-point probe setup with a Jandel 4-pin four-point probe head

3.3 Stretchability characterization

3.3.1 Preparation of elastomer PDMS

The elastomer PDMS, adopted as the substrate for stretchable OECTs, is fabricated by blending elastomer and curing agent (weight ratio 10:1), spin coating on the glass substrate and baking on a hot plate at 100 ºC for 1 h. Ahead of the PEDOT:PSS deposition, the obtained PDMS substrates are cleaned by exposure to UV/O_3 for 20 min.

3.3.2 Electromechanical test

The stretchability of PEDOT:PSS films on PDMS is clarified by transient current measurements at different applied strain percentages, defined as the length change upon stretching (ΔL) divided by the initial length of the PDMS substrate (L) and multiplied by 100%. To allow comparison between different samples, the currents are normalized with respect to the initial value (unstretched samples). To benchmark the current variation, we use the ratio [$\Delta I/I_{0x}$], where ΔI indicates the current change between the released and stretched states and I_{0x} is the current in the released state after the first application of x% preset strain. Thus, a low value of [$\Delta I/I_{0x}$] indicates a small current variation between the stretched and the released states (strain-insensitive), as required for stretchable OECTs. On the other hand, a high [$\Delta I/I_{0x}$], i.e., a large current variation between the stretched and the released state (strain-sensitive), can be exploited in devices such as pressure sensors. Another

parameter that can be acquired here is the elongation at break, which defines the maximum strain that PEDOT:PSS can endure without forming throughout cracks and losing all conducting paths.

3.4 Self-healing test

Self-healing test is employed to evaluate the ability of conducting polymers to recover the electrical property upon the external damages with/without the trigger of water. The drop-cast PEDOT:PSS films are shaped into a size of ≈(6.0 × 1.5) cm with different thicknesses. The current is measured with electrical probe station via placing tungsten probes on conducting polymer films. The cuts are performed manually using different razor, surgical, ceramic blades, a quartz microscope slide and a micro-scratcher. The details of self-healing tests are described in section 5.6 and 6.6. The healing efficiency and response time can be extracted from the current versus time profile.

3.5 Microfabrication and characterization of stretchable OECTs

3.5.1 Microfabrication

The microfabrication is an important step to obtain OECTs. Generally, Au electrodes are first patterned on the PDMS elastomer. In order to avoid the contamination of commercial photoresists on PDMS, a parylene transfer method is used here. 1 μm parylene layer is evaporated on the pre-cleaned flexible PET substrate. Commercial photolithography with AZ-900 photoresist and reactive ion etching are applied to create patterns on parylene. Then patterned parylene is transferred on the prepared PDMS substrate due to the stronger adhesion between PDMS and parylene layer. In the following E-beam evaporation, Au source/drain contacts (40 nm thickness with 4 nm Cr/Ti as adhesion layer) are deposited on PDMS using parylene layer as a mask. Patterned Au electrodes are obtained via peeling off the Parylene film. Then PEDOT:PSS films are spin-coated on PDMS substrate, and negative fluorinated photoresist (OSCoR 4000, Orthogonal, Inc.) is used to pattern the PEDOT:PSS channel in the OECTs.

3.5.2 Characterization of stretchable OECTs

We use either 0.1 M NaCl aqueous solution confined in an elastic well made of stretchable tape (3 M VHB 4905) or a cut and paste polyampholyte hydrogel containing NaCl as the electrolyte for OECTs. As the gate electrode for devices using aqueous electrolytes, we use activated carbon

(PICACHEM BP9) on carbon fiber paper (Spectracorp 2050, 10 mils) and a planar PEDOT:PSS stripe is adopted for those using a hydrogel electrolyte. Liquid metal EGaIn are applied at the source-drain electrodes to facilitate the probing. The strain is applied in situ with a LabVIEW software controlled tensile tester, and the transistor electrical characteristics are measured with an Agilent B2900A source measure unit controlled with Quick IV Measurement software at the same time (Figure 3.2).

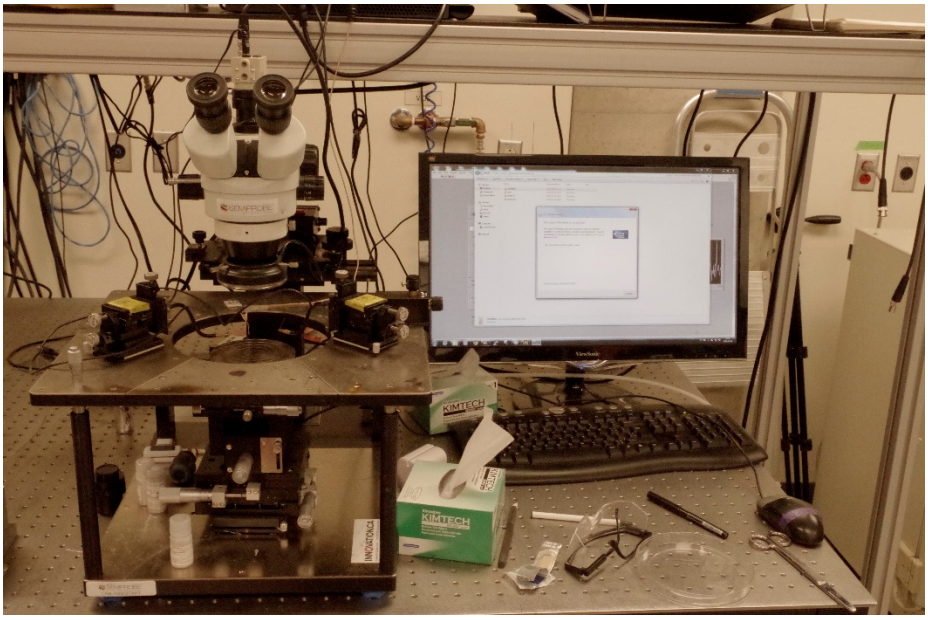

Figure 3.2 The probing system used to measure the transistor characteristics

3.6 Composition characterization

3.6.1 X-ray photoelectron spectroscopy

For conducting polymer PEDOT:PSS films, X-ray photoelectron spectroscopy (XPS) is used to identify the elements (i.e., S, C, O) and their chemical states based on the photoelectric effect. At high or ultra-high vacuum conditions, a beam of X-rays irradiates the testing material, resulting in the electron population spectra. The material properties are obtained via analyzing the number of ejected electrons and kinetic energy. In our experiments, the XPS test of conducting polymer films is performed using a VG ESCALAB 3MKII system with Mg-Ka X-ray source in an ultra-high vacuum (Figure 3.3). The limitation of this powerful technique is that it can only detect elemental composition of material on the surface.

3.6.2 Fourier-transform infrared spectroscopy

Fourier-transform infrared spectroscopy, or FTIR spectroscopy is a technique using infrared light to scan test samples and observe chemical properties. Mid-infrared region (400 to 4000 cm^{-1}) spectra will usually be obtained by measuring the absorbed radiation due to the conversion into vibrational and/or rotational energy by sample molecules. The peaks in the spectra corresponding to frequencies of light are absorbed because they match the natural vibration of the molecules or chemical structures, making this technique quite useful for the chemical identification for both organic and inorganic compounds. Intensity of the FTIR spectra is measured as the percent of transmittance of the radiation with respect to reference. In the FTIR test of conducting polymer films, the spectra of PEDOT:PSS films is performed using a PerkinElmer FTIR Spectrum Two spectrometer.

CHAPTER 4 TUNING THE ELECTROMECHANICAL PROPERTIES OF PEDOT:PSS FILMS FOR STRETCHABLE TRANSISTORS

4.1 Introduction

Stretchable electronic devices, such as light-emitting diodes, solar cells, transistors, and capacitors, are attracting enormous interest for applications in wearable electronics and bioelectronics. Organic conducting polymers have emerged among the most promising materials for stretchable electronics because of their high electrical conductivity, ease of processing on a wide range of substrates, stability in water and biocompatibility. In particular, organic electrochemical transistors (OECTs) based on the conducting polymer poly(3,4-ethylenedioxythiophene) doped with polystyrene sulfonate (PEDOT:PSS) are regarded as revolutionary tools to replace conventional bulkier systems for many in vitro and in vivo bioelectronic applications, including high resolution mapping of cell activity and flexible self-powered biosensors for electrophysiological signal monitoring.

To fabricate fully stretchable OECTs, the mechanical properties of PEDOT:PSS, which is inherently brittle, need to be modified by blending it with elastomers or surfactants. Mixtures of PEDOT:PSS with elastomers yield conductive gels. However, for OECTs, thin films are preferred to gels since a low thickness favours a reversible and fast doping/dedoping process, leading to a high ON/OFF ratio and a fast response time. Stretchable PEDOT:PSS thin films can be obtained by blending PEDOT:PSS and surfactants, which act as soft domains to absorb the external strain and reduce the electrostatic interactions between PEDOT and PSS. Blends of PEDOT:PSS and surfactants are easily processable on stretchable substrates and can yield stretchable ultrathin films with a high conductivity. However, the effect of the processing parameters such as film thickness and baking temperature on the stretchability of PEDOT:PSS films is yet to be investigated. To push forward their applications in developing strain-insensitive OECTs, further optimization of the electromechanical properties of PEDOT:PSS thin films is needed to minimize the current change with the strain. An additional challenge for fabricating fully stretchable OECTs is that they require stretchable metal contacts. Stretchable conductors such as liquid metals, although increasingly used in stretchable electronics, are not suitable as electrodes for OECTs due to their limited electrochemical stability and biocompatibility.

Our group has demonstrated fully stretchable PEDOT:PSS OECTs, by combining parylene transfer-patterning and orthogonal lithography on an elastomer substrate maintained under strain during the fabrication process. However, the resulting devices have a periodic wavy surface (buckled) profile, which is a challenge to achieve seamless contact with skin or living tissues. In addition, buckled devices present out-of-plane patterns, which are difficult to encapsulate and disadvantageous for devices that require planar interfaces. Therefore, further development of nonbuckled stretchable OECTs is highly desirable to decrease the fabrication complexity and to increase the device yield. Towards this goal, Marchiori et al. recently described laser-patterned serpentine metallic interconnects for stretchable OECTs, which leads to PEDOT:PSS OECTs showing unchanged performance up to 11% strain.

In this work, we report strain-insensitive stretchable OECTs on polydimethylsiloxane (PDMS) substrates, fabricated with conventional technologies, without prestretching the substrates. Our OECTs maintain similar performance up to 30% strain (the maximum strain the human skin can tolerate). The stretchability is maximized by fine tuning the composition, reducing the thicknesses and decreasing the baking temperature of PEDOT:PSS films. By interposing a thin parylene layer between the PDMS substrate and the PEDOT:PSS film, we are able to improve the ON/OFF ratio and the transconductance of the devices to levels comparable to OECTs on rigid substrates.

4.2 Results and discussions

Figure 4.1(a-i) shows the fabrication process of stretchable OECTs on PDMS, which is similar to that previously reported for buckled devices (fabricated on an elastomer substrate maintained under strain during the fabrication process). Briefly, Au contacts are patterned on a PDMS substrate, attached on a supporting glass slide, via transfer-patterning of a parylene shadow mask prepatterned on polyethylene terephthalate. Subsequently, a PEDOT:PSS film is spin-coated on the substrate and patterned using orthogonal lithography. The PDMS substrate with the PEDOT:PSS film is then peeled-off from the supporting glass substrate. Figure 4.1j shows the cross-section of one of the geometries we adopted for stretchable OECTs. For that system the electrolyte (0.1 M NaCl aqueous solution) was confined in an elastic well made of stretchable tape (3M VHB 4905), and activated carbon on carbon paper used as the gate electrode. Our stretchable OECTs show no macroscopic

physical damage at different strains (Figure 4.1k). Additionally, they can be arbitrarily stretched, twisted, and placed in conformable contact with the skin (Figure 4.1l).

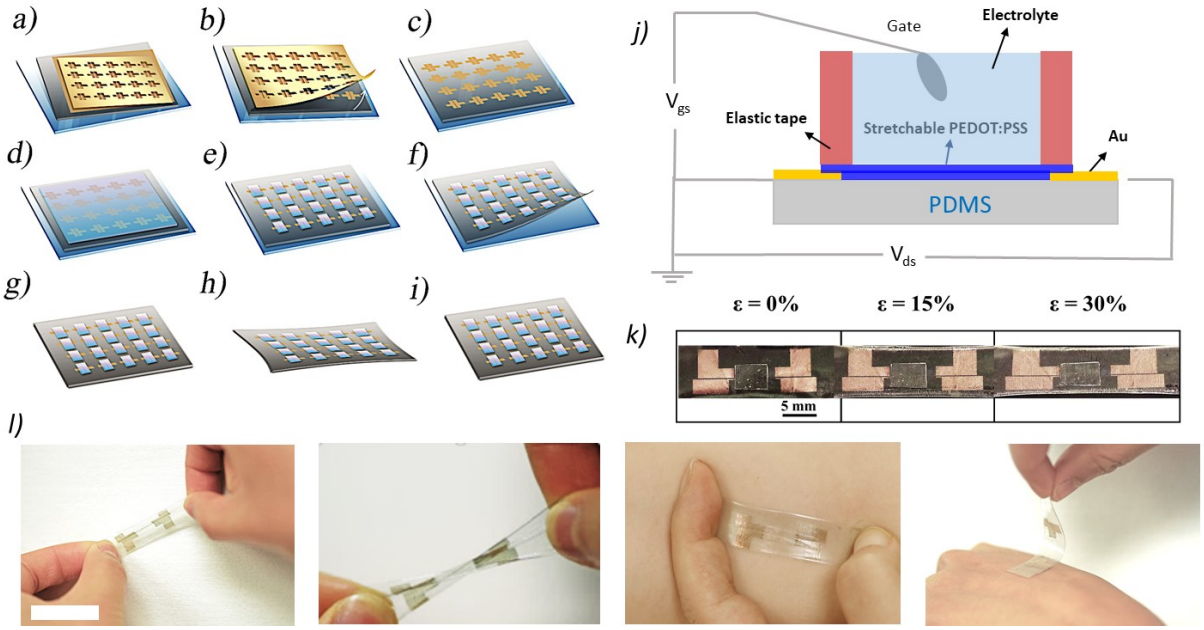

Figure 4.1 a-i) Process flow for the fabrication of stretchable OECTs on nonbuckled PDMS: a) transfer of a prepatterned parylene mask from a polyethylene terephthalate (PET) sheet to a PDMS substrate temporarily attached on a glass slide, b,c) Ti (4 nm)/Au (25 nm) deposition and parylene removal, d) spin coating of 50 nm PEDOT:PSS (with 5 v/v% glycerol and 1 v/v% Capstone FS-30), e) patterning of PEDOT:PSS via orthogonal photoresist lithography and oxygen reactive ion etching, f,g) peeling off PDMS from glass slide, h) applying a 30% strain to the devices, i) releasing the strain to obtain a stretchable OECT, j) schematic image of one of the device structures used for stretchable OECTs, k) optical images of stretchable OECTs at 0%, 15%, and 30% strain (ε), where an elastic tape is attached on top, and l) optical images of our nonbuckled stretchable OECT (with channel length of 8 mm and channel width of 2 mm) being stretched, twisted, and placed in contact with skin. The scale bar is 1 cm.

On-skin bioelectronic applications require devices whose electrical properties are not significantly affected within an applied strain of 30% (Figure SA1, Supporting Information), the maximum strain tolerated by human skin. To achieve this goal the following processing conditions were identified: the addition of 1 v/v% fluorosurfactant (Capstone FS-30) to the PEDOT:PSS suspension,

a thickness of 25 nm for the Au electrodes and of 50 nm for the PEDOT:PSS channel. The devices were baked for 1 h at 100 °C and a 30% strain was applied prior to measurements. The importance of this last step will be discussed in detail later.

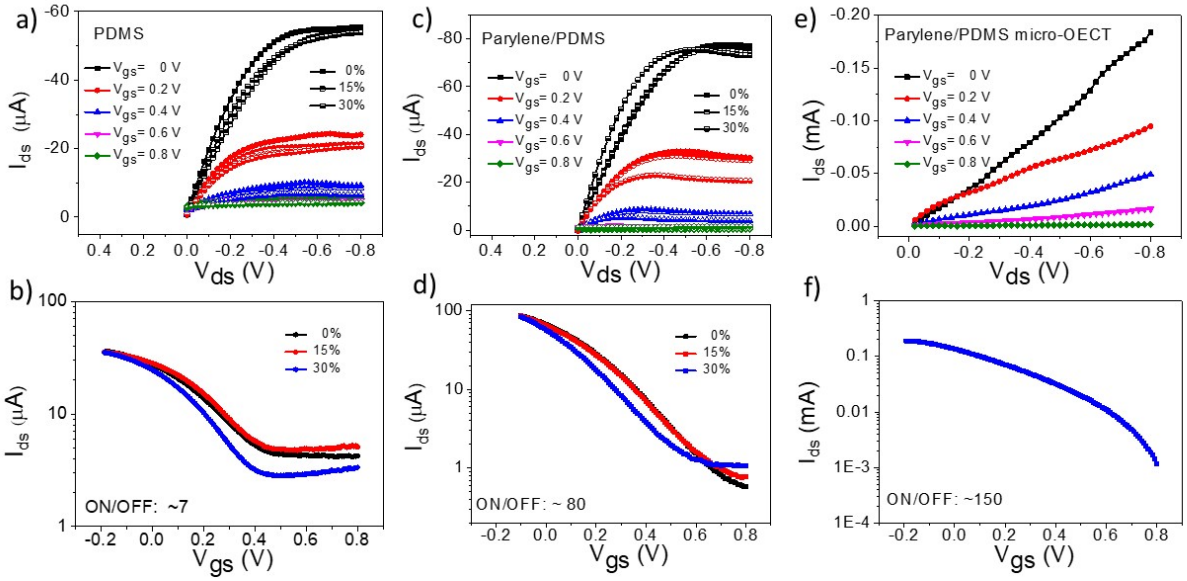

Figure 4.2 Output and transfer curves of our nonbuckled stretchable OECTs using an activated carbon gate electrode and 0.1 M NaCl solution as the electrolyte. PEDOT:PSS is mixed with 5 v/v% glycerol and 1 v/v% Capstone FS-30. The films were baked at 100 °C for 1 h. The thickness of the PEDOT:PSS channel and the Au electrode are 50 and 25 nm respectively. a) output curves of OECTs on PDMS at 0%, 15%, 30% strain, b) transfer curves of OECTs on PDMS at 0%, 15%, 30% strain, c) output curves of OECTs on parylene/PDMS at 0%, 15%, 30% strain, d) transfer curves of OECTs on parylene/PDMS at 0%, 15%, 30% strain. The channel length and width are 8 and 2 mm (W/L of 1/4) respectively. e) Output curves of micro-OECTs on parylene/PDMS and f) transfer curve of micro-OECTs on parylene/PDMS. The channel length and width are 10 and 4000 µm (W/L of 400).

The output and transfer characteristics of the OECTs, measured at 0%, 15%, and 30% strain, show the typical behavior of PEDOT:PSS OECTs working in depletion mode (Figure 4.2a,b). Large device dimensions (channel length, L, of 8 mm and a width, W, of 2 mm) were here chosen to facilitate electrical measurements during stretching. It is worth noting that applied strains up to 30% did not significantly affect the device electrical performance in terms of output and transfer curves.

From the transfer curves, we observed a strain-insensitive transconductance (i.e., source-drain current, I_{ds}, sensitivity to gate voltage, V_{gs}, variations, Figure SA2, Supporting Information). We extracted a maximum transconductance of about 70 μS (V_{gs} = 0.1 V, Figure SA2, Supporting Information), and an ON/OFF ratio of ≈7 (0% strain, Ids (V_{gs} = 0)/I_{ds} (V_{gs} = 0.8)), both lower compared to that of devices with the same geometry on glass or PET substrates, which typically show a transconductance around 1 mS and an ON/OFF ratio above 100. We obtained similar results in our previous report on stretchable OECTs for buckled devices, which we attributed to leakage of impurities or PDMS monomers at the PEDOT:PSS/PDMS interface.

The transconductance and the ON/OFF ratio of the devices were improved by interposing a thin parylene interlayer (1 μm thick) between PDMS and PEDOT:PSS. Parylene on PDMS can be deposited directly or transferred via a plastic carrier. We observed that parylene films directly deposited on PDMS can be stretched up to 30% with microcracks, while films transferred via a plastic carrier show the appearance of much larger cracks at lower strains (<10%) (Figure SA3 a,b, Supporting Information). The parylene interlayer likely acts as a smoother interface to prevent the diffusion of impurities such as uncured monomers or oligomers, from PDMS to the PEDOT:PSS channel, facilitating dedoping of PEDOT:PSS at the interface and thus leading to high performance of OECTs despite the presence of microcracks under strain (Figure SA3c,d, Supporting Information). The output and transfer curves in presence of the parylene interlayer show minor changes within 30% strain (Figure 4.2c,d). Additionally, the ON/OFF ratio is increased to about ≈80, (i.e., about a factor of 10 higher than that of the devices on PDMS) and the maximum transconductance, at V_{gs} = −0.1 V, to 200 μS (i.e., about three times higher than the devices on PDMS, Figure SA2, Supporting Information). To further validate our method, we fabricated micro-OECTs (with L = 10 μm and W = 4000 μm) on parylene/PDMS. Such devices show a higher ON/OFF ratio of 150 (Figure 4.2e,f) and a transconductance of 0.4 mS (Figure SA2, Supporting Information), i.e., similar to that of OECTs with same geometry on rigid substrates.

The high stretchability of the OECTs discussed above is achieved by fine tuning the electromechanical properties of PEDOT:PSS films, depending on the film thickness, baking temperature, and the strain applied prior to measurements. We clarify the role of these factors on film stretchability by transient current measurements of PEDOT:PSS films on PDMS at different applied strain percentages, defined as the length change upon stretching (ΔL) divided by the initial

length of the PDMS substrate (L) and multiplied by 100%. To allow comparison between different samples, the currents were normalized with respect to the initial value (unstretched samples). To benchmark the current variation, we used the ratio [$\Delta I/I_{0x}$], where ΔI indicates the current change between the released and stretched states and I0x is the current in the released state after the first application of x% preset strain. Thus, a low value of [$\Delta I/I_{0x}$] indicates a small current variation between the stretched and the released states (strain-insensitive), as required for stretchable OECTs. On the other hand, a high [$\Delta I/I_{0x}$], i.e., a large current variation between the stretched and the released state (strain-sensitive), can be exploited in devices such as pressure sensors.

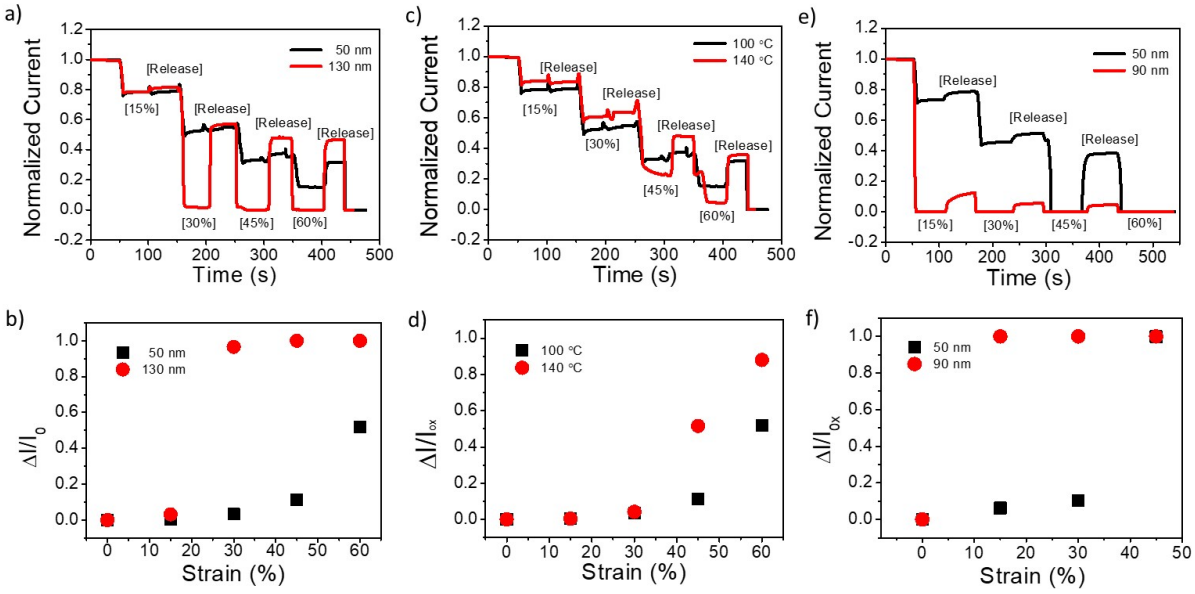

Figure 4.3 Normalized current versus time at different applied strain percentages a,c,e) and $\Delta I/I_{0x}$ versus strain percentage b,d,f) of PEDOT:PSS films on PDMS. A constant voltage of 1 V is applied for all measurements. ΔI indicates the current changes upon stretching and I_{0x} the current in the released state after the application of x% strain. The strain is applied for 50 s in the sequence of 0%, 15%, 0%, 30%, 0%, 45%, 0%, and 60%, 0%, a,b) 130 nm thick and 50 nm thick films baked at 100 °C for 1 h, c,d) 50 nm thick films baked at 100 and 140 °C for 1 h, e,f) 50 nm thick and 90 nm thick films on parylene/PDMS baked at 100 °C for 1 h.

The effect of thickness on the film stretchability is shown in Figure 4.3a. For the 130 nm thick PEDOT:PSS film, after the first application of a 15% strain (preset strain), the current decreases by ≈20%. Notably, in the subsequent 0%-15%-0% strain cycles, the current remains unchanged,

thus yielding a small [$\Delta I/I_{0x}$] of about 0.03 (Figure 4.3b; Figure SA1, Supporting Information). That is, the conductivity of the film becomes insensitive to external strains (within x%) after the first application of x% preset strain (here x = 15%). However, for 130 nm thick films, this conclusion only applies to strains up to 15%. For example, upon increasing the preset strain to 30%, the current decreases sharply to the noise level. When the film is released, instead of being stable, it recovers to ≈50% of the initial value, thus yielding a [$\Delta I/I_{0x}$] of about 1 (Figure 4.3b). Significantly, decreasing the PEDOT:PSS thickness dramatically minimizes $\Delta I/I_{0x}$ at a wide strain range. For example, for the 50 nm thick film, a lower [$\Delta I/I_{0x}$] is obtained (Figure 4.3b) even after increasing the preset strain up to 45% strain, demonstrating reducing thickness of PEDOT:PSS films is effective in realizing strain-insensitive OECTs.

The effect of baking temperature on film stretchability, at a fixed thickness of 50 nm, is shown in Figure 4.3c,d. We observed that decreasing the baking temperature from 140 to 100 °C not only increases the stretchability, but also decreases the [$\Delta I/I_{0x}$], especially under higher strains. For example, PEDOT:PSS films baked at 140 ºC show high [$\Delta I/I_{0x}$] of ≈0.9 between 0% and 60% strain, while films baked at 100 °C show much lower values of 0.5. Overall, these results point out that, beyond reducing film thickness, decreasing the baking temperature of PEDOT:PSS films on PDMS is also an effective way to minimize its sensitivity to external strains.

The above conclusions also apply when a parylene interlayer is interposed between PDMS and PEDOT:PSS (Figure 4.3e). For example, at 30% strain, 50 nm thick PEDOT:PSS films maintain a small [$\Delta I/I_{0x}$] of about 0.1 while 90 nm thick films show a [$\Delta I/I_{0x}$] of ≈1 at 15% strain (Figure 4.3f). However, PEDOT:PSS on parylene/PDMS shows inferior stretchability with respect to that on PDMS, which is likely due to the cracking of the parylene interlayer under strain (Figure SA3, Supporting Information), which is transferred to the PEDOT:PSS film (Figure SA4, Supporting Information). Nevertheless, PEDOT:PSS film with 50 nm thickness on parylene/PDMS show stable current and excellent cyclic stability (60 cycles) between 0% and 30% strains (Figure SA5, Supporting Information), making them suitable candidates for stretchable OECTs.

4.3 Conclusion

We have demonstrated that stretchable OECTs can be developed with standard fabrication methods such as evaporation of Au electrodes and spin coating of PEDOT:PSS on PDMS, without

prestretching the substrate. The highly stretchable and strain-insensitive PEDOT:PSS OECTs are obtained by reducing the thickness and decreasing the baking temperature of the PEDOT:PSS films. High performance strain-insensitive OECTs are obtained by modifying the PDMS surface with 1 μm thick parylene interlayer. Our work paves the way for developing stretchable and high-performance organic electronics for wearable biomedical applications.

4.4 Experimental Section

The PEDOT:PSS aqueous suspension (Clevios PH1000) was purchased from Heraeus Electronic Materials GmbH (Leverkusen, Germany). Glycerol (99.5%+ purity) was purchased from Caledon Laboratories Ltd. (Georgetown, ON). Capstone FS-30 was purchased from Sigma-Aldrich. The liquid metal gallium-indium eutectic (EGaIn) 495425 was purchased from Sigma-Aldrich. The fluorinated photoresist kit, including a negative tone chemically amplified photoresist (OSCoR 4000), a developer (Orthogonal developer 700) and a stripper (Stripper 103), was supplied by Orthogonal Inc. (Rochester, NY, USA). Glass slides were purchased from Corning. PDMS (Sylgard 184 silicone elastomer kit) was purchased from Dow Corning. Polyethylene terephthalate (PET) sheets were purchased from Policrom Inc (Bensalem, PA, USA). Parylene (Parylene C) was purchased from SCS coating.

As stretchable substrates, 300 μm thick PDMS sheets were used, pretreated with UV/O_3 for 20 min prior to PEDOT:PSS deposition. PEDOT:PSS films were processed by spin coating a mixture of Clevios PH1000, 5 v/v% glycerol and 1% Capstone FS-30 at different speeds and different baking temperatures. The PEDOT:PSS thickness was measured with a profilometer (Dektak 150) using a 12.5 μm stylus tip with a 10 mg stylus force and the following values were obtained: about 130 nm (1000 rpm), 70 nm (2000 rpm), and 50 nm (4000 rpm) for PDMS, and 90 nm (1500 rpm) and 50 nm (3000 rpm) for parylene/PDMS. For these measurements, the films were transferred from PDMS onto glass using a water-soluble tape (3M 5414). The Ti and Au film were deposited by thermal electron-beam (E-beam) evaporation at 1 Å s^{-1}.

OECTs were fabricated following a procedure reported previously for buckled PDMS substrates: Au electrodes were patterned via parylene transfer-patterning and PEDOT:PSS films were patterned with orthogonal photolithography. A 0.1 M NaCl aqueous solution, confined in an elastic

well made of stretchable tape (3M VHB 4905), was used as the electrolyte. Liquid metal EGaIn was applied at the source-drain electrodes to facilitate probing.

The transient current measurements were carried out on PEDOT:PSS films with a width of 10 mm and a length of 5 mm included between gallium-indium eutectic electrodes.

Electrical measurements were carried out using an electrical probe station and an Agilent B2900A source measure unit controlled with Quick IV Measurement software in ambient conditions. The strain was applied in situ with a LabVIEW software-controlled tensile tester.

CHAPTER 5 ARTICLE 1: HIGHLY STRETCHABLE PEDOT:PSS ORGANIC ELECTROCHEMICAL TRANSISTORS ACHIEVED VIA POLYETHYLENE GLYCOL ADDITION

This article has been published in the journal "Flexible and Printed Electronics" in 2019. This article reports the enhanced stretchability and conductivity of PEDOT:PSS films via the addition of plasticizer polyethylene glycol (PEG). The OECTs fabricated on elastomer substrates based on PEDOT:PSS/PEG films show superior performance in terms of both mechanical compliance and transistor characteristics. The supporting information for this article is reprinted in Appendix A of this thesis.

5.1 Authors

Yang Li[1], Shiming Zhang[2], Xinda Li[1], Venkata Ramana Nitin Unnava[1], Fabio Cicoira[1],*

[1] Department of Chemical Engineering, Polytechnique Montréal, Montreal, Quebec H3C 3A7, Canada

[2] Center for Minimally Invasive Therapeutics, California NanoSystems Institute, University of California, Los Angeles, California 90095, United States

E-mail: fabio.cicoira@polymtl.ca

5.2 Abstract

Organic electrochemical transistors (OECTs) are widely used in biosensing and bioelectronics, due to their ability to convert ionic signals into electronic signals and their high transconductance. Stretchable OECTs are particularly suited for on-skin and on-organ bioelectronics, since they are able to record or transmit signals under mechanical strain. Most stretchable OECTs are based on the conducting polymer poly(3, 4-ethylenedioxythiophene) doped with polystyrene sulfonate (PEDOT:PSS), which needs to be appropriately processed to yield stretchable films. Here we report stretchable OECTs that are obtained by modifying the mechanical properties of PEDOT:PSS films via the addition of low-molecular weight polyethylene glycol (PEG), which acts as a plasticizer. The presence of PEG in the films prevents the formation of cracks under strain while maintaining a high electrical conductivity, thus resulting in improved electromechanical properties. In particular,

the addition of PEG leads to a higher channel thickness and increased ion mobility in the films, thus resulting in stretchable OECTs with high transconductance and fast response time. This work shows that high stretchability, high transconductance and fast response time can be simultaneously obtained in OECTs, paving the way for their applications in conformable devices at the human-machine interface.

5.3 Introduction

Increasing demand for intelligent, wearable and integrated electronics has driven the unprecedented interest in stretchable electronic devices, such as sensors[132], transistors[133], solar cells[134], batteries and capacitors[135, 136]. Organic electrochemical transistors (OECTs) are already widely used in bioelectronics, where a combined electronic-ionic transport is required[44, 57, 137, 138]. Stretchable OECTs are highly demanded for on-skin or on-organ applications because of their ability to show strain-insensitive electric performance.

Currently, most OECTs use thin films of the conducting polymer poly(3, 4-ethylenedioxythiophene) doped with polystyrene sulfonate (PEDOT:PSS) as channel material, because of its high conductivity, biocompatibility, ease of process and stability in water at a physiological pH[28, 139]. As PEDOT:PSS films are, in general, inherently brittle, several approaches have been proposed to improve their mechanical properties, in order to incorporate them in stretchable devices. Stretchable PEDOT:PSS-based OECTs have been demonstrated by our group via a combination of parylene transfer, orthogonal patterning and buckling of PEDOT:PSS films on a pre-stretched elastomer. These devices showed almost unchanged transistor performance up to 30% strain[140]. An alternative approach used a laser patterning method to fabricate stretchable metallic interconnections on elastomers to yield OECTs with a maximum stretchability of 38% while maintaining a transconductance as high as 0.35 mS[141]. Matsuhisa *et al* fabricated stretchable Au conductors controlling the strain-induced microcrack propagation in Au thin films by varying the evaporation rate. These Au conductors were utilized to fabricate stretchable OECTs, based on PEDOT:PSS, with a high transconductance both at 0% strain (0.54 mS) and 140% strain (0.14 mS)[142]. Recently, our group also demonstrated stretchable OECTs on PDMS, able to maintain stable performance up to 30% strain, by decreasing the thickness of PEDOT:PSS films to ~50 nm and using a baking temperature to 100 °C[143].

Decreasing film thickness is a well-known method to obtain better stretchability of thin films of conducting polymers or metals on elastomers, due to a transition from a 3D packing to a 2D percolating structure and a reduced mechanical mismatch with the substrate[142-146]. However, as the transconductance of OECTs is proportional to the channel thickness[57], a compromise must be reached to balance the electrical and mechanical properties of the films.

Another widely-used approach to yield stretchable films is to modify the mechanical properties conducting polymers by blending them with plasticizers, such as Capstone FS-30 (Zonyl)[40, 47], Triton X-100[33] and ionic liquids[31], whose effect is to decrease the Young's modulus and to increase the elongation at the break. Low-molecular-weight polyethylene glycol (e.g., PEG 400) has been proven to act as a plasticizer in polymer processing, e.g., for poly(lactic acid), by decreasing the Young's modulus and increasing the elongation at the break[147-150]. In addition, when blended with electrolytes, PEG has shown to lead to an improvement of ion transport[151]. Moreover, low-molecular-weight PEG shows high aqueous solubility, antifouling properties[152], and a moderate ability to enhance conductivity of PEDOT:PSS[29]. This ensemble of properties makes it an interesting candidate as a plasticizer for applications in bioelectronic devices based on PEDOT:PSS.

In this work, we achieved highly stretchable OECTs by using PEG 400 as a plasticizer for PEDOT:PSS films. The PEG 400 remains inside the films after baking, and improves the electromechanical properties by limiting the formation of cracks under the strain. This allowed us to fabricate high transconductance OECTs keeping similar performance between 0% and 45% strain. As PEG also favours ion transport in the films, our OECTs showed a faster response time compared to reference devices.

5.4 Experimental

5.4.1. Materials

The PEDOT:PSS aqueous suspension (Clevios PH1000) was purchased from Heraeus Electronic Materials GmbH (Leverkusen, Germany). PEG 400, the liquid metal Gallium-Indium eutectic (EGaIn) 495425 and Capstone FS-30 (Zonyl) were purchased from Sigma-Aldrich. Glycerol (99.5 + % purity) was purchased from Caledon Laboratories Ltd (Georgetown, ON). The Orthogonal

photoresist kit was supplied by Orthogonal Inc. Glass slides were purchased from Corning. Polydimethylsiloxane (PDMS, Sylgard 184 silicone elastomer kit) was purchased from Dow Corning.

5.4.2. PEDOT:PSS film preparation

The PEDOT:PSS/PEG films were deposited onto PDMS substrates by spin coating a mixture of Clevios PH1000, 4 v/v% PEG 400, 1 v/v% fluorosurfactant Capstone FS-30 and 5 v/v% glycerol. Control samples without PEG 400 were also prepared. The two kinds of samples described above are named as PEDOT:PSS/PEG and PEDOT:PSS films. The PDMS substrates (160 μm thick) were cleaned by exposure to UV/O_3 for 20 min. Among all PEGs with different molecular weights, PEG 400 was selected as a plasticizer for PEDOT:PSS due to its liquid form at room temperature and ease of process. After deposition, the films were baked at 100 °C for 1 h. The film thickness was measured with a profilometer (Dektak 150) using a 12.5 μm stylus tip with a 10 mg force, after transferring them from PDMS onto glass using a water-soluble tape (3 M 5414). We observed thicknesses of ~300 nm (1000 rpm), and ~100 nm (4000 rpm) for PEDOT:PSS/PEG films and ~50 nm (4000 rpm) for PEDOT:PSS films. The difference in thickness for films deposited at the same spin coating speed is due to the presence of PEG in the films after baking.

5.4.3. Characterization of films

The optical microscopy images were obtained with a Carl Zeiss AX10 microscope. The electromechanical properties of the films were evaluated by measuring the change of the current flowing in the films as a function of time during stretching and release cycles at different applied tensile strain percentage[153]. The latter is defined as [(L' − L)/L] × 100%, where L and L' denote the relaxed and stretched lengths of the PDMS substrate, respectively. Two EGaIn *contacts* were applied at the extremities of the films to facilitate the electrical contact. The current was normalized with respect to the value measured for unstretched films. As a figure of merit to assess the electromechanical properties of the films, we used the *ratio* $\Delta I/I_{0x}$, where ΔI indicates the current variation between the stretched and released state, and I_{0x} is the current in the released state after the first application of x% strain (preset strain). A low value of $\Delta I/I_{0x}$ indicates that the electrical properties are not significantly affected by mechanical deformation, which is a desirable property for stretchable OECTs[143]. Scanning electron microscopy (SEM) measurements were performed

with a JEOL JSM-7600TFE Field Emission Scanning Electron Microscope (FE-SEM). X-ray photoelectron spectroscopy (XPS) was performed using a VG ESCALAB 3MKII system with Mg-Ka X-ray source in an ultra-high vacuum.

5.4.4. Polyampholyte hydrogel electrolyte synthesis

The polyampholyte hydrogel synthesis has been described previously[154]. Briefly, 1 M Sodium 4-vinylbenzenesulfonate (NaSS) and 1 M [3-(methacryloylamino)propyl] trimethylammonium chloride (MPTC) with 4,4-Azobis(4-cyanovaleric acid) (thermal initiator, 0.25 mol%, respect to the amount of NaSS and MPTC) were dissolved in deionized water to form the precursor solution. The precursor solution was heated at 70 °C in the convection oven for 6 h to yield the as-prepared hydrogel. Then, the as-prepared hydrogel was purified in deionized water to remove unreacted monomers. The purified hydrogel was further dialyzed in the electrolyte solution (0.1 M NaCl solution) to let ions diffuse inside the hydrogel.

5.4.5. OECT fabrication and characterization

OECTs were fabricated following our previously reported procedure: Au contact pads (thickness ~20 nm with a ~2 nm Ti adhesion layer) were patterned via parylene transfer and the PEDOT:PSS channels with orthogonal photolithography[140, 143]. As the electrolyte, we used either a 0.1 M NaCl aqueous solution confined in an elastic well made of stretchable tape (3 M VHB 4905) or a cut and paste polyampholyte hydrogel containing NaCl. As the gate electrode, we used activated carbon on carbon paper for devices using aqueous electrolytes[153] and a planar PEDOT:PSS stripe for those using a hydrogel electrolyte. Liquid metal EGaIn was applied at the source-drain electrodes to facilitate the probing. The transistor electrical characteristics were measured with an Agilent B2900A source measure unit controlled with Quick IV Measurement software, and the strain was applied *in situ* with a LabVIEW software controlled tensile tester.

5.5 Results and discussions

The molecular structures of the chemicals used in this work as well as the preparation steps of films and devices are shown in scheme 5.1. The films obtained from mixtures containing Clevios PH 1000 and 4 v/v% PEG 400 show a conductivity of ~200 S cm^{-1}, which increases up to ~450 S cm^{-1} upon addition of 5 v/v% glycerol and 1 v/v% Capstone.

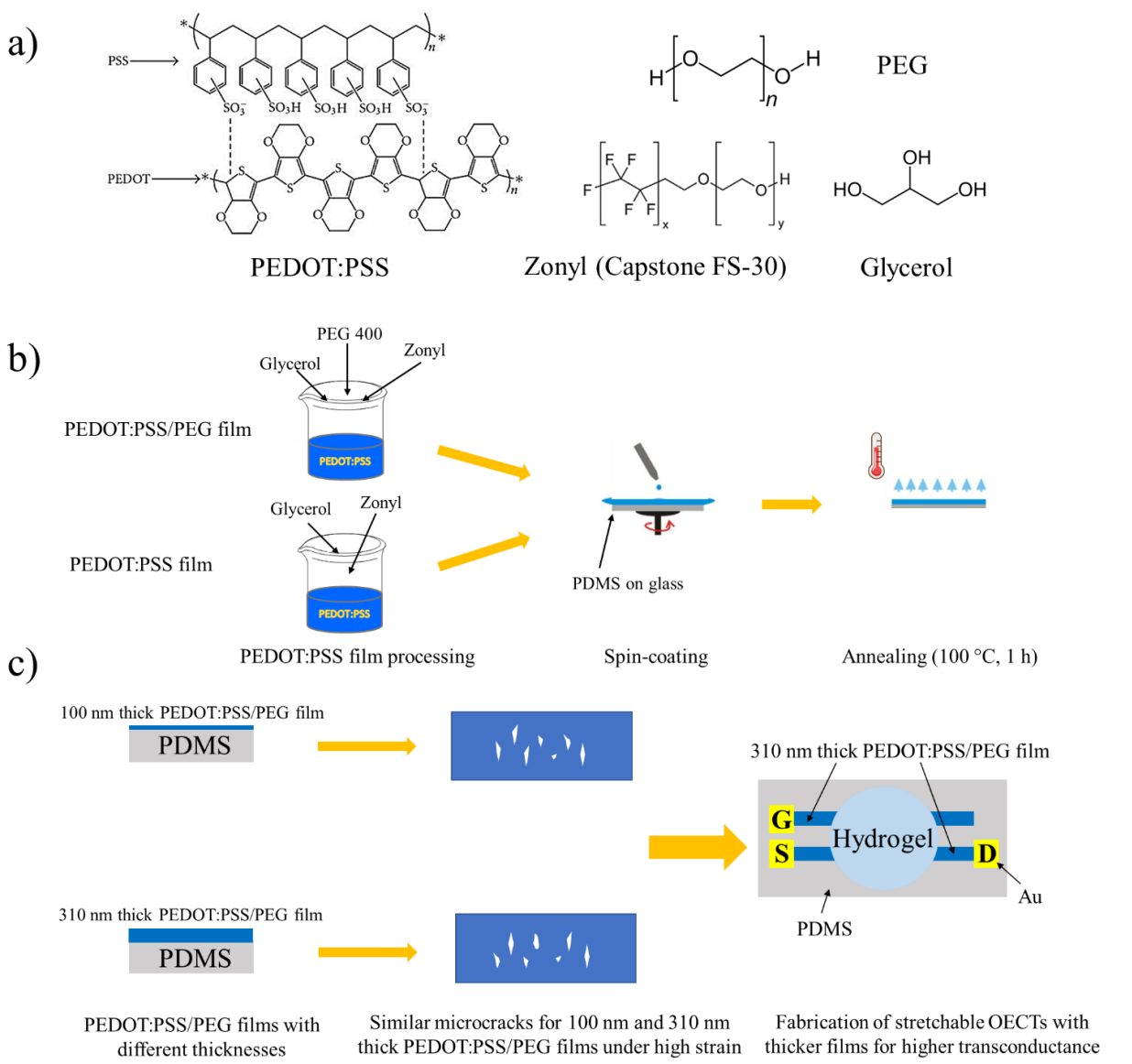

Scheme 5.1 a) Molecular structures of PEDOT:PSS, glycerol, fluorosurfactant (Zonyl) and PEG, b) schematic overview of the sample preparation steps for PEDOT:PSS films and PEDOT:PSS/PEG films and c) schematic overview of the fabrication of stretchable OECTs with thick PEDOT:PSS/PEG films

The optical microscopy images of PEDOT:PSS (~50 nm thick) and PEDOT:PSS/PEG (~100 and ~300 nm thick) films under 15%, 30%, 45% and 60% strains are shown in Figure 5.1. No significant crack formation is observed at 15% and 30% strain for all films. When the strain reaches 45%, a high density of cracks is observed on ~50 nm thick PEDOT:PSS films (Figure 5.1c). As

shown by preliminary SEM investigation, the cracks propagate through the entire film thickness (Figure SB1). The length and density of cracks increase at the application of 60% strain, in accordance with our previous study[143]. The addition of PEG significantly affects the formation of cracks: both ~100 and ~300 nm thick PEDOT:PSS/PEG films show short and sparse cracks up to 45% and 60% strain. Interestingly, increasing the film thickness does not impact the density and the length of the cracks, unlike to what we previously observed for PEDOT:PSS films without PEG[143].

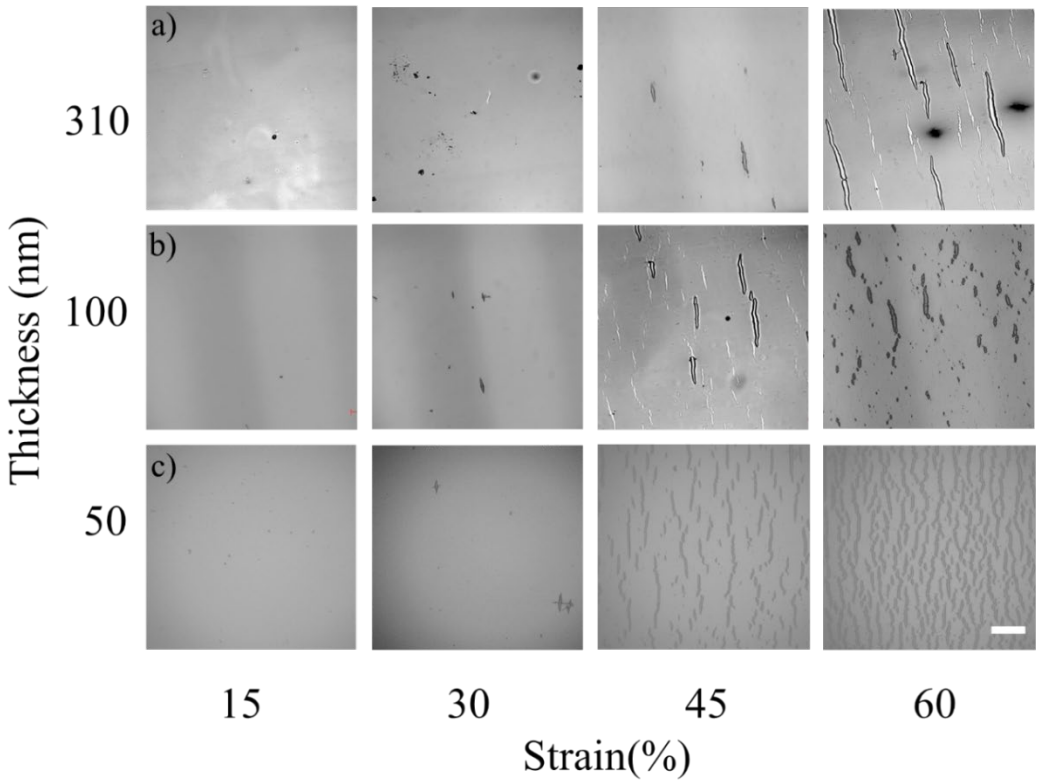

Figure 5.1 Optical microscopy images under strain of ~300 nm thick PEDOT:PSS/PEG film (a), ~100 nm thick PEDOT:PSS/PEG film (b) and ~50 nm thick PEDOT:PSS film on PDMS substrate. All films were baked at 100 °C for 1 h. The scale bar is 200 μm.

The shape and density of cracks have an important effect on the current flowing in the films under strain (Figure 5.2a) and on the $\Delta I/I_{0x}$ (Figure 5.2b). In absence of cracks, or at low crack density, there is a small difference in current between the stretched and released state, which results in a small $\Delta I/I_0x$. Long and high density cracks partially interrupt the electrical conducting path during

stretching, resulting in a drop of the current. When the strain is released, the cracks reconnect in part and the current is partially recovered, thus resulting in a large $\Delta I/I_{0x}$. The ~50 nm thick PEDOT:PSS films maintain a small $\Delta I/I_{0x}$ (less than 0.05) under 15% and 30% strain. At strain of 45% or larger, there is a clear increase of $\Delta I/I_{0x}$ (Figure 5.2b), which reaches almost 1 at 75% applied strain. The addition of PEG clearly improves the electromechanical properties of the films, by leading to a smaller $\Delta I/I_{0x}$, which remains below 0.1 up to 60% strain. At strains of 75% or higher the $\Delta I/I_{0x}$ increases up to a value of about 0.8 at 120% strain.

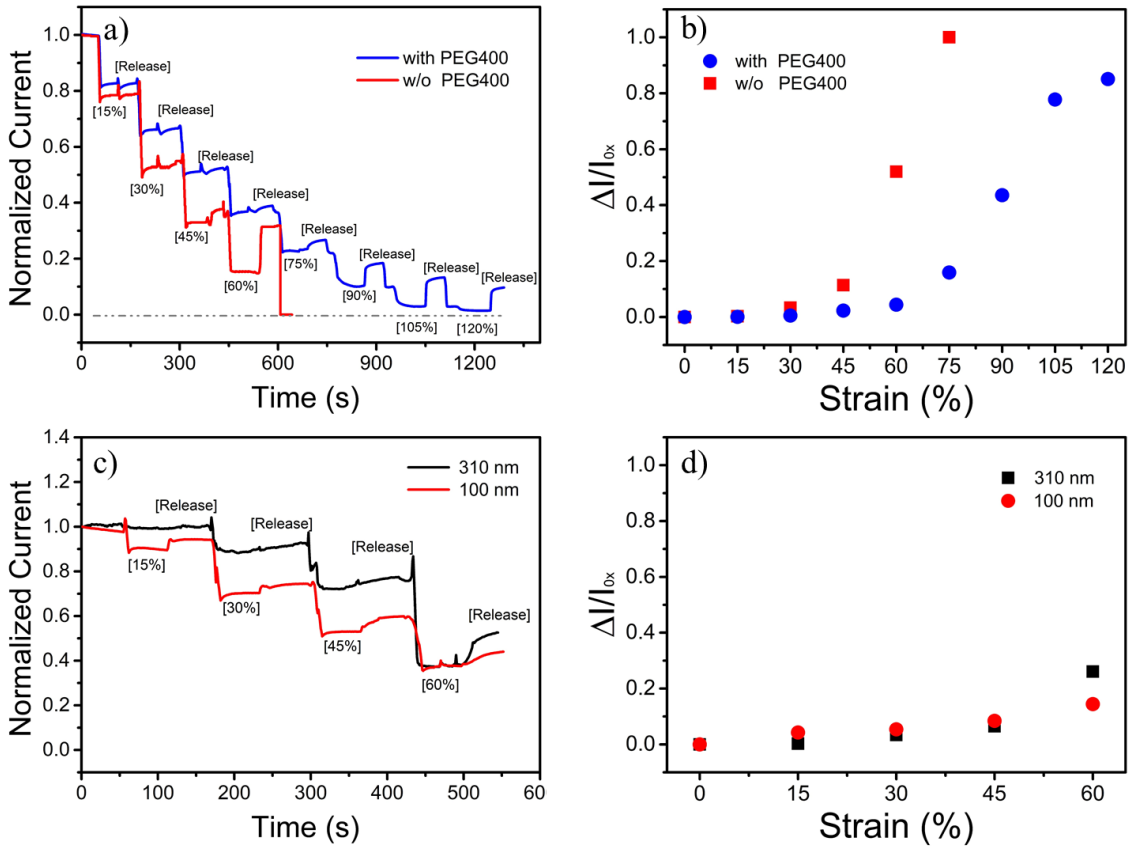

Figure 5.2 Normalized current versus time at different applied strain percentages (a) and $\Delta I/I_{0x}$ versus strain percentage (b) for PEDOT:PSS/PEG and PEDOT:PSS films on PDMS. The thickness is ~50 nm for PEDOT:PSS film and ~100 nm for PEDOT:PSS/PEG films. Same plots for PEDOT:PSS/PEG films with ~100 and ~300 nm thickness (c) and (d). A constant voltage of 0.2 V is applied. The applied strain is increased in 15% per step and the strain rate is 2.5%/s. For each cycle, the samples are kept in the stretched and released state for 50 s. All films were baked at

100 °C for 1 h. In each experiment, at least 4 films were measured to ensure the results are repeatable.

We have recently shown that the electromechanical properties of PEDOT:PSS films strongly depend on the thickness[143]. Thin films (~50 nm) show better electromechanical characteristics than thick ones (~130 nm), due to a lower density of strain-induced cracks[143]. However, for OECT fabrication, a high film thickness would be preferred to maximize the device transconductance[57]. The effect of PEDOT:PSS/PEG film thickness on the electromechanical properties is shown in Figure 5.2c. At 15% strain, the normalized current of ~300 nm thick film remains unchanged while that of ~100 nm film drops by 15%. At 30% and 45% strain, the ~300 nm film still maintains 90%, and 75% of the initial current. Notably, the $\Delta I/I_{0x}$ value of ~300 nm film is similar but slightly lower than that of ~100 nm film when the applied strain is 45% or less (Figure 5.2d). When the strain reaches 60%, the current of both ~300 and ~100 nm films drops to 40% of the initial value, and ~100 nm film exhibits a smaller $\Delta I/I_{0x}$ value. Since increasing the thickness of PEDOT:PSS/PEG films from ~100 to ~300 nm does not significantly affect the $\Delta I/I_{0x}$ value, we fabricated OECTs using ~300 nm PEDOT:PSS/PEG films to achieve larger transconductance without sacrificing the electromechanical properties.

The enhanced stretchability of PEDOT:PSS/PEG films is attributed to the plasticizing effect of PEG, which remains in the film after baking. We investigated the composition of PEDOT:PSS and PEDOT:PSS/PEG films by XPS. Clear shifts in C(1s) and O(1s) core level spectra indicates the presence of PEG 400 (Figure SB2)[29]. It is also worthwhile to mention that the presence of PEG probably increases the background noise in the XPS spectra (Figure SB2a). In the S(2p) spectra, the peak between 166 and 172 eV is attributed to sulfur atoms of PSS, whereas the double peak between 162 and 166 eV is attributed to sulfur atoms of PEDOT[28, 155]. This is consistent with the higher thickness of PEDOT:PSS/PEG films with respect to PEDOT:PSS ones processed in the same conditions. According to a previous study[49], the PEG remaining in the films functions as a soft matrix, with PEDOT:PSS particles embedded on it. The hydrogen bonds between PEG and PSS modify the interaction between PEDOT and PSS, leading to the enhanced stretchability[49]. Overall, when PEG is present in the film, the adverse effect of increasing the film thickness on electromechanical properties is compensated by improved plasticity.

To gain more insight on the stability of ~300 nm PEDOT:PSS/PEG film, a stretch-release cycle test at 30% and 45% strain was performed. The samples were stretched for 50 s and released for the same amount of time for 100 times. The film resistance, calculated through the applied voltage and measured current, increases during the first of three stretch-release cycles, then it reaches a stable value, that is maintained up to 100 cycles for both 30% and 45% strain (Figure 5.3a). The result demonstrates an excellent cyclic stability towards stretch-release cycles, which can be explained by the fact that the shape and density of the cracks do not change significantly between the 3rd and the 100th stretch-release cycles (Figure 5.3b).

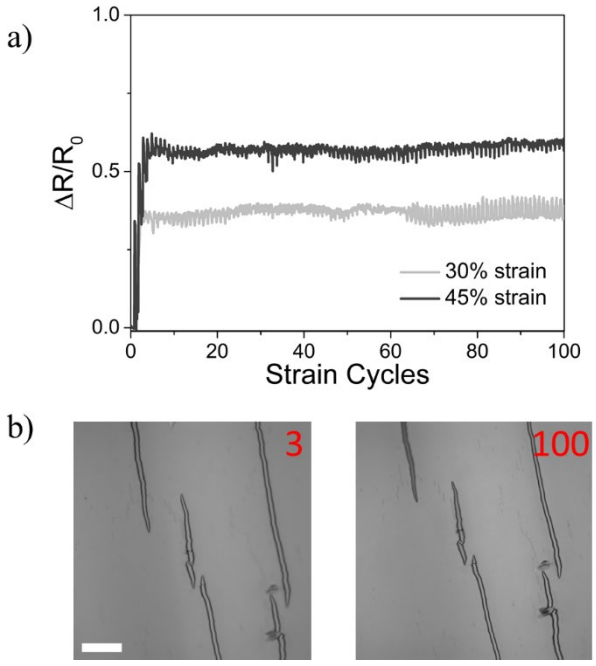

Figure 5.3 Resistance change during 100 stretch-release cycles from 0% to 30% and 0% to 45% strain for PEDOT:PSS/PEG film (~300 nm thick) on PDMS (a). Density and shape od cracks for a ~300 nm thick PEDOT:PSS/PEG film (100 °C baking for 1 h) after 3 and 100 strain cycles at 45% strain (b). R_0 is the initial resistance of PEDOT:PSS/PEG film before stretching. The scale bar is 200 μm.

The stretchable OECTs were fabricated on PDMS according to a method previously reported by our group[140, 143]. We used a stretchable polyampholyte hydrogel or an aqueous electrolyte as the gating medium. To facilitate probing on the tensile tester, large devices were used (channel length, L, of 8 mm and a width, W, of 2 mm). On the basis of the results shown in Figure 5.3, we

pre-stretched the PEDOT:PSS/PEG films by applying 45% strain for three times to reach a stable current.

For the hydrogel-gated OECTs (video S1), a planar PEDOT:PSS stripe parallel to the channel was used as the gate (Figure 5.4a). These devices show similar transfer characteristics when operated at 0% and 45% strain (Figure SB3). These results demonstrate that our hydrogel electrolyte can efficiently gate PEDOT:PSS/PEG film at different strains. However, the low mobility of ions inside the hydrogel limits the performance of OECTs (ON/OFF ratio ~5).

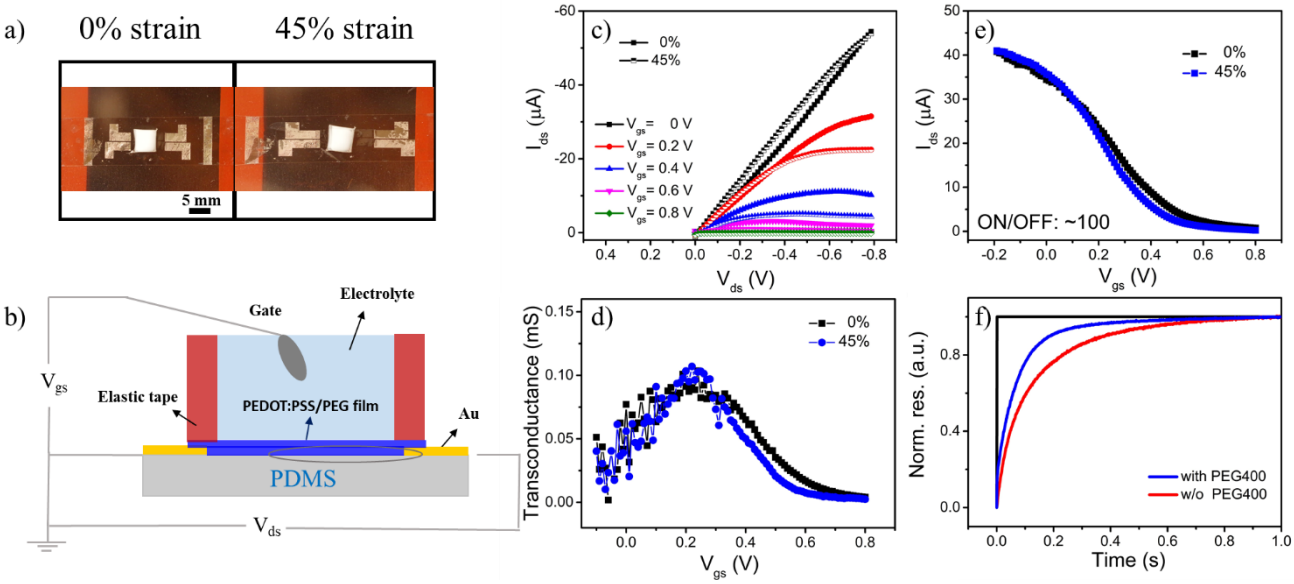

Figure 5.4 Optical images of stretchable OECTs using PEDOT:PSS/PEG channel and gate electrode and polyampholyte hydrogel containing NaCl electrolyte at 0% and 45% strain (a); schematic image of device structure of stretchable OECTs using an aqueous electrolyte and an activated carbon gate (b). Electrical characteristic of stretchable OECTs based on PEDOT:PSS/PEG films on PDMS, using an activated carbon gate electrode and 0.1 M NaCl aqueous solution as electrolyte (c)-(f): output curves (c), transconductance (d) and transfer curves (e) at 0% and 45% strain, normalized time response of I_{ds} during de-doping (V_g = 0.4 V) in presence and in absence of PEG 400 into the films (f). The black step indicates the pulse of 0.4 V gate voltage. All films were baked at 100 °C for 1 h. The thicknesses of PEDOT:PSS/PEG and PEDOT:PSS film are ~300 nm and ~130 nm, respectively. The channel length and width are 8 and 2 mm.

To achieve better device performance, we also fabricated stretchable OECTs using an aqueous electrolyte (0.1 M NaCl solution) confined in an elastic well made of stretchable tape (3 M VHB 4905). Activated carbon on carbon paper was used as the gate electrode (Figure 5.4b)[153]. The output and transfer characteristics (Figure 5.4c, 4.4e) show that the device performance is similar at 0% and 45% strain. These properties make our devices suitable for on-skin bioelectronic (30% strain) and for applications where larger strains are required, such as heartbeat monitoring electronics and sensors applied on joints or knees[156]. Four devices were measured to calculate the transconductance and ON/OFF ratio. The values of ON/OFF ratio range from 50 to 160. We extracted a maximum transconductance of about 0.1 mS (V_{gs} = 0.2 V, Figure 5.4d) and an average ON/OFF ratio of 100 (I_{ds} (V_{gs} = 0 V)/I_{ds} (V_{gs} = 0.8 V), Figure 5.4e), both higher compared to devices with the same geometry using PEDOT:PSS films without PEG, which show a transconductance of ~0.07 mS and an ON/OFF ratio of ~10 (Figure SB4)[143]. The low ON/OFF ratio of OECTs on PDMS are likely due to impurities of unreacted monomers present at PDMS surface and to an irregular morphology[157, 158]. The beneficial effect of PEG on the ON/OFF ratio is still under investigation. However, we hypothesize that the PEG present in the film prevents or reduces the diffusion of unreacted monomers towards the conducting PEDOT regions, thus reducing its impact on the electrical properties. Interestingly, OECTs based on PEDOT:PSS/PEG channels also show a faster response time than those based on PEDOT:PSS (Figure 5.4f), even at high channel thickness (~300 nm). This is likely because the presence of glycol groups in PEG 400 facilitates the mobility of cations[54, 159].

5.6 Conclusion

In this work, we showed that the addition of PEG 400 to PEDOT:PSS processing mixtures strongly improves the electromechanical properties of films on PDMS substrates. When used as channels in OECTs, such films result in a higher stretchability and improved electrical performance. Optical microscopy images show that the presence of PEG significantly reduces the formation of cracks in the films, thus resulting in small variation of the film resistance up to 45% strain. Interestingly, increasing the film thickness from ~100 to ~300 nm does not deteriorate the electromechanical properties. Due to the presence of hydroxyl groups, which likely facilitate ion transport, these stretchable OECTs also show faster response time compared to devices without PEG. This work

provides an easy method to enhance the electro-mechanical properties of conducting polymer films and paves the way for high performance stretchable OECTs for applications as conformable biosensors and bio-electronic devices.

5.7 Acknowledgements

This work is supported by grants NSERC Discovery and Department of National Defence Discovery supplement, awarded to FC. YL is grateful to the Centre de Recherche sur les Systèmes Polymères et Composites à Haute Performance (CREPEC) and Polytechnique Montréal for partial financial support. VRNU is grateful to Nanyang University for financial support through the CN Young Scholars Programme.

CHAPTER 6 ARTICLE 2: AUTONOMIC SELF-HEALING OF PEDOT:PSS ACHIEVED VIA POLYETHYLENE GLYCOL ADDITION

This article has been published in the journal "Advanced Functional Materials" in 2020. This article reports that fast, repeatable and autonomic electrical healing PEDOT:PSS is achieved by blending it with the bio-compatible PEG. The PEG incorporation also improves the conductivity, softness and stability of the conducting polymer film. The supporting information for this article is reprinted in Appendix B of this thesis.

6.1 Authors

Yang Li[1], Xinda Li[1], Shiming Zhang[2], Leslie Liu[1], Natalie Hamad[1], Sanyasi Rao Bobbara[1], Damiano Pasini[3], Fabio Cicoira[1]

[1] Department of Chemical Engineering, Polytechnique Montréal, Montréal, Quebec H3C 3A7, Canada

[2] Center for Minimally Invasive Therapeutics, California NanoSystems Institute, University of California, Los Angeles, California 90095, United States

[3] Department of Mechanical Engineering, McGill University, Montreal, Quebec, H3A0C3, Canada

Email: fabio.cicoira@polymtl.ca.

6.2 Abstract

Self-healing electronic materials are of primary interest for bioelectronics and sustainable electronics. In this work, autonomic self-healing of films obtained from mixtures of the conducting polymer poly(3,4-ethylenedioxythiophene) doped with polystyrene sulfonate (PEDOT:PSS) and polyethylene glycol (PEG) is reported. The presence of PEG in PEDOT:PSS films decreases the elastic modulus and increases the elongation at break, thus leading to a softer material with enhanced self-healing characteristics. In situ imaging of the cutting/healing process shows that the healing mechanism is likely due to flowing back of the material to the damaged area right after the cutting.

6.3 Introduction

Self-healing materials are able to recover their functionalities after being damaged, via a process that can be spontaneous (autonomic), or triggered by an external input[95, 98, 109, 110, 160-163]. Materials showing autonomic self-healing are highly desired, in particular for applications such as bioelectronics and wearable electronics, where frequent damages may occur due to mechanical movement or prolonged contact with living tissues and biological fluids[85, 164-171]. Several approaches have been proposed to achieve such kind of materials. Song et al. reported an aerogel framework fabricated via in situ polymerization of *N*-isopropylacrylamide on sulfur-containing Ag nanowires with an electrical conductivity of 93 S cm^{-1}, exhibiting autonomic self-healing due to the strong reversible Ag-S bonds[172]. Autonomic self-healing, resulting from the ion-dipole interactions, was also found in ionic conductors consisting of ionic liquids in a poly(vinylidene fluoride-*co*-hexafluoropropylene) matrix, which showed a conductivity ranging between $\approx 10^{-5}$ and 10^{-9} S cm^{-1}[163, 173]. Lu et al. reported autonomic self-healing of a stretchable polymer complex composed of poly(2-acrylamido-2-methyl-1-propanesulfonic acid), poly-aniline and phytic acid, which also acts as a strain sensor[174]. Other types of autonomic self-healing materials make use of micro-capsules of conductive agents, such as liquid metal or silver paste, embedded into a polymer matrix[175-189]. The conducting polymer poly(3,4-ethylenedioxythiophene) doped with polystyrenesulfonic acid (PEDOT:PSS) is attracting enormous interest as self-healing material, due to its widespread use in bioelectronics and wearable electronics. Our group demonstrated that PEDOT:PSS films can be healed electrically by water after being cut by a razor blade and show autonomic self-healing when wetted with water before being cut[104]. However, wet PEDOT:PSS films are extremely fragile and their autonomic healing behavior vanishes after drying. A possible strategy to achieve autonomic self-healing in PEDOT:PSS films is to modify their mechanical properties via mixing with other polymers. Along this line, it has been shown that mixtures of PEDOT:PSS with the surfactant Triton X-100 show autonomic self-healing and can be used for deformable electronics and stretchable thermoelectrics[109, 110]. However, as Triton X-100 is potentially harmful[190], alternative approaches need to be explored to develop self-healing materials for applications in bioelectronics.

We have recently reported that adding polyethylene glycol (PEG) to PEDOT:PSS films significantly improves the performance of stretchable organic electrochemical transistors, by

reducing the density of the cracks in the films upon stretching[191]. PEG, also known to act as a moderate electrical conductivity enhancer for PEDOT:PSS[29, 191, 192], has been already used to modify the mechanical properties of several polymers, by decreasing the Young's modulus and increasing the elongation at break[149, 151]. The biocompatibility and anti-fouling properties of PEG make it interesting for applications in bioelectronics[193-195]. On the basis of these results, we believe that the presence of PEG in PEDOT:PSS films can lead to significant changes of the self-healing properties. In this work we explore the self-healing properties of films obtained from blends of PEDOT:PSS and PEG. We show that films processed from a mixture of PEDOT:PSS aqueous suspension and PEG exhibit repeatable autonomic self-healing when cut by sharp blades, even in presence of the conductivity enhancer glycerol. The self-healing can be switched from autonomic to water-enabled by varying the PEG amount in the film, the molecular weight of PEG or by soaking PEG-containing films in methanol. We found that the addition of PEG decreases the Young's modulus and increases the elongation at break of PEDOT:PSS films, thus leading to a soft and viscoelastic material.

6.4 Results and discussion

Preliminary experiments revealed that to achieve films showing autonomic healing, at least 3% PEG needs to be added to the PEDOT:PSS aqueous suspension. The addition of lower amounts leads to water induced healing. For our studies we focused on films obtained from mixtures of PEDOT:PSS and 4% PEG-400, as this composition is safely beyond the threshold required for autonomic self-healing. Free standing films obtained from mixtures of PEDOT:PSS and 4% PEG-400 (thickness ≈15 μm, electrical conductivity ≈200 S cm^{-1}) show autonomic self-healing upon multiple cuts (black curve in Figure 6.1a, Figure SC1, Video S1, Supporting Information), with a healing efficiency close to 100%. An identical behavior was observed when 5 v/v% glycerol was added to the processing mixture, leading to an increase of the electrical conductivity to ≈400 S cm^{-1} (cyan curve in Figure 6.1a). The time-lapse current measurements (Figure 6.1b) show that the process takes place rapidly, with healing times ranging between ≈50 and 800 ms. The autonomic self-healing is observed for cut widths ranging between ≈10 and 60 μm (i.e., about 4 times the film thickness), achieved with blades of different sharpness (Table SC1, Supporting Information). The SEM images of healed films (Figure 6.1c,d, Figure SC3, Supporting Information) show that,

although the damage induced by the blade can be clearly distinguished, there are no discontinuities between the two sides of the cut. The autonomic self-healing vanishes when the cut width is increased to ≈100 µm, using the edge of a quartz microscope slide (Figure SC2, Supporting Information).

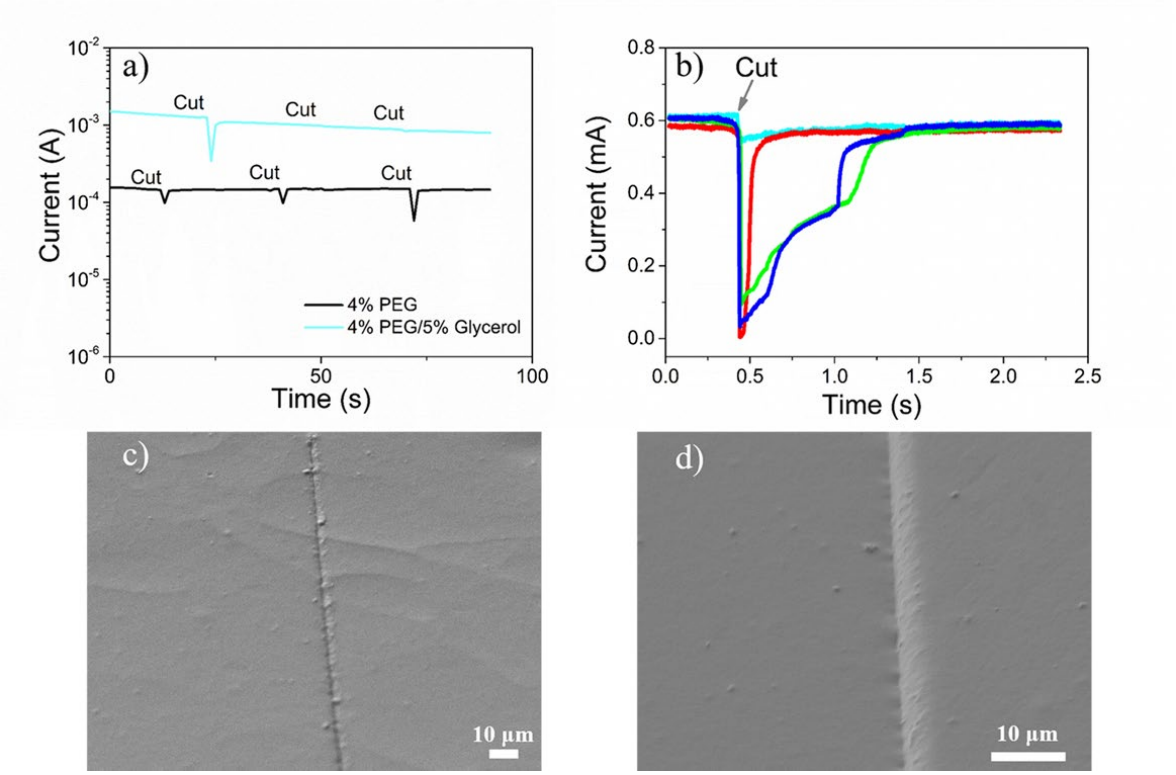

Figure 6.1 a) Current versus time plots during several cuts in different regions of films processed from mixtures containing PEDOT:PSS and 4% PEG-400, with or without 5% glycerol. b) Time-lapse current measurements during the cut/healing process for four different films processed from mixtures containing PEDOT:PSS and 4% PEG-400. c,d) SEM images of the cut and healed regions with different magnifications. The voltage applied during the healing test was 0.2 V. The thickness of the films was ≈15 µm.

As shown above, the addition of PEG to the film-processing mixture is essential to achieve autonomic self-healing. To confirm that PEG is still present at the end of the film processing, we performed thermogravimetric analysis (TGA, Figure 6.2a) and Fourier-transform infrared spectroscopy (FTIR, Figure SC4, Supporting Information). TGA curves of pristine PEDOT:PSS films show a sharp weight loss above 300 °C, due to the decomposition of thiophene[196]. Films

containing PEG-400 show a different behavior, with a main weight loss occurring between 150 and 300 °C, likely due to the vaporization of PEG-400. The weight loss is more pronounced for samples containing 4 v/v% and 10 v/v% PEG-400, where it reaches ≈80%. In the FTIR spectra, the peaks at 2875 cm^{-1} (C-H stretching) and 1645 cm^{-1} (C-O-H bending), as well as the broad band at 3300 cm^{-1} (O-H stretching band of the hydroxyl group), confirm the presence of PEG in the films[29, 197-199]. It is worthwhile to mention that the shape of FTIR bands is might due to the "Christiansen effect", which leads to the higher transmittance of the samples compared to the reference air[200]. The intensities of the peaks at 2875 and 1645 cm^{-1} and of the broad band gradually increase with increasing PEG amount (Figure SC4, Supporting Information), which indicates that the hydroxyl groups of PEG form hydrogen bonding with the hydroxyl groups of other PEG molecules and with the sulfonate groups of PEDOT:PSS[197-199]. The total hydrogen bonding contribution is enhanced with the increase of PEG amount, due to the availability of more hydroxyl groups. This is also reflected in the shift of onset temperature for weight decrease in the TGA curves of conducting polymer films containing larger amounts of PEG-400 (Figure 6.2a) [199, 201, 202]. The presence of PEG is further confirmed by X-ray photoelectron spectroscopy (XPS), via the shift of C(1s) and O(1s) core level spectra (Figure SC5, Supporting Information), in agreement with our recent work[191].

To evaluate the impact of PEG on the mechanical properties of the films under study, we performed tensile stress-strain measurements and dynamic mechanical analysis (DMA) of PEDOT:PSS films processed from pristine PEDOT:PSS solution and from PEDOT:PSS solutions containing different concentrations of PEG-400. A maximum of 10% PEG was added to the PEDOT:PSS processing solution, as higher amounts (≈15%) yielded a dough-like suspension, which could not be used to make freestanding films. Stress-strain responses (Figure 6.2b and Figure SC6, Supporting Information) show almost linear behavior for all films. Additionally, as the PEG content increases the slope (Young's modulus) decreases. Pristine PEDOT:PSS films show elongation at break (percentage increase in length that occurs before breaking under tension) of ≈0.5% upon the application of a stress of ≈4.5 MPa. Increasing the PEG content leads to an increase of the elongation at break, that is, ≈4% upon the application of a stress of ≈3.8 MPa for 1 v/v% PEG-400, ≈6.5% upon the application of a stress of ≈1.5 MPa for 4 v/v% PEG-400 and ≈8.5% upon the application of a stress of ≈0.3 MPa for 10 v/v% PEG-400. The plots of the Young's

modulus and the elongation at break (versus the amount of PEG in the film processing mixture (Figure 6.2c, data extracted from the stress-strain responses shown in Figure SC6, Supporting Information) show that increasing the PEG content leads to a gradual decrease of the modulus from ≈800 MPa (pristine PEDOT:PSS) to ≈4 MPa (10 v/v% PEG), and a gradual increase of the elongation at break from ≈1% to ≈9%. These results clearly indicate that increasing the amount of PEG leads to softer films. It is important to point out that the film conductivity increases from a few S cm^{-1} to ≈350 S cm^{-1} upon addition of 1% PEG, then decreases to ≈200 S cm^{-1} upon addition of 4% PEG (Table 6.1). To investigate the viscoelastic properties, we performed DMA at variable stress frequencies. The storage modulus E', which is a measure of the elastic response, does not show a strong dependence on frequency, whereas the loss modulus E'', which expresses the viscous response, increases with frequency. Both E' and E'' decrease with increased PEG content, especially at concentrations of 4 and 10 v/v% PEG (Figure 5.2d,e), with the viscous component remaining lower than the elastic one. The behavior of E' parallels that of the Young's modulus and confirms that the addition of PEG leads to softer films. The relative ratio ($\tan \delta = E''/E'$) between loss and storage modulus (damping factor) is almost constant for all films up to a frequency of 40 Hz. In the 40-100 Hz range, it shows a steep increase for 4 and 10 v/v% PEG contents (Figure 6.2f). The latter result points to an increased tendency of the material to dissipate energy, that is, to a more pronounced viscoelastic behavior, likely due to the mobility of the PEG chains.

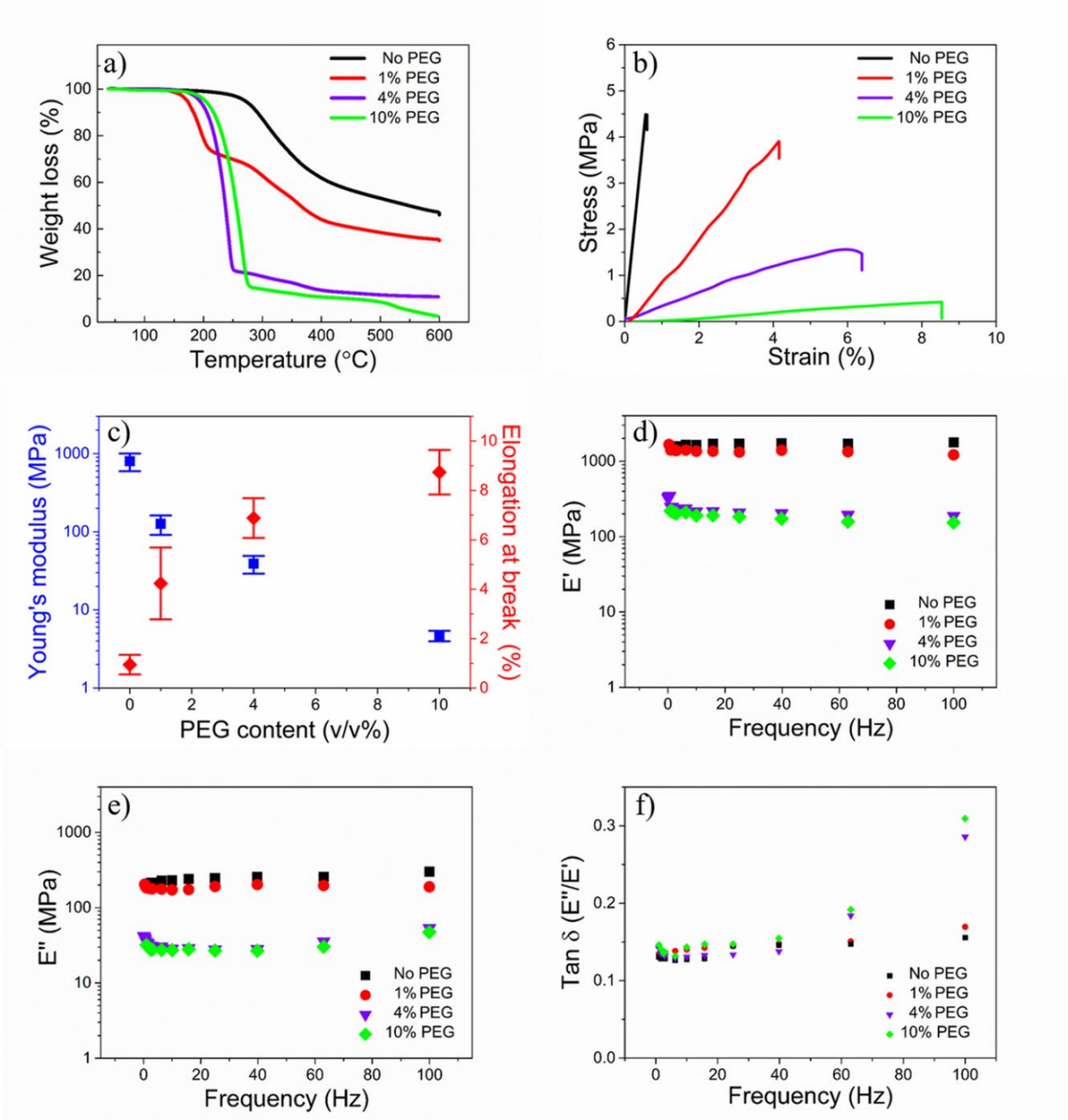

Figure 6.2 Thermal and mechanical properties of films processed from mixtures of PEDOT:PSS and different amounts of PEG-400. a) Thermogravimetric analysis; b) stress-strain curves; c) Young's modulus and break elongation as a function of the PEG-400 content; d) storage modulus (E'); e) loss modulus (E''); f) mechanical damping factor (tan δ = E''/E') for different PEG-400 contents, obtained via DMA in the frequency range 100-0.01 Hz. The thickness of the films used for mechanical tests was ≈100-150 μm.

Table 6.1 Summary of healing behaviors and electrical conductivity of PEDOT:PSS/PEG films

Processing mixture/treatment	Healing Behavior	Electrical Conductivity (S cm^{-1})
PEDOT:PSS/1%PEG-400	Water-enabled	356±23
PEDOT:PSS/4%PEG-400	Autonomic	201±13
PEDOT:PSS/4%PEG-400/5%Glycerol	Autonomic	373±52
PEDOT:PSS/4%PEG-400 after methanol soaking	Water-enabled	1399±87
PEDOT:PSS/4%PEG-200	Autonomic	237±27
PEDOT:PSS/4%PEG-1500	Autonomic	118±15
PEDOT:PSS/4%PEO-100000	Partial autonomic and water-enabled	58±13
PEDOT:PSS/4%PEO-5000000	Water-enabled	17±9

Although further investigations are needed to establish a clear correlation between mechanical properties and self-healing behavior, our results suggest that autonomic self-healing is favored by the softness and viscoelasticity provided to PEDOT:PSS films by increasing amounts of PEG. For instance, films processed from mixtures containing 4% PEG, characterized by a pronounced softness and viscoelasticity, show autonomic self-healing. On the other hand, decreasing the amount of PEG to 1%, leads to mechanical properties similar to those of pristine PEDOT:PSS and, as a consequence, to a change from autonomic to water-induced healing (Figure 6.3a,b)[104]. SEM images confirm that the gap of ≈15 μm created by the cut (Figure 6.3c) is fully healed by water (Figure 6.3d).

With the aim to increase the conductivity of autonomically healable films, we carried out methanol soaking (20 min followed by 20 min drying at 140 °C)[33, 35, 39], which led to an increase from ≈200 S cm^{-1} to ≈1400 S cm^{-1} (Table 6.1). TGA curves (Figure 6.3e) show that this treatment leads to a behavior similar to pristine PEDOT:PSS films, thus indicating that the conductivity enhancement is most likely due to the dissolution of the insulating PEG during methanol soaking[33, 35, 39]. The PEG dissolution, however, led to a switch from autonomic to water-enabled healing (Figure 6.3f). Re-immersing the films in PEG for about 30 min led only to a partial recovery of the autonomic healing (Figure SC7, Supporting Information). Therefore, although it suppresses autonomic healing, methanol soaking can be exploited to achieve water-healable films with high conductivity. The self-healing performance of PEG containing PEDOT:PSS films also depends on the molecular weight of PEG. In addition to PEG-400, we investigated PEG-200, PEG-1500, PEO-100000, and PEO-5000000, by keeping the added amount constantly to 4 v/v%. Films containing PEG-200 show autonomic healing (Figure SC8a, Supporting Information) and a conductivity similar to that achieved with PEG-400. The use of PEG-1500 leads to a decrease of the healing efficiency to ≈80% (Figure SC8b, Supporting Information). Films containing polyethylene oxide (PEO, molecular weight 100 000) show a partial autonomic healing, which can be completed by wetting the damaged area with water (Figure SC8c, Supporting Information). Films containing PEO-5000000 show only water-enabled healing (Figure SC8d, Supporting Information). This decrease in autonomic healing efficiency can be attributed to the lower mobility of the longer chains of high molecular weight PEG, which may lead to increased stiffness, thus hindering the flow back of material to the damaged area after cut. It is also worth noticing that increasing the molecular weight of PEG results in a significant conductivity decrease, as reported in the literature[29]. The self-healing behavior and the electrical conductivity of films processed from different PEDOT:PSS/PEG mixtures are summarized in Table 6.1.

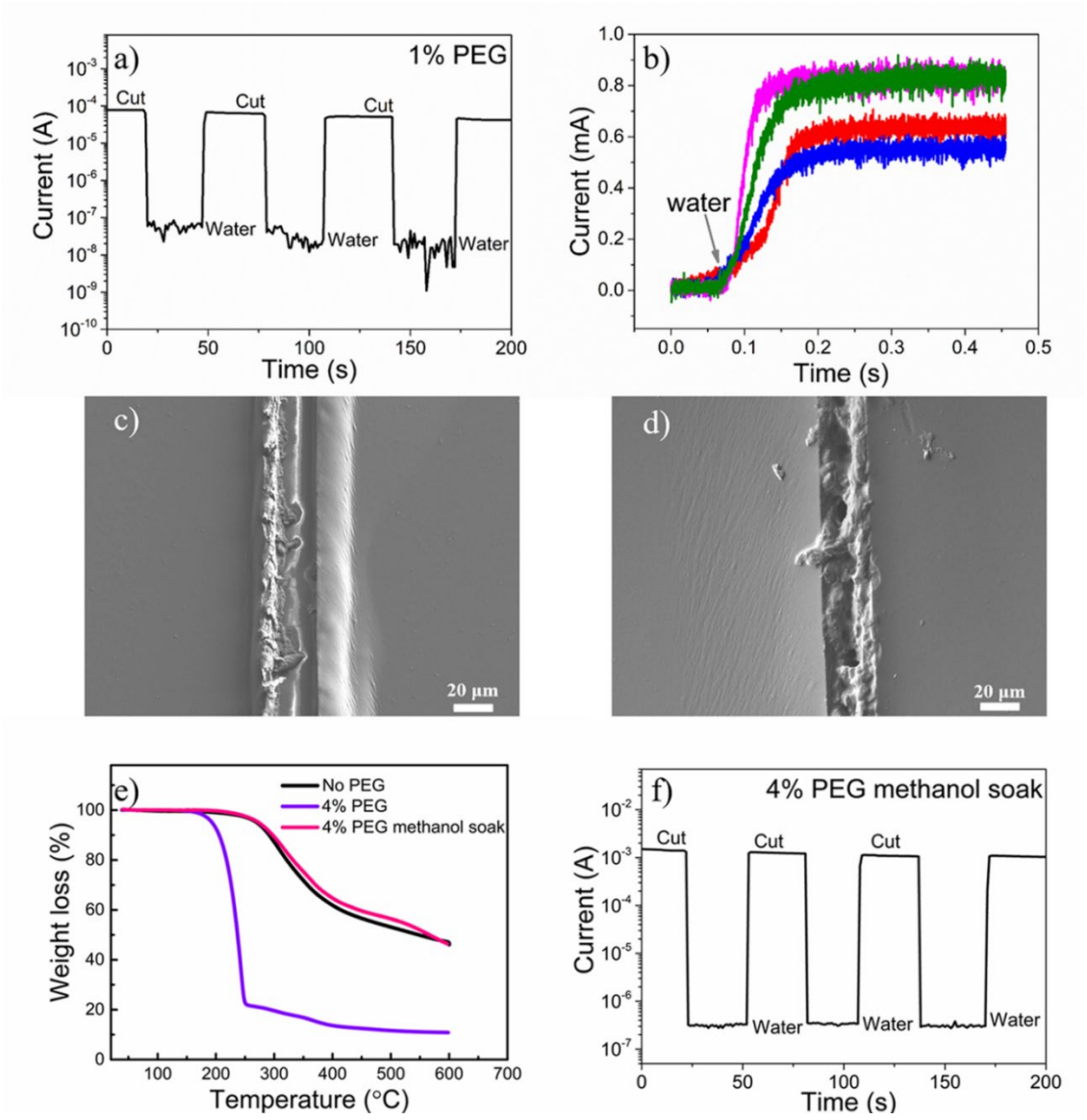

Figure 6.3 a) Current versus time plot of a film processed from a mixture containing PEDOT:PSS and 1% PEG-400 during several cuts and water healings in different regions; b) time-lapse current measurements of the healing process of PEDOT:PSS/1%PEG films; SEM images of the damaged area c) before and d) after healing; e) TGA curves of PEG containing PEDOT:PSS films before and after soaking in methanol compared to pristine PEDOT:PSS films; f) current versus time plot of a film processed from a mixture containing PEDOT:PSS and 4% PEG-400 and rinsed in methanol upon several cuts and water healings in different regions. The voltage applied during the healing test was 0.2 V. The thickness of the films was ≈15 µm (methanol soaking can lead to a thickness decrease).

In our previous work, we hypothesized that swelling may play a role in the mechanism of water induced healing[104]. To validate our hypothesis, here we measured the swelling (i.e., weight gain upon the water immersion) of PEDOT:PSS films containing various amounts of PEG-400 (Figure 6.4a). As pristine PEDOT:PSS films were too brittle to handle for this experiment, we replaced them with films containing 5% of glycerol. Soaking for 10 min in water led to a weight increase of ≈300% for PEDOT:PSS films containing glycerol and 1% PEG. This high swelling ability may explain the water-enabled self-healing. A higher amount of PEG causes the weight increase to drop to ≈90% for 2 v/v% PEG-400 and ≈30% for 4 v/v% PEG-400. No further changes were observed upon soaking for longer times. Interestingly, upon increasing the PEG content, the weight of dry films increases, in accordance with TGA (Figure 6.2a), while that of wet films remains almost constant (Figure 6.4b). A similar trend was observed by exposing the films to water vapor in a humidity chamber with a relative humidity (RH) of ≈95% (Figure SC9, Supporting Information). In agreement with the literature, the reduced swelling of films containing PEG is likely due to partial removal of PSS, which is responsible for the high swelling of PEDOT:PSS[203-205]. A similar behavior is found for the surfactant Triton X-100, which has also been reported to induce autonomic healing of PEDOT:PSS films (Figure SC10, Supporting Information)[109, 110]. We found that Triton-containing PEDOT:PSS films show autonomic or water-enabled healing depending on the amount added to PEDOT:PSS (Figure SC11, Supporting Information), as in the case of PEG.

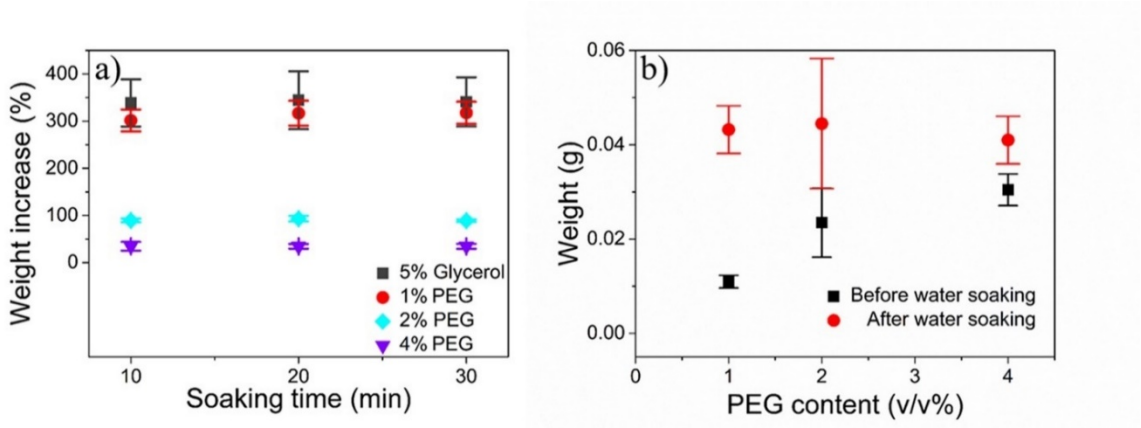

Figure 6.4 a) Weight increase versus water soaking time of PEDOT:PSS films containing different amounts of PEG-400; b) weight of PEDOT:PSS films containing different amounts of PEG-400 before and after water soaking for 10 min.

To prove that swelling does not play a significant role in autonomic healing of PEDOT:PSS films containing 4% PEG, we performed cut/healing experiments in dry conditions in a N_2 purged glove box, after baking the film in situ for 14 h at 140 °C. Notably, the autonomic self-healing after multiple cuts was observed even in these conditions (Figure SC12, Supporting Information), thus excluding any significant role of water trapped in the hygroscopic PEG matrix. The limited swelling provides PEG-containing PEDOT:PSS films with an excellent stability during wetting and drying cycles, while pristine PEDOT:PSS films show a considerable shrinking in the same conditions (Figure SC13, Supporting Information). This property can be exploited for the fabrication of electrodes for biomedical devices operated under high humidity conditions, e.g., in incubators for neonatal intensive care units, where swelling can cause dramatic shape change, leading to a detachment from the skin and device failure.

To further investigate the healing process, we performed in situ imaging of the cut/healing process, using a micro scratcher equipped with an inverted optical microscope. Imaging during the cutting process (Video S2, Supporting Information, and Figure 6.5a, where the brighter part corresponds to the blade and the dark part of the film being cut) reveals that the gap created by the cut becomes narrower as the blade moves forward. Imaging right after completion of the cut shows that the gap is completely healed and no longer visible (Video S3, Supporting Information, Figure 6.5b), in agreement with SEM images. These results clearly indicate that, just after being cut, the material rapidly flows back to the damaged area, likely due to the viscoelastic properties imparted by PEG.

It has been reported that PEG chains present in the films screen the ionic interaction between PEDOT and PSS by forming hydrogen bonding with PSS. This leads to a phase separation between PEDOT and PSS, and favors the formation of aggregated PEDOT domains, enhancing the film conductivity (Scheme I in Figure 6.5c)[29]. The PEG chains also function as a soft matrix for PEDOT:PSS particles and endow a well-mixed and strong entanglement between hydrophilic PSS chains, thus favoring the flowing-back of material towards the damaged area after cutting (Scheme II in Figure 6.5c). A further contribution to the healing process, and thus to the rebuilding of the PEDOT-PEDOT conducting pathways in the PEG matrix, might be the formation of hydrogen bonds between PEG-PEG, PSS-PSS, and PEG-PSS chains at the interfaces of the gap (Scheme II in Figure 6.5c)[29, 49, 109, 110].

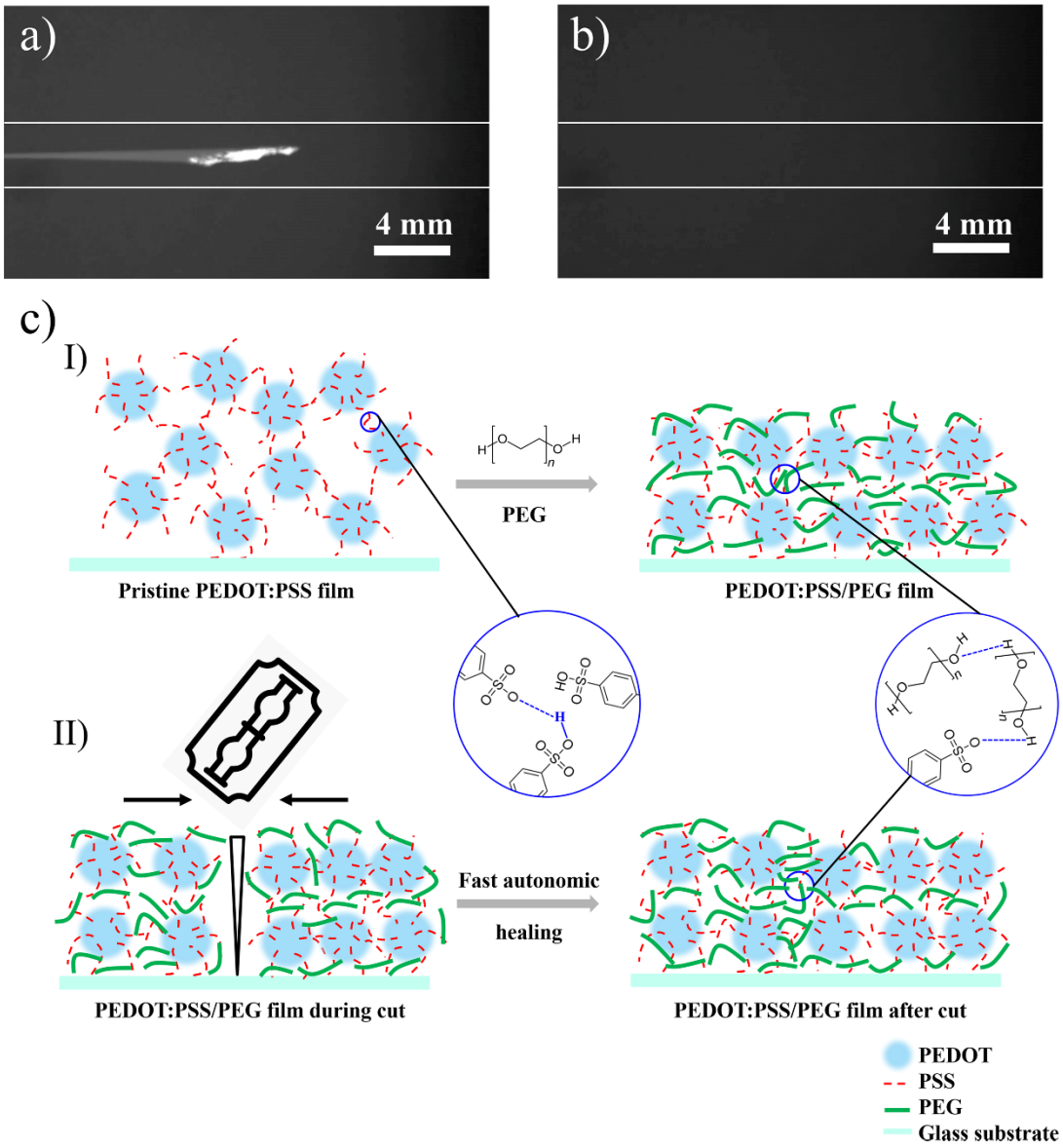

Figure 6.5 a) Optical images of a PEDOT:PSS/PEG film while being cut by the micro scratcher and b) after the cut. The white lines have been added to highlight the cut region. c, I) Scheme of the soft matrix effect played by PEG chains in PEDOT:PSS films; c, II) Scheme of the proposed mechanism for the autonomic healing of PEDOT:PSS/PEG film. The chemical structures in the circles represent the H-bonds between two PSS chains, between two PEG chains, and between a PSS and a PEG chain.

6.5 Conclusion

We have shown that PEDOT:PSS films containing PEG-400 show autonomic self-healing in dry conditions, even in the presence of the conductivity enhancer glycerol. In situ imaging of the cutting/healing process shows that, just after cutting, the two parts of the film reconnect by flowing back to the damaged area. The autonomic self-healing is attributed to the change of mechanical properties induced by PEG, which leads to a lower elastic modulus, a larger elongation at break and more enhanced viscoelastic properties with respect to pristine PEDOT:PSS films. The self-healing behavior of PEDOT:PSS/PEG films depends on the molecular weight and the amount of the PEG added to the processing mixture. Low-molecular weight PEG (200 and 400) favors autonomic self-healing, likely because of the high mobility of short molecular chains. Films containing higher molecular weight PEO (100 000 or 5 000 000) or a lower amount of PEG (e.g., 1 v/v %) do not heal autonomically and rather show water induced healing, which can be explained by water swelling of the films. We believe that this work will propel the development of healable electronics for wearable or biomedical applications.

6.6 Experimental section

Materials

The PEDOT:PSS aqueous suspension (Clevios PH1000) was purchased from Heraeus Electronic Materials GmbH (Leverkusen, Germany). Glycerol (99.5+% purity) was purchased from Caledon Laboratories Ltd. (Georgetown, ON). PEG 200, 400, and 1500, PEO 1 00 000 and 50 00 000 and the liquid metal gallium-indium eutectic (EGaIn 495 425) were purchased from Millipore Sigma. All chemicals were used without further treatment. Glass slides (Corning 2947-75 × 50) were purchased from Corning Incorporated.

Processing and Characterization of PEDOT:PSS Films

The mixtures to process the films were prepared by mixing Clevios PH1000 with PEG or PEO and glycerol in a centrifugal mixer (Thinky M310) at 2000 rpm for 5 min. As PEG-1500, 1 00 000, and 50 00 000 are solid at room temperature, their volume was calculated by dividing the weight by the density. The films were deposited by drop-casting (≈0.5 mL of mixture) on glass slides and successively baked on a hot plate with the following sequence: 50 °C for 1 h, 90 °C for 2 h, and

finally 140 °C for 6 h. The gradual temperature increase permitted to obtain continuous films without the formation of bubbles, which could be easily detached from the glass slides[104]. The film thickness was measured with a profilometer (Dektak 150) using a 12.5 μm stylus tip with a 10 mg load. Optical microscopy images were obtained with a Carl Zeiss Axio microscope. SEM measurements were performed with a JEOL JSM-7600TFE field emission scanning electron microscope with a voltage of 5.0 kV (LEI) under a vacuum of 10^{-4} Pa. XPS was performed using a VG ESCALAB 3MKII system with Mg-Ka X-ray source in an ultra-high vacuum. FTIR was performed using a PerkinElmer FTIR Spectrum Two spectrometer. Electrical conductivity measurements were carried out on thin films (thickness ≈200 nm) deposited by spin-coating at 1000 rpm and baked at 140 °C for 1 h. Sheet resistances were measured by a four-point probe (Jandel engineering) connected to an Agilent B2902A voltage-current source measure unit.

Self-Healing Tests

Self-healing experiments were carried out in ambient air on films with a size of ≈(6.0 × 1.5) cm, and a thickness of ≈15 μm. Electrical contacts were made via two tungsten probes immersed into EGaIn contacts at the two sides of the film and the current was measured with an electrical probe station equipped with national instruments NI PXIe-1062Q source-measure unit controlled by Labview software. The cuts for the self-healing experiments were performed manually using different razor, surgical and ceramic blades (specifications reported in Table S1, Supporting Information) and a quartz microscope slide (Micro-Tec 51-001113, (76.2 × 25.4 mm) × 1 mm). The size of the cuts induced by the different blades was measured on pristine PEDOT:PSS films, which do not show autonomic healing. A droplet (≈40 μL) of deionized (DI) water (18.2 MΩ cm at 25 °C, Millipore) was used as the healing agent for water-enabled healing experiments. The time for current recovery is referred as the healing time; the ratio $\eta=(I_{healed}-I_{damaged})/(I_{pristine}-I_{damaged}$, where I is the current measured for pristine, damaged, and healed films, as the healing efficiency. For the time-lapse current measurement, the PEDOT:PSS/PEG film was connected with a sensing series resistor. The output voltage on the sensing resistor was measured after applying 100 mV of the input voltage. The plotted current was calculated from the relation $I = V_{resistor}/R$. The actual voltage drop across the PEDOT:PSS/PEG films under test was less than 100 mV. For real-time imaging of the cutting/healing processes, the cuts were performed with titanium-coated trimmer blades (Fiskars) mounted a Micro Scratcher (MST³, CSM instruments SA) equipped with an

inverted microscope (Zeiss Axioscope A1). The force applied by the cutting blade to the film was 200 mN and the blade moving speed was 2 cm min^{-1}.

Thermogravimetric Analysis

TGA was performed on a TG Q500 (TA Instruments). 5 mg samples of pristine PEDOT:PSS film or PEDOT:PSS/PEG films were transferred into platinum pans to perform the test. The TGA curves were acquired between 40 and 600 °C (heating rate of 10 °C s^{-1}) under nitrogen atmosphere (flow rate of 60 mL min^{-1}).

Mechanical Tests

Mechanical tests are performed on three or more PEDOT:PSS films with different PEG amounts. These films, all with a dimension 5 cm × 1.5 cm × 100-150 μm (length × width × thickness), were prepared by drop-casting the mixture in an aluminum mold, followed by baking at 140 ºC for 3h. Tensile tests were conducted at room temperature with a mechanical tester (Instron ElectroPuls E10000) equipped with a 500 N load cell. The Young's modulus of each specimen was calculated by the linear fitting of stress-strain curves at low strain (<1%). The DMA test of these films was performed at room temperature with a DMA 2980 (TA Instruments) in the thin-film testing configuration. The tests were carried out in frequency sweeping mode from 100 to 0.01 Hz. The oscillation amplitude was 30 μm. The static force applied to the sample was 0.01 N.

Swelling Test

PEDOT:PSS films were weighed by an analytic balance (Sartorius BP 210 D) right after baking to record their initial mass and successively soaked in DI water or transferred into a Cole-Parmer humidity-controlled chamber (03323-14) for 10-30 min. They were then removed from the water and transferred onto a piece of lint-free paper using tweezers. The water on the surface of the films was dried off and the samples were weighed for a second time. The mass increase of each sample was calculated using the following formula, where M_w is the mass of the wet film and M_D is mass of dry film.

$$\text{Weight Increase (\%)} = (M_w - M_D)/M_D \times 100$$

Films containing glycerol or PEG are easy to peel off from the glass substrate after baking and stable during water soaking process. Swelling of pristine PEDOT:PSS films could not be assessed, because they are difficult to handle and break apart when soaked in water.

6.7 Acknowledgement

The authors are grateful to Jo'Elen Hagler and Biporjoy Sarkar for fruitful discussions. This work was supported by grants NSERC Discovery and Defence Research and Development Canada Discovery supplement, awarded to F.C. Y.L. is grateful to the Centre de Recherche sur les Systèmes Polymères et Composites à Haute Performance (CREPEC) and Polytechnique Montréal for partial financial support. N.H. acknowledges support from FRQNT through a Scholarship for Reentering the Research Community. The authors are grateful to the CMC Microsystems for financial support through the program MNT financial assistance. The authors have also benefited from the support of FRQNT and its Regroupement stratégique program, through a grant awarded to RQMP. The supporting information file was revised on July 23, 2020 after initial online publication.

CHAPTER 7 ARTICLE 3: TAILORING THE SELF-HEALING PROPERTIES OF CONDUCTING POLYMER FILMS

This article has been published in the journal “Macromolecular Bioscience” in 2020. This article reports the tailoring of the healing property of PEDOT:PSS films via diverse processing methods. The supporting information for this article is reprinted in Appendix C of this thesis.

7.1 Authors

Yang Li[1], Shiming Zhang[2], Natalie Hamad[1], Kyoungoh Kim[1], Leslie Liu[1], Michael Lerond[1], and Fabio Cicoira[1]

[1] Department of Chemical Engineering, Polytechnique Montréal, Montréal, Québec, H3C3J7, Canada

[2] California NanoSystems Institute, University of California, Los Angeles, California 90095, United Statesartment of Chemical Engineering, Polytechnique Montréal, Montréal, Québec, Canada

E-mail: fabio.cicoira@polymtl.ca

7.2 Abstract

The conducting polymer polyethylenedioxythiophene doped with polystyrene sulfonate (PEDOT:PSS) has received great attention in the field of wearable bioelectronics due to its tunable high electrical conductivity, air stability, ease of processability, biocompatibility, and recently discovered self-healing ability. It has been observed that blending additives with PEDOT:PSS or post-treatment permits the tailoring of intrinsic polymer properties, though their effects on the water-enabled self-healing property have not previously been established. Here, it is demonstrated that the water-enabled healing behavior of conducting polymers is decreased by crosslinkers or by acid post-treatment. Organic dopants of PEDOT have high water swelling ratios and lead to water-enabled healing, while inorganic dopants fail in the healing of PEDOT. The water-enabled healing of two isolated PEDOT:PSS squares with a 5 μm width gap and a thickness less than 1 μm is shown. This work will help pave the way for the further development of conducting polymer-based self-healable bioelectronics and flexible and stretchable electronics.

7.3 Introduction

Recent advances in wearable electronics and bioelectronics have brought a great deal of attention to self-healing organic electronic materials[95, 98, 99, 206-209], which have been used in devices, such as sensors[210-212], field-effect transistors (FETs)[213, 214], electrochemical transistors (ECTs)[104], and energy storage devices[215, 216]. The organic conducting polymer poly(3,4-ethylene-dioxythiophene): polystyrene sulfonate (PEDOT:PSS) is an excellent candidate for self-healable electronics, as it combines water-induced or autonomic self-healing with high conductivity and ease of the process[28, 104, 110, 139]. After reporting water induced self-healing of PEDOT:PSS films[104], we have shown recently that adding the biocompatible polymer polyethylene glycol (PEG) to PEDOT:PSS aqueous suspensions yields softer films showing autonomic healing[217]. It had been reported that PEDOT:PSS mixed with the surfactant Triton X-100 forms a conducting polymer dough that is capable of recovering current autonomically, due to enhanced viscoelasticity[109, 110]. Moreover, a PEDOT:PSS hydrogel, formed by mixing PEDOT:PSS aqueous suspension and 4-dodecylbenzenesulfonic acid (DBSA), achieves both electrical and mechanical healing after cutting and pasting[118]. Cao et al. reported a stretchable PEDOT:PSS hydrogel in poly(*N*-isopropyl acrylamide) (PNIPAM) matrix can be healed at room temperature without external stimulus due to multiple dynamic hydrogen bonds among PSS^-@PNIPAM shells[218].

Although autonomic or water-induced healing has been demonstrated for several PEDOT:PSS formulations, some important questions remain unanswered. For instance, it is still unclear how the healing process is affected by compounds added during PEDOT:PSS film processing to modify the film adhesion properties, such as crosslinkers, or by treatments carried out to increase the electrical conductivity, such as acid soaking[31, 32, 38, 46, 143, 191, 219-221]. Moreover, it is unclear if self-healing properties extend to other forms of PEDOT containing counterions other than PSS, obtained by chemical or electrochemical polymerization. Such forms of PEDOT are of interest since in small dopants, such as *para*-toluene sulfonate (or tosylate, Tos), trifluoromethanesulfonate (or triflate, OTf), and ClO_4^-, lead to an enhanced electrical conductivity (>1000 S cm^{-1}) due to a more compact PEDOT-PEDOT stack[222-224].

In this work, we studied the water-enabled self-healing of the following systems: PEDOT:PSS films processed in presence of the crosslinker 3-(glycidyloxypropyl)trimethoxysilane (GOPS); PEDOT:PSS films post-treated with sulfuric acid; PEDOT:Tos and PEDOT:OTf films obtained by chemical polymerization; and PEDOT:ClO_4 obtained by electrochemical polymerization. We showed that i) the presence of GOPS in the film as well as a long post-treatment with sulfuric acid significantly impair the healing ability; ii) films of PEDOT:Tos as well as PEDOT:OTf show water-enabled healing; iii) electropolymerized PEDOT:ClO_4 films do not show water-induced healing. The self-healing properties were found to be strictly related to the ability of the materials to swell in water. In addition, we demonstrated that water is able to bridge 5 μm wide gaps between PEDOT:PSS films, generated by photolithography and oxygen plasma etching. These explorations of the healing ability of diverse PEDOT films will significantly complement and advance knowledge in the field of self-healable materials and pave the way for the innovation of multiple healable bioelectronics.

7.4 Results and discussion

Since swelling of PSS in water plays a primary role in water-induced self-healing, we expect that any change of PSS concentration in the films would lead to a change in self-healing properties. Previous studies indicate that GOPS molecules can cross-link with PSS anions, other GOPS molecules and glass substrates, enhancing the adhesion of PEDOT:PSS film[225-227], and that a sulfuric acid treatment is able to remove PSS and substitute it with HSO_4^-[34, 37, 228]. Therefore, both treatments are expected to change the self-healing properties of PEDOT:PSS (Figure 7.1).

GOPS, in concentrations between 0.5 and 1% v/v, is often added to PEDOT:PSS aqueous suspensions to improve adhesion on glass substrates (Figure 7.1)[28, 225]. We performed self-healing experiments on films obtained from mixtures containing 0.5, 1, and 5% v/v of the conductivity enhancer glycerol[138, 229, 230]. In agreement with the literature, the GOPS addition lowers the conductivity from ≈800 S cm^{-1} (no GOPS) to ≈350 S cm^{-1} (0.5% v/v GOPS) and ≈300 S cm^{-1} (1% v/v GOPS) (Table 7.1)[28, 225]. Higher amounts of GOPS were not considered, as they lead to a considerable decrease of electrical conductivity. Experiments show that the presence of GOPS clearly leads to a decrease of healing efficiency from ≈90% to ≈65% for 0.5% GOPS, and ≈15% for 1% GOPS (Figure 7.2a; Table 7.1). The healing time, averaged of three different

cuts, increases from ≈0.2 to ≈3.5 s for 0.5% GOPS and ≈7.5 s for 1% GOPS (Figure 7.2b,c; Table 7.1). As the healing is thought to be a result of swelling in water[104], we evaluated the change of the swelling properties of PEDOT:PSS films containing different amounts of GOPS, with respect to films containing 5% glycerol[217]. Films without GOPS show a weight gain of ≈340% after water soaking for 10 min, without further changes for longer soaking times. The presence of GOPS leads to a substantial decrease of the weight gain: from ≈290% for 0.5% v/v GOPS and ≈150% for 1% v/v GOPS (Figure 7.2d). It is necessary to point out here that PEDOT:PSS possesses a core-shell structure with a weight ratio of 1:2.5 between PEDOT and PSS, and the excess PSS contributes remarkably to the high swelling of PEDOT:PSS film (Figure 7.1)[203-205]. As described in the literature, crosslinking reactions may involve the epoxy ring of GOPS and the sulfonate groups of excess PSS, the methoxysilane group of GOPS, and the glass substrate as well as the methoxysilane groups of different GOPS molecules (Figure 7.1)[28, 225]. A higher amount of GOPS likely leads to the formation of more cross-linking bonds surrounding PSS shells, hindering the water uptake of PSS and restricting the volume expansion upon water uptake[231]. The decrease of swelling upon GOPS addition also affects the water-enabled healing ability of PEDOT:PSS by creating barriers for the propagation of PSS and PEDOT to the cut area after water drops, leading to prolonged healing time and thus lowering healing efficiency.

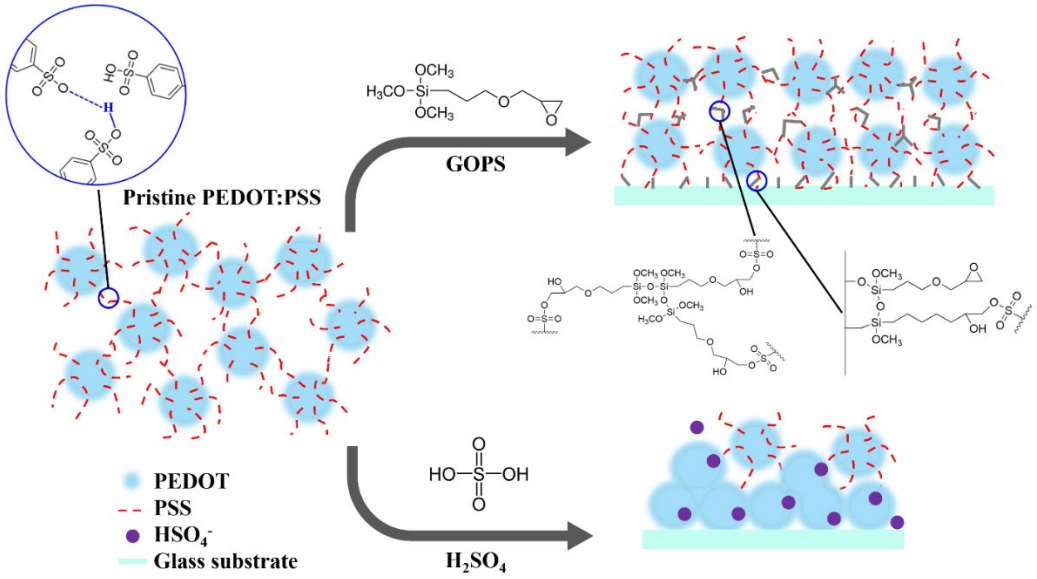

Figure 7.1 Schematic diagram of proposed PEDOT:PSS molecular structure changes via crosslinker addition and acid post-treatment. The chemical structures in the left circle represent the H-bonds between two PSS chains inside the pristine PEDOT:PSS film. The addition of crosslinker GOPS induces three main interactions, involving GOPS-PSS, GOPS-GOPS, GOPS-glass (shown in the circles and zoom area), increasing the film water-stability and adhesion on glass. Sulfuric acid soaking removes excess PSS and replace it with HSO_4^-, leading to the conformational change of PEDOT chains[34, 37, 225, 228].

Post-treatment with strong acids, such as sulfuric and triflic acid, besides increasing electrical conductivity, is also expected to influence water-enabled healing due to the removal of PSS^- from the films[34, 37, 228]. We evaluated the self-healing performance of PEDOT:PSS films soaked in concentrated sulfuric acid for 10, 20, and 30 min and found that after such treatments, the films still retain water-enabled healing upon several cuts (Figure 7.3a), although with a decreased efficiency of ≈93%, ≈75%, and ≈70% for immersions of 10, 20, and 30 min, respectively. The corresponding healing times gradually increase from ≈0.3 to ≈4 s (Figure 7.3b). The water-induced healing properties are practically suppressed for samples immersed in sulfuric acid for three days, which only show a transient current raise, probably due to the ionic current induced by water droplets (Figure 7.3c). The absence of healing is also confirmed by scanning electron microscopy (SEM), which reveals that water cannot heal the gap (Figure SD1, Supporting Information). Notably, the sulfuric acid post-treatment substantially raises the electrical conductivity of

PEDOT:PSS films from ≈0.1 S cm^{-1} to ≈1100, ≈2000, ≈2400, and ≈2550 S cm^{-1} after soaking in concentrated sulfuric acid for 10, 20, 30, and 3 days, respectively (Table 7.1). We found that increasing the duration of the sulfuric acid post-treatment dramatically decreases the swelling ability of PEDOT:PSS films (Figure 7.3d): the weight increase of conducting polymer films after water soaking drops from ≈350% (untreated sample) to ≈150% (1-day treatment) and ≈75% (3-day treatment).

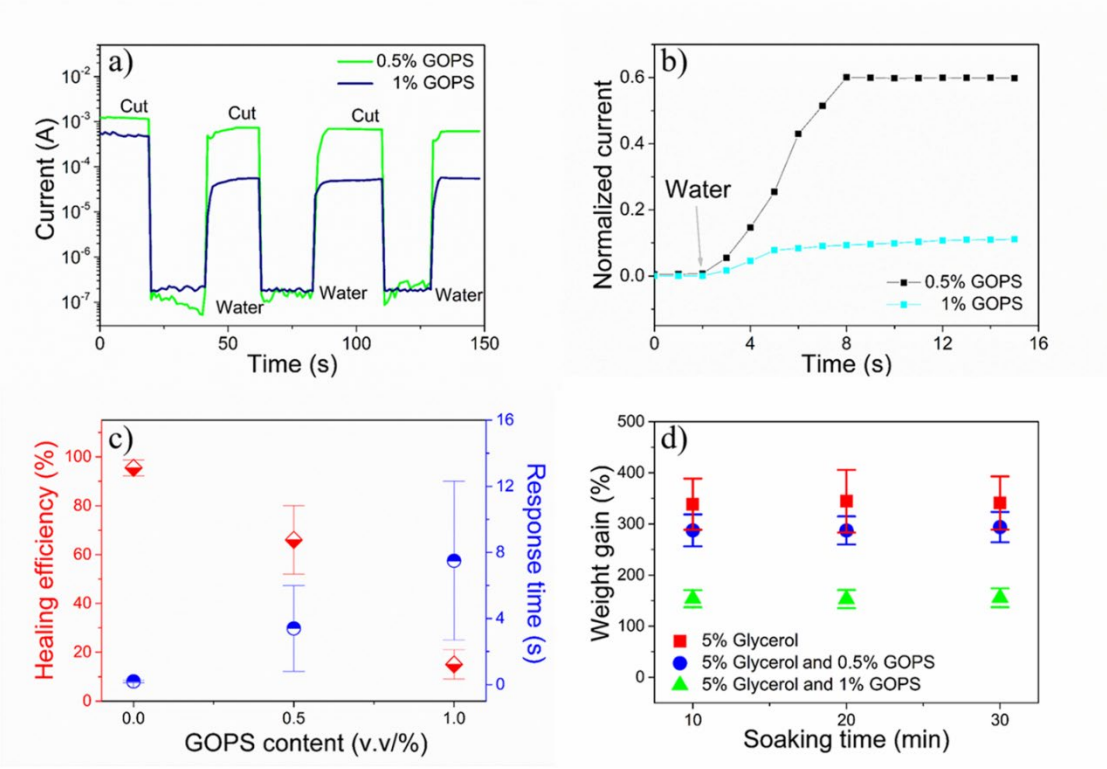

Figure 7.2 Healing and swelling properties of films processed from mixtures containing PEDOT:PSS, 5% glycerol and different amounts of GOPS ($N = 6$). a) Current versus time during several cuts in different areas, b) current versus time during the water-triggered healing process after one cut, c) healing efficiency and response time versus different amounts of GOP, and d) water uptake versus soaking time. The current in (b) is normalized to the initial current before cutting. The healing time and healing efficiency in (c) were extracted by calculating the average value of healing process parameters in (b) upon one cut from 6 samples. The films were first baked at 50 °C for 1 h, then at 90 °C for 2 h and finally at 140 °C for 6 h. The thickness of films was ≈5 μm.

It is worth pointing out that both sodium chloride (NaCl) and phosphate buffer saline (PBS) solutions lead to healing performance similar to those achieved with DI water (Figure SD3, Supporting Information).

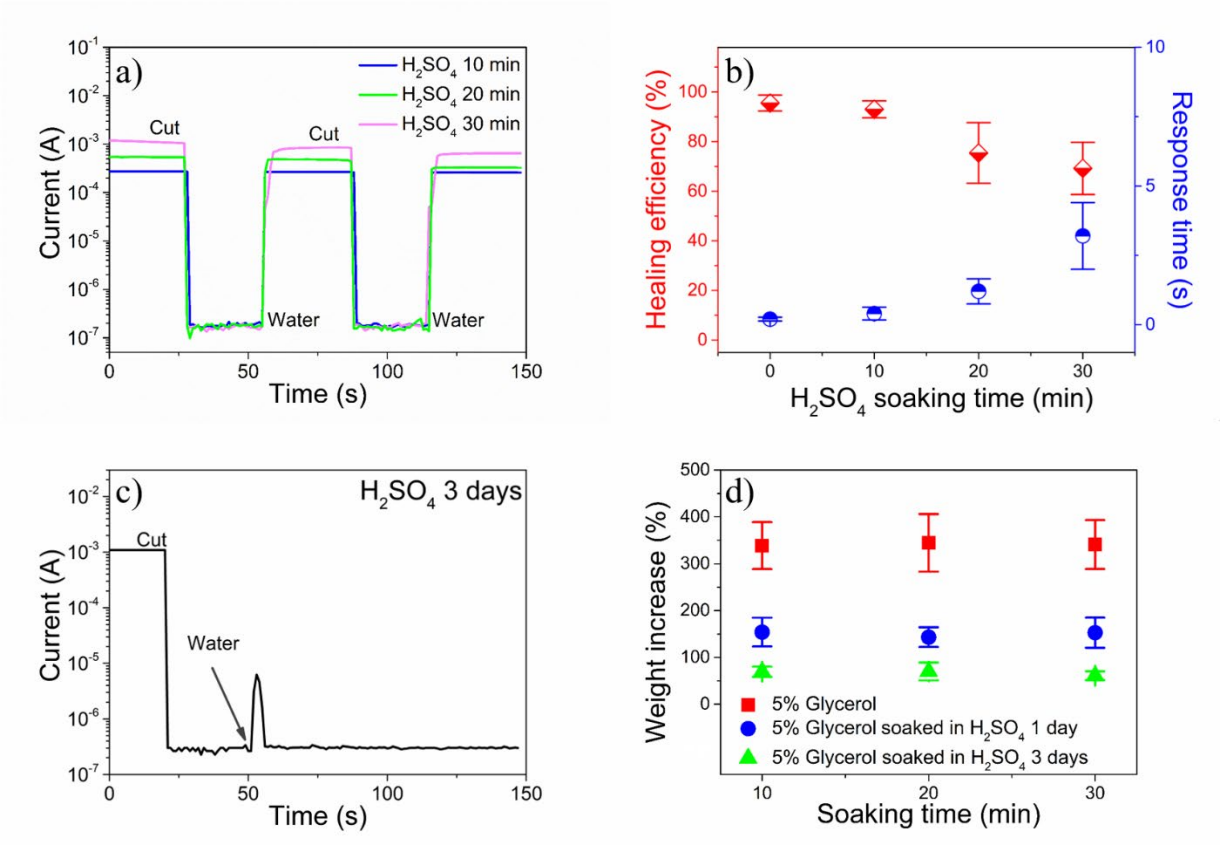

Figure 7.3 Healing and swelling properties of PEDOT:PSS films after soaking in sulfuric acid for different times (N = 6). a) Current versus time profile of pristine PEDOT:PSS films after sulfuric acid treatment for 10, 20, and 30 min after several cuts in different areas of the films; b) healing efficiency and response time of pristine PEDOT:PSS films versus sulfuric acid treatment time; c) current versus time profile of pristine PEDOT:PSS films after sulfuric acid treatment for 3 days after the one-time blade cut; d) water uptake versus soaking time of films processed from mixture of PEDOT:PSS and 5% glycerol after sulfuric acid post-treatment for different times. The healing time for samples soaked in sulfuric acid for 3 days in (c) cannot be calculated since there is almost no healing behavior. The thickness of films before soaking was ≈5 µm.

To investigate the composition change of PEDOT:PSS films after sulfuric acid post-treatment, we performed X-ray photoelectron spectroscopy (XPS). In the S(2p) spectra of untreated PEDOT:PSS films (Figure SD2, Supporting Information), the peak between 166 and 172 eV is attributed to sulfur atoms of PSS, whereas the double peak between 162 and 166 eV is attributed to sulfur atoms of PEDOT[28, 155]. After sulfuric acid treatment, we observe an increase of the PEDOT/PSS signal ratio. While the position of the PEDOT peaks remains unchanged, the PSS peak is replaced with a broader signal at lower binding energy, which, based on literature data, can be attributed to both residual sulfonate groups from PSS and sulfate groups from HSO_4[232]. To quantify the composition change, we calculated the featured peak areas of PSS and PEDOT chains and found that the PEDOT/PSS ratio increases from ≈0.4 to ≈1.2 after 3 days of sulfuric acid post-treatment. Although XPS only provides information about the very top layers of the films (≈1-10 nm), the increase of PEDOT/PSS ratio and the shift of the PSS peak suggests that excess insulating PSS^- is significantly replaced by HSO_4^- (Figure 7.1), also leading to the conformational change of the conjugated PEDOT chains and the reduction of barriers for inter-chain and inter-domain hopping, which would also explain the increase of electrical conductivity (Table 7.1)[233]. Overall, swelling test and XPS analysis indicate that increasing the time of the sulfuric acid post-treatment leads to removal of PSS, with consequent impairment of healing ability.

In addition, as the swelling of PEDOT:PSS occurs from both sides of a cut, the cut width (or gap width) plays a primary role in the healing performance. Here we found that, on ≈5 μm thick PEDOT:PSS films, water induced healing could be achieved on cuts obtained with different razor, surgical and ceramic blades, which produced widths ranging from ≈10 to ≈50 μm[217].

Table 7.1 Summary of healing behaviors and electrical conductivity of PEDOT:PSS after different processing methods and PEDOT with different dopants

Processing methods/ Conducting polymer name	Conductivity (S cm^{-1})	Healing response time (s)	Healing efficiency (%)
Glycerol (5 v/v%)	780±33	0.2±0.07	95.5±3.3
GOPS (0.5 v/v%) and glycerol (5 v/v%)	343±31	3.4±2.6	66±14
GOPS (1 v/v%) and glycerol (5 v/v%)	300±95	7.5±4.8	15±6
H_2SO_4 (pristine PEDOT:PSS soaked 10 min)	1080±234	0.4±0.23	93±3.4
H_2SO_4 (pristine PEDOT:PSS soaked 20 min)	1950±460	1.2±0.45	75.4±12.2
H_2SO_4 (pristine PEDOT:PSS soaked 30 min)	2430±572	3.2±1.2	69.2±10.5
H_2SO_4 (pristine PEDOT:PSS soaked 3 days)	2555±431	No healing	No healing
PEDOT:Tos	1636±364	0.28±0.14	94.3±3.6
PEDOT:OTf	2234±547	0.29±0.15	94.1±4.2
PEDOT:ClO_4		No healing	No healing

** The conductivity of PEDOT:ClO_4 could not be accessed due to the difficulty of achieving thin films via electro-polymerization and achieved thick films are too porous to get an accurate value during profilometry scans*

Creating cuts manually with razor blades presents several reproducibility issues, as the cut size might depend on the force applied by the operator and the angle of the blade with respect to the film. In order to achieve a controlled cut size, we adopted a novel method based on lithography and oxygen reactive ion etching (see the Experimental Section for details), which permits the patterning of squares of PEDOT:PSS films (thickness to ≈500 nm) on a glass substrate, separated by gaps with widths ranging from 5 to 100 µm (Figure SD4, Supporting Information)[44]. Even if the reactive ion etching can significantly change the chemistry of the PEDOT:PSS films, we found that a water drop enabled us to bridge gaps having a width of 5 µm and led to a significant increase in the current flowing between them (Figure 7.4a). Optical microscopy images and profilometry scans perpendicular to the channel clearly confirm the presence of material in the gap after wetting, even after water evaporation (Figure 7.4b,c, Figure SD5, Supporting Information). However, for larger gaps (10-100 µm), water droplets cannot successfully "heal" the gap, likely due to the limited volume expansion of thin PEDOT:PSS films during swelling.

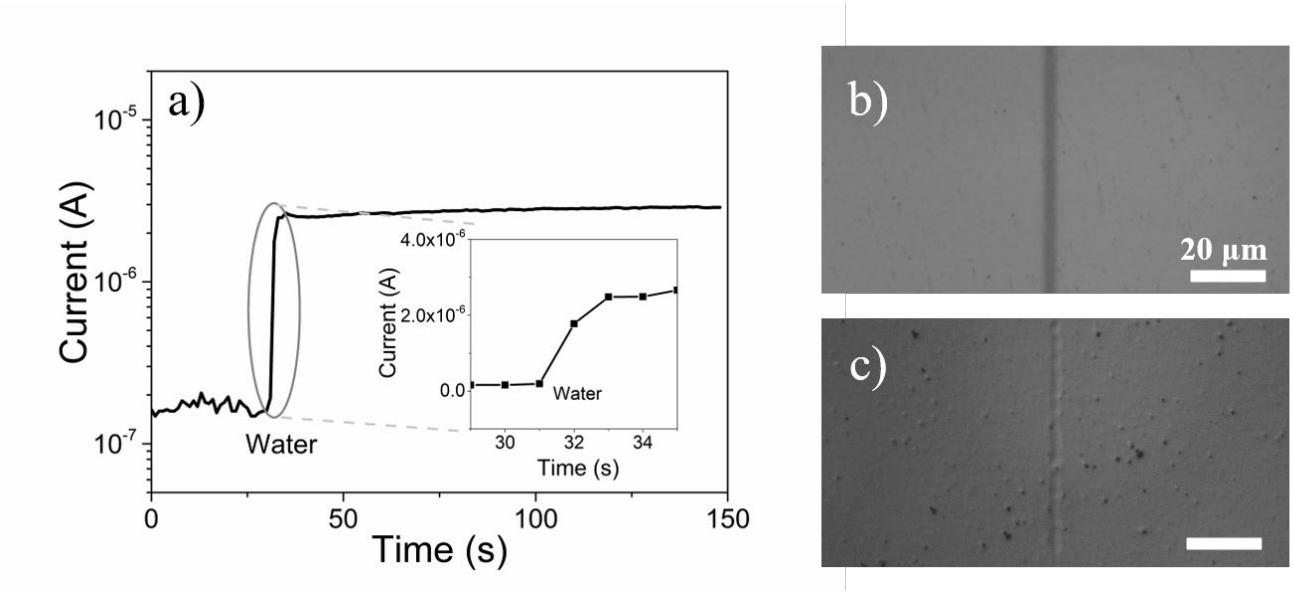

Figure 7.4 a) Current versus time profile of PEDOT:PSS squares and 5 µm width gap patterned by photolithography before and after the water drop on the gap area, and b) the optical images of PEDOT:PSS patterned squares before and c) after the water drop and baking. The thickness of PEDOT:PSS squares was kept to ≈500 nm. The applied voltage was 0.2 V.

So far, we have discussed different methods used to tailor the water-enabled healing behavior of conducting polymer PEDOT:PSS. Besides PSS, other dopants such as *para*-toluene sulfonate, trifluoromethanesulfonate, and inorganic anions are used in PEDOT-based conducting polymers for wearable electronics and bioelectronics (Figure SD6, Supporting Information)[82, 223, 232]. We produced PEDOT:Tos and PEDOT:OTf films via chemical polymerization, which showed electrical conductivities of ≈1600 and ≈2200 S cm^{-1}, respectively. Interestingly, the healing experiments showed that these materials can also be healed repeatedly by water, similarly to PEDOT:PSS (Figure 7.5a). Healing experiments were also carried out on conducting polymer films synthesized by electropolymerization and transferred to a glass substrate (details described in the experimental section). Here ClO_4^- is adopted as the dopant for PEDOT in electropolymerization because to small dopants generally have better electrochemical properties with respect to larger ones (e.g., PSS)[81, 82, 234, 235]. In this case, upon one cut, the water droplet cannot restore the initial current of PEDOT:ClO_4 film, and only induces a transient ionic current flow similar to that observed in PEDOT:PSS films soaked in sulfuric acid for 3 days (Figure 7.5a). The difference between the water-enabled healing abilities of these various conducting polymers is probably based on their ability to swell in water. To confirm this hypothesis, we performed water-soaking tests. PEDOT:Tos and PEDOT:OTf films show a slightly lower but still consistent weight increase compared to PEDOT:PSS upon immersion in water for 10 min, reaching values of ≈310% and ≈250%, respectively. PEDOT:ClO_4 films do not show any weight gain under the same conditions (Figure 7.5b). We hypothesize that organic dopants (Tos, OTf) occupy larger volumes compared to the inorganic dopant (ClO_4^-), leading to a less compact structure of the conducting polymer, and provide the film with many sites which may interact with water molecules, leading to significant volume expansion[17, 204, 236, 237]. The $HSO_4^-$and ClO_4^- are reported to be similar in size, with a thermochemical radius of 0.225 and 0.221 nm, respectively[236]. This can also explain why PEDOT:PSS films, after soaking in sulfuric acid for 3 days, lose their water-enabled healing behavior due to the removal or replacement of PSS with HSO_4^-. However, the different swelling behavior of the PEDOT films investigated in this work deserves further investigation, as differences might arise from several factors, such as the size and type of dopants, the film morphology and the PEDOT chain length[82, 232, 238].

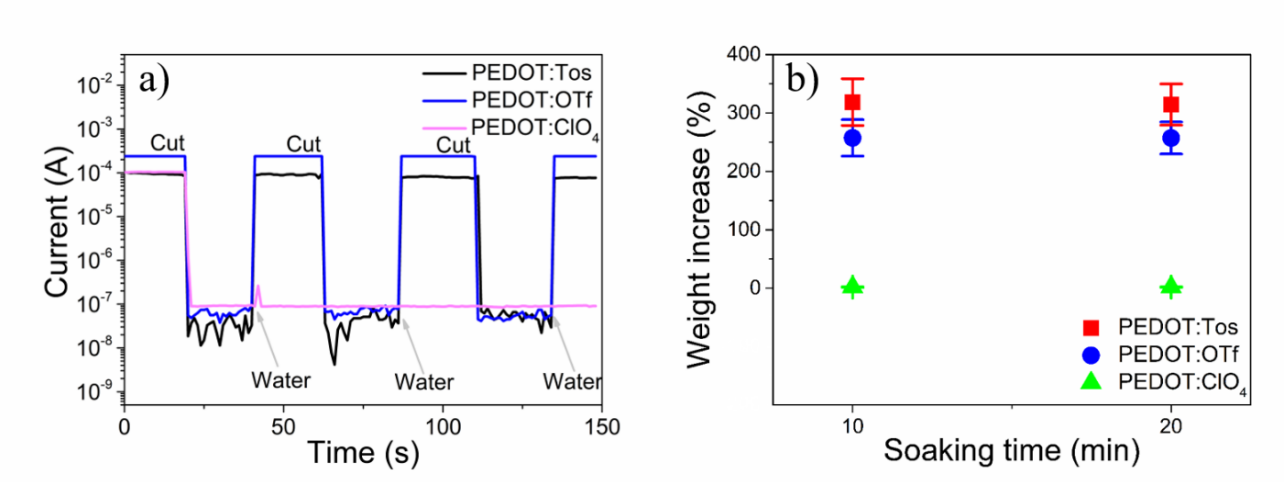

Figure 7.5 a) Current versus time profile of PEDOT:Tos and PEDOT:OTf film after several cuts in different areas of film, and of PEDOT:ClO_4 film after one-time blade cut and b) water uptake versus soaking time profile of different PEDOT films (N = 4). The thickness was ≈4-6 µm for PEDOT:Tos and PEDOT:OTf, and between 3 and 8 µm for PEDOT:ClO_4 films.

7.5 Conclusion

We demonstrated that the water-enabled healing ability of PEDOT:PSS can be tailored via processing. The presence of GOPS and sulfuric acid treatment weaken or eliminate water-enabled healing. Replacing the dopant PSS with other organic anions (Tos^- or OTf^-) results in films showing water-enabled healing, while replacement with the inorganic dopant ClO_4^- leads to suppression of the phenomenon, due to poor swelling ability. Finally, we showed that water "healing" can be achieved on 5 µm wide gaps, created by photolithography and etching, between two isolated squares of PEDOT:PSS films (thickness ≈500 nm). We believe this work will stimulate the development of future organic healable wearable electronics and biomedical applications.

7.6 Experimental section

Materials

The PEDOT:PSS aqueous suspension (Clevios PH1000) and Fe(III) *p*-toluenesulfonate in *n*-butanol (Clevios CB 54 V3) were purchased from Heraeus Electronic Materials GmbH (Leverkusen, Germany). Glycerol (99.5+% purity) was purchased from Caledon Laboratories Ltd.

(Georgetown, ON). (3-Glycidyloxypropyl)trimethoxysilane (GOPS), sulfuric acid (95%-98%), imidazole, $LiClO_4$, 3,4-ethylenedioxythiophene (EDOT), polyethylene glycol-polypropylene glycol-polyethylene glycol (PEG-PPG-PEG, M_w = 5800), *N*-methyl-2-pyrrolidone (NMP), ethanol and liquid metal gallium-indium eutectic (EGaIn 495425), phosphate buffer saline (PBS) tablets and sodium chloride (NaCl) were purchased from MilliporeSigma. Fe (III) trifluoromethanesulfonate ($Fe(OTf)_3$) was purchased from Alfa Chemicals. Deionized water (18.2 MΩ cm at 25 °C, Millipore), PBS (pH = 7.4), and NaCl solutions were used for healing experiments. PBS solutions were prepared from tablets dissolved in 200 mL deionized water yielding a solution of 0.01 phosphate buffer, 0.0027 m potassium chloride, and 0.137 m sodium chloride. The concentration of NaCl solutions was 0.01 m. All materials and chemicals were used without further treatment. Glass slides (Corning 2947—75 × 50) were purchased from Corning Incorporated.

PEDOT:PSS Processing and Patterning

Additives (glycerol, GOPS) were mixed with Clevios PH1000 in a centrifugal mixer (Thinky M310) at 2000 rpm for 5 min. Glycerol does not interfere in the water-enabled healing behavior but can raise the electrical conductivity of PEDOT:PSS, so it was added together with GOPS into PEDOT:PSS suspension in the experiments because GOPS deteriorates film conductivity[28, 104, 225]. The films were processed by drop-casting PEDOT:PSS mixtures (≈0.5 mL) onto glass substrates. After drop casting, the films were baked on a hot plate with the following sequence: 50 °C for 1 h, 90 °C for 2 h, and finally 140 °C for 6 h. The gradual temperature increase permitted us to obtain continuous films without the formation of bubbles. The thickness of the films was kept to ≈5μm, as we have previously shown that films with thicknesses ranging between 1 and 10 μm show very similar healing performance[104].

Soaking of films in sulfuric acid was carried out in a glass petri dish. After soaking, films were rinsed with DI water to remove excess acid and dried on a hot plate at 140 °C for 15 min.

PEDOT:PSS films used for self-healing tests on lithographically induced gaps were deposited by spin coating two layers from Clevios PH1000 suspension on precleaned glass slide at 700 rpm for 30 s to get a thicker film. Thicker film here was desired for healing test according to our previous work[104]. The sample was baked at 140 °C for 1 h after the deposition of each layer. A Karl Suss

MA-6/BA-6 mask aligner (wavelength 365 nm, intensity of 8 mW cm^{-2}) was used for photolithography. Oxygen reactive ion etching was performed with an ENI OEM-6 apparatus.

Synthesis of PEDOT:OTf

PEDOT:OTf was synthesized by chemical polymerization of EDOT in presence of the oxidant $Fe(OTf)_3$ in a mixture of 72 wt% ethanol, 8 wt% NMP, and 20 wt% PEG-PPG-PEG[222]. 126 mg of $Fe(OTf)_3$ were dissolved in 1 mL of solvent mixture and sonicated for 2 h. This solution was mixed with 20 µL of EDOT for 30 s and then sonicated for 10 s, and finally was drop-cast or spin-coated at 1000 rpm on a glass substrate. The resulting films were baked on a hot plate at 120 °C for 40 min, rinsed twice with ethanol and dried. The film thickness of was ≈4-6 µm.

Synthesis of PEDOT:Tos

PEDOT:Tos was synthesized by chemical polymerization of EDOT in the presence of the oxidant Fe (III) *p*-toluenesulfonate[223]. A solution composed of 2 mL of Fe(III) *p*-toluenesulfonate in *n*-butanol and 0.073 g imidazole was stirred in a centrifugal mixer (Thinky M310) at 2000 rpm for 30 min. Then 0.1 mL of EDOT was added into the solution and mixed by the centrifugal mixer at 2000 rpm for 30 s. Then the solution was drop-cast or spin-coated at 1000 rpm for 30 s on the glass substrate. Then the samples were baked at 140 °C for 20 min, rinsed twice with ethanol and dried in nitrogen. The film thickness of was ≈4-6 µm.

Synthesis of PEDOT:ClO_4

Electropolymerization of PEDOT:ClO_4 was carried out galvanostatically in an acetonitrile solution containing 30 × 10^{-3} m EDOT monomer and 120 × 10^{-3} m $LiClO_4$ in a three-electrode electrochemical cell, using a Bio-Logic VSP-300 potentiostat equipped with the EC-Lab software[82]. Silver/silver chloride (Ag/AgCl) was used as the reference electrode, a Pt wire as the counter electrode, and a stainless-steel sheet with a size of ≈(6 × 1) cm as the working electrode. All working electrodes were rinsed in acetone, IPA, and deionized water and dried with nitrogen. The solutions were degassed for 10 min with nitrogen prior to electropolymerization and a nitrogen blanket was maintained during the electropolymerization to limit the oxygen concentration in the solution and avoid unwanted oxidation reactions[239]. After electrodeposition, the PEDOT:ClO_4 films were gently transferred from the stainless-steel sheet to the glass slide using a thermal release film tape (TFA1106, Koan Hao Technology Co Ltd.) because of the higher adhesion force of

PEDOT:ClO_4 film onto tape with respect to the stainless-steel sheet. Then the glass slide was baked at 120 °C for 5 min to ensure the decomposition of the tape. The films were finally gently rinsed with deionized water and dried on a hot plate at 140 °C for 20 min. The film thickness was of ≈3-8 μm.

Film Characterization

The film thickness was measured with a profilometer (Dektak 150) using a 12.5 μm stylus tip with a 10 mg load. Optical microscopy images were obtained with a Carl Zeiss microscope. SEM was performed with a JEOL JSM-7600TFE field emission (FE-SEM) with a voltage of 5.0 kV (LEI) under a vacuum of 10^{-4} Pa. Electrical conductivity measurements were carried out on thin films deposited by spin coating at 1000 rpm and baked at 140 °C for 1 h. Sheet resistance was measured by a four-point probe (Jandel Engineering) connected to an Agilent B2902A voltage-current source measure unit. XPS was performed using a VG ESCALAB 3MkII system with MgK X-ray source in an ultrahigh vacuum.

Self-Healing Test

Self-healing experiments were carried out in ambient air on films with a size of ≈(6.0 × 1.5) cm, and a thickness of ≈15 μm. Electrical contacts were made via two tungsten probes immersed into EGaIn contacts at the two sides of the film and the current was measured with an electrical probe station equipped with a National Instruments NI PXIe-1062Q source-measure unit controlled by Labview software. The voltage applied in the healing test was 0.2 V. A droplet (≈40 μL) of deionized (DI) water (18.2 MΩ cm at 25 °C, Millipore) was used as the healing agent for water-enabled healing. The time for current recovery is referred as the healing time; the ratio $\eta=(I_{healed}-I_{damaged})/(I_{pristine}-I_{damaged})$, where I is the current measured for pristine, damaged, and healed films, as the healing efficiency.

Swelling Test

PEDOT:PSS films were weighed by an analytic balance (Sartorius BP 210 D) right after baking to record their initial mass and successively soaked in DI water for 10-30 min. They were then removed from the water and transferred onto a piece of lint-free paper using tweezers. The water on the surface of the films was dried off and the samples were weighed for a second time. The mass

increase of each sample was calculated using the following formula, where M_w is the mass of the wet film and M_D is mass of dry film

$$\text{Weight Increase (\%)} = (M_w - M_D)/M_D \times 100$$

7.7 Acknowledgments

This work was supported by grants NSERC Discovery and Department of National Defence Discovery supplement and IDEAS CFPMN1-008, awarded to F.C. Y.L. is grateful to the Centre de Recherche sur les Systèmes Polymères et Composites à Haute Performance (CREPEC) and Polytechnique Montréal for partial financial support. N.H. acknowledges support from FRQNT through a Scholarship for Reentering the Research Community. The authors are grateful to CMC Microsystems for support through the program MNT financial assistance.

CHAPTER 8 GENERAL DISCUSSION

In the following, the results of Chapter 4 to 7 are discussed as a whole with reference to the literature presented in Chapter 2. A detailed study of the fundamental properties of PEDOT:PSS is presented in this thesis, and many insights have been gained in terms of processing, mechanical stretchability and self-healing ability. Advanced methods have been developed to enhance both stretchability and transistor performance of stretchable OECTs. We also demonstrate a facile method to achieve autonomic healing behavior of PEDOT:PSS and are able to tailor the healing performance of conducting polymer films via processing methods.

In the chapter 4, OECTs were fabricated on PDMS elastomer substrate via adding fluorosurfactant Zonyl to obtain stretchability. However, the strain range for the stable operation of OECTs is up to 30%, and there is a trade-off between the stretchability and transistor performance when a ultrathin parylene layer is deposited between the PEDOT:PSS channel and elastomer substrate. To solve this problem, we hypothesize that if the secondary plasticizer can also improve the conductivity and ion transport of PEDOT:PSS, the transistor performance of the stretchable OECTs may also be improved. As a result, in the article 1, we enhanced both stretchability and the transistor performance via the addition of PEG. Due to the excellent plasticizing effect of PEG, we have shown that PEG can increase the strain-insensitive range and failure strain of PEDOT:PSS film on PDMS. More importantly, PEG addition creates a thickness-independent strain-insensitive range for PEDOT:PSS films, allowing us to fabricate stretchable OECTs with thicker film for higher transconductance. This is a very important discovery in the field of stretchable OECTs, because usually channel material thickness is lowered to obtain better stretchability, while the transconductance is sacrificed.

The knowledge we gained in article 1 inspired us to achieve the autonomic healing behavior of PEDOT:PSS film via using PEG to change the mechanical properties. Since polymer chain diffusion plays an important role in the healing ability of polymers, we also hypothesize that change of flow ability of PEDOT:PSS after plasticizer addition may lead to the variation of healing property. In article 2, we used PEG to soften PEDOT:PSS film and achieve repeatable, fast, and high-efficiency autonomic healing. We also found that the healing behavior of PEDOT:PSS/PEG

film can be tuned from autonomic healing to water-enabled healing by decreasing PEG addition amount, post treatment with methanol, and increasing the molecular weight of PEG.

As the water enabled healing behavior of PEDOT:PSS is hypothesized mainly to be related with the swelling, we believe that any change of PSS concentration in the films would lead to a change in self-healing properties. In article 3, we further studied the healing behavior of PEDOT under diverse processing conditions or synthetic methods. We confirmed that the swelling of dopants plays the importance role in the healing behavior of conducting polymers. The presence of crosslinker GOPS as well as a long-time post-treatment with concentrated sulfuric acid significantly decrease the swelling and impair the healing ability of PEDOT:PSS. Organic dopants of PEDOT have high water swelling ratios and lead to water-enabled healing, while inorganic dopants fail in the healing of PEDOT. Besides, we preliminarily studied the effect of cut width and film thickness on healing of PEDOT:PSS. The cuts made by various blades on ~ 5 μm thick PEDOT:PSS film with width ranging from ~ 10 to ~ 50 μm are all healed by water. The "healing" of nanoscale PEDOT:PSS film (~ 500 nm) is also achieved by narrowing down the gap to ~5 μm via photolithography and reactive ion etching. From article 2 and article 3, we have gained more profound understanding of the healing behavior of conducting polymers.

We believe the principle we adopt in Article 1 for fabrication of high-performance stretchable electronics as well as the knowledge regarding to the self-healing properties of conducting polymers in Article 2 and Article 3, will pave the way to self-healing wearable electronics in the areas of conductors, surface coatings, energy storage devices, and biomedical sensors. Despite there are still limitations for the materials or devices (discussed in chapter 9), this thesis contributes to the advancement of technology in organic bioelectronics and we believe a significant improvement can be realized in the near future to meet the requirements for commercial applications.

CHAPTER 9 CONCLUSION AND RECOMMANDATIONS

This thesis explored the possibility to tune the stretchability and healing property of conducting polymer PEDOT:PSS for organic bioelectronics. We further improved the device performance of our stretchable OECTs previously reported and gained deeper knowledge about the healing behavior of the conducting polymer PEDOT:PSS. A lot of work have been done on enhancing the stretchability of PEDOT:PSS, reporting a maximum fracture strain of 800%[31]. However, our goal is totally different because we want to have a maximum strain that allows us to have stable during stretching and releasing. As for the healing, we mainly work on the healing property of conducting polymers, which has been done by very few groups. And we want to enhance the healing property of PEDOT:PSS without sacrificing the biocompatibility, since our target is organic bioelectronics.

Our first goal is to fabricate stretchable OECTs on PDMS substrate without buckling method and improve the transistor performance without sacrificing stretchability. We have demonstrated that the addition of PEG can both increase the stretchability of PEDOT:PSS films, enabling us to fabricate OECTs with thicker channel film for higher transconductance. In addition, OECTs fabricated with PEDOT:PSS/PEG channel also shows higher ON/OFF ratio and faster response time. However, the mechanism of performance improvement is still not well understood. Future study can focus on the detailed effects of PEG addition on PEDOT:PSS film, such as the improved ionic transport and overall lowered impedance, as well as possible antifouling and anti-freezing properties. Furthermore, due to the good solubility of PEG in water, the long-term stability of these OECTs operating with aqueous electrolyte needs to be improved. Compared with thin PEDOT:PSS films, PEDOT hydrogels described in the literature review section have much smaller modulus and comparable mechanical properties to human tissues. Despite the promising future of these hydrogels in the organic bioelectronics, they suffer a poor stability due to the loss of water. In the future, PEG could be exploited as a stabilizer for PEDOT hydrogels due to its non-volatile property.

Our second goal is to develop a stable, biocompatible, and autonomically healable conductor based on PEDOT:PSS and obtain a deeper understanding on the water-enable behavior of PEDOT:PSS. We have shown that addition of PEG can significantly soften the PEDOT:PSS and leads to a repeatable autonomic healable conductor with high healing efficiency and fast response time. Via in situ cutting monitoring and mechanical characterization, we hypothesize that PEDOT:PSS/PEG

film can achieve healing via flowing back to damaged areas. The PEG addition also helps conducting polymer film to obtain good water-stability and air-stability.

The swelling abilities of PEDOT based materials are believed to be likely related to their healing behaviors. We have successfully proved that the healing performance of PEDOT based material can be tuned by varying processing methods, dopants or polymerization methods. We also have preliminarily demonstrated that the healing performance of PEDOT:PSS films is associated with the film thickness and the cut width, which needs to systematically investigated in the future.

Self-healable conducting polymers are recent-established materials for the next-generation electronics. In terms of the future work, the first challenge is to improve the healing property of PEDOT-based material. Molecular structure design could be an alternative to gain healing ability, via side chain grafting on the backbone or incorporation of specific ions upon doping, providing more possible dynamic bonding sites. However, their effects on molecular chain alignment and stacking, and the trade-off between conductivity and healing ability needs further investigation. Substantial efforts need to be contributed to improving the healing performance of the current healable materials, including increasing the healing efficiency with ultra-short response time (less than 0.1 s). Processing PEDOT:PSS with plasticizer and hydrogel network can render the healable composite with fast recovery speed and high efficiency. However, with the arising of bioelectronics, biocompatible plasticizers and/or hydrogel network are often required to enable the further implementation of on-skin or in vivo applications. The second concern is the stability or reliability of self-healing materials based on PEDOT and its composites. For instance, physical molecular diffusion assisted by the high water ratio inside hydrogels cannot guarantee the eternal healing performance due to the unavoidable water evaporation at ambient conditions. The dynamic reversible bonds embedded in healable materials are often sensitive to temperature, affecting the mechanical properties. The third challenge is to provide healable materials with the ease of tunable healing performance. Taking advantage of the excellent processability of PEDOT, the tunable and diverse healing performance can significantly endow PEDOT-based materials with more functionalities in potential applications, such as optoelectronic devices and actuators.

REFERENCES

[1] T. Someya, Z. Bao, and G. G. Malliaras, "The rise of plastic bioelectronics," *Nature,* vol. 540, pp. 379-385, 2016.

[2] D. Ohayon and S. Inal, "Organic Bioelectronics: From Functional Materials to Next-Generation Devices and Power Sources," *Advanced Materials,* vol. 32, p. 2001439, 2020.

[3] D. T. Simon, E. O. Gabrielsson, K. Tybrandt, and M. Berggren, "Organic bioelectronics: bridging the signaling gap between biology and technology," *Chem. Rev,* vol. 116, pp. 13009-13041, 2016.

[4] S. J. Benight, C. Wang, J. B. H. Tok, and Z. Bao, "Stretchable and self-healing polymers and devices for electronic skin," *Progress in Polymer Science,* vol. 38, pp. 1961-1977, 2013.

[5] M. Berggren and A. Richter-Dahlfors, "Organic Bioelectronics," *Advanced Materials,* vol. 19, pp. 3201-3213, 2007.

[6] F. Jonas, W. Krafft, and B. Muys, "Poly(3, 4-ethylenedioxythiophene): Conductive coatings, technical applications and properties," *Macromolecular Symposia,* vol. 100, pp. 169-173, 1995.

[7] Z. Rahimzadeh, S. M. Naghib, Y. Zare, and K. Y. Rhee, "An overview on the synthesis and recent applications of conducting poly(3,4-ethylenedioxythiophene) (PEDOT) in industry and biomedicine," *Journal of Materials Science,* vol. 55, pp. 7575-7611, 2020.

[8] B. D. Paulsen, K. Tybrandt, E. Stavrinidou, and J. Rivnay, "Organic mixed ionic–electronic conductors," *Nature Materials,* vol. 19, pp. 13-26, 2020.

[9] "Twenty-five years of conducting polymers," *Chemical Communications,* pp. 1-4, 2003.

[10] J. J. Urban, "One model to rule them all," *Nature Materials,* vol. 16, pp. 157-159, 2017.

[11] Y. van de Burgt, A. Melianas, S. T. Keene, G. Malliaras, and A. Salleo, "Organic electronics for neuromorphic computing," *Nature Electronics,* vol. 1, pp. 386-397, 2018.

[12] H. He, L. Zhang, X. Guan, H. Cheng, X. Liu, S. Yu*, et al.*, "Biocompatible Conductive Polymers with High Conductivity and High Stretchability," *ACS Applied Materials & Interfaces,* vol. 11, pp. 26185-26193, 2019.

[13] M. J. Donahue, A. Sanchez-Sanchez, S. Inal, J. Qu, R. M. Owens, D. Mecerreyes*, et al.*, "Tailoring PEDOT properties for applications in bioelectronics," *Materials Science and Engineering: R: Reports,* vol. 140, p. 100546, 2020.

[14] S. Kee, N. Kim, B. Park, B. S. Kim, S. Hong, J.-H. Lee*, et al.*, "Highly Deformable and See-Through Polymer Light-Emitting Diodes with All-Conducting-Polymer Electrodes," *Advanced Materials,* vol. 30, p. 1703437, 2018.

[15] P. Friederich, A. Fediai, S. Kaiser, M. Konrad, N. Jung, and W. Wenzel, "Toward Design of Novel Materials for Organic Electronics," *Advanced Materials,* vol. 31, p. 1808256, 2019.

[16] D. N. Nguyen and H. Yoon, "Recent advances in nanostructured conducting polymers: from synthesis to practical applications," *Polymers,* vol. 8, p. 118, 2016.

[17] J. Ouyang, "“Secondary doping” methods to significantly enhance the conductivity of PEDOT:PSS for its application as transparent electrode of optoelectronic devices," *Displays,* vol. 34, pp. 423-436, 2013.

[18] J. Tsukamoto, "Recent advances in highly conductive polyacetylene," *Advances in Physics,* vol. 41, pp. 509-546, 1992.

[19] J. L. Bredas and G. B. Street, "Polarons, bipolarons, and solitons in conducting polymers," *Accounts of Chemical Research,* vol. 18, pp. 309-315, 1985.

[20] I. Zozoulenko, A. Singh, S. K. Singh, V. Gueskine, X. Crispin, and M. Berggren, "Polarons, Bipolarons, And Absorption Spectroscopy of PEDOT," *ACS Applied Polymer Materials,* vol. 1, pp. 83-94, 2019.

[21] G. Tourillon and F. Garnier, "New electrochemically generated organic conducting polymers," *Journal of Electroanalytical Chemistry and Interfacial Electrochemistry,* vol. 135, pp. 173-178, 1982.

[22] T. Horii, Y. Li, Y. Mori, and H. Okuzaki, "Correlation between the hierarchical structure and electrical conductivity of PEDOT/PSS," *Polymer Journal,* vol. 47, pp. 695-699, 2015.

[23] N. M. Nair, J. K. Pakkathillam, K. Kumar, K. Arunachalam, D. Ray, and P. Swaminathan, "Printable Silver Nanowire and PEDOT:PSS Nanocomposite Ink for Flexible Transparent Conducting Applications," *ACS Applied Electronic Materials,* vol. 2, pp. 1000-1010, 2020.

[24] P. Wang, M. Hu, H. Wang, Z. Chen, Y. Feng, J. Wang*, et al.*, "The Evolution of Flexible Electronics: From Nature, Beyond Nature, and To Nature," *Advanced Science,* p. 2001116, 2020.

[25] Y. Xia and J. Ouyang, "Significant Different Conductivities of the Two Grades of Poly(3,4-ethylenedioxythiophene):Poly(styrenesulfonate), Clevios P and Clevios PH1000, Arising from Different Molecular Weights," *ACS Applied Materials & Interfaces,* vol. 4, pp. 4131-4140, 2012.

[26] X. Fan, W. Nie, H. Tsai, N. Wang, H. Huang, Y. Cheng*, et al.*, "PEDOT:PSS for Flexible and Stretchable Electronics: Modifications, Strategies, and Applications," *Advanced Science,* vol. 6, p. 1900813, 2019.

[27] J. Y. Kim, J. H. Jung, D. E. Lee, and J. Joo, "Enhancement of electrical conductivity of poly(3,4-ethylenedioxythiophene)/poly(4-styrenesulfonate) by a change of solvents," *Synthetic Metals,* vol. 126, pp. 311-316, 2002.

[28] S. Zhang, P. Kumar, A. S. Nouas, L. Fontaine, H. Tang, and F. Cicoira, "Solvent-induced changes in PEDOT:PSS films for organic electrochemical transistors," *APL Materials,* vol. 3, p. 014911, 2015.

[29] D. Alemu Mengistie, P.-C. Wang, and C.-W. Chu, "Effect of molecular weight of additives on the conductivity of PEDOT:PSS and efficiency for ITO-free organic solar cells," *Journal of Materials Chemistry A,* vol. 1, pp. 9907-9915, 2013.

[30] D. Huang, T. Goh, J. Kong, Y. Zheng, S. Zhao, Z. Xu*, et al.*, "Perovskite solar cells with a DMSO-treated PEDOT:PSS hole transport layer exhibit higher photovoltaic performance and enhanced durability," *Nanoscale,* vol. 9, pp. 4236-4243, 2017.

[31] Y. Wang, C. Zhu, R. Pfattner, H. Yan, L. Jin, S. Chen*, et al.*, "A highly stretchable, transparent, and conductive polymer," *Science Advances,* vol. 3, p. e1602076, 2017.

[32] D. Alemu, H.-Y. Wei, K.-C. Ho, and C.-W. Chu, "Highly conductive PEDOT:PSS electrode by simple film treatment with methanol for ITO-free polymer solar cells," *Energy & Environmental Science,* vol. 5, pp. 9662-9671, 2012.

[33] J. Y. Oh, M. Shin, J. B. Lee, J.-H. Ahn, H. K. Baik, and U. Jeong, "Effect of PEDOT Nanofibril Networks on the Conductivity, Flexibility, and Coatability of PEDOT:PSS Films," *ACS Applied Materials & Interfaces,* vol. 6, pp. 6954-6961, 2014.

[34] Y. Xia, K. Sun, and J. Ouyang, "Solution-Processed Metallic Conducting Polymer Films as Transparent Electrode of Optoelectronic Devices," *Advanced Materials,* vol. 24, pp. 2436-2440, 2012.

[35] N. Kim, S. Kee, S. H. Lee, B. H. Lee, Y. H. Kahng, Y.-R. Jo*, et al.*, "Highly Conductive PEDOT:PSS Nanofibrils Induced by Solution-Processed Crystallization," *Advanced Materials,* vol. 26, pp. 2268-2272, 2014.

[36] Y. Xia and J. Ouyang, "Significant Conductivity Enhancement of Conductive Poly(3,4-ethylenedioxythiophene): Poly(styrenesulfonate) Films through a Treatment with Organic Carboxylic Acids and Inorganic Acids," *ACS Applied Materials & Interfaces,* vol. 2, pp. 474-483, 2010.

[37] W. Jang, S. Ahn, S. Park, J. H. Park, and D. H. Wang, "Counterbalancing of morphology and conductivity of poly(3,4-ethylenedioxythiophene) polystyrene sulfonate based flexible devices," *Nanoscale,* vol. 8, pp. 19557-19563, 2016.

[38] J. Ouyang, "Solution-Processed PEDOT:PSS Films with Conductivities as Indium Tin Oxide through a Treatment with Mild and Weak Organic Acids," *ACS Applied Materials & Interfaces,* vol. 5, pp. 13082-13088, 2013.

[39] S.-S. Yoon and D.-Y. Khang, "Roles of Nonionic Surfactant Additives in PEDOT:PSS Thin Films," *The Journal of Physical Chemistry C,* vol. 120, pp. 29525-29532, 2016.

[40] S. Savagatrup, E. Chan, S. M. Renteria-Garcia, A. D. Printz, A. V. Zaretski, T. F. O'Connor*, et al.*, "Plasticization of PEDOT:PSS by Common Additives for Mechanically Robust Organic Solar Cells and Wearable Sensors," *Advanced Functional Materials,* vol. 25, pp. 427-436, 2015.

[41] C. Yeon, G. Kim, J. W. Lim, and S. J. Yun, "Highly conductive PEDOT:PSS treated by sodium dodecyl sulfate for stretchable fabric heaters," *RSC Advances,* vol. 7, pp. 5888-5897, 2017.

[42] B. Fan, X. Mei, and J. Ouyang, "Significant Conductivity Enhancement of Conductive Poly(3,4-ethylenedioxythiophene):Poly(styrenesulfonate) Films by Adding Anionic Surfactants into Polymer Solution," *Macromolecules,* vol. 41, pp. 5971-5973, 2008.

[43] G. Latessa, F. Brunetti, A. Reale, G. Saggio, and A. Di Carlo, "Piezoresistive behaviour of flexible PEDOT:PSS based sensors," *Sensors and Actuators B: Chemical,* vol. 139, pp. 304-309, 2009.

[44] S. Zhang, E. Hubis, C. Girard, P. Kumar, J. DeFranco, and F. Cicoira, "Water stability and orthogonal patterning of flexible micro-electrochemical transistors on plastic," *Journal of Materials Chemistry C,* vol. 4, pp. 1382-1385, 2016.

[45] U. Lang, N. Naujoks, and J. Dual, "Mechanical characterization of PEDOT:PSS thin films," *Synthetic Metals,* vol. 159, pp. 473-479, 2009.

[46] M. Vosgueritchian, D. J. Lipomi, and Z. Bao, "Highly Conductive and Transparent PEDOT:PSS Films with a Fluorosurfactant for Stretchable and Flexible Transparent Electrodes," *Advanced Functional Materials,* vol. 22, pp. 421-428, 2012.

[47] D. J. Lipomi, J. A. Lee, M. Vosgueritchian, B. C. K. Tee, J. A. Bolander, and Z. Bao, "Electronic Properties of Transparent Conductive Films of PEDOT:PSS on Stretchable Substrates," *Chemistry of Materials,* vol. 24, pp. 373-382, 2012.

[48] M. Y. Teo, N. Kim, S. Kee, B. S. Kim, G. Kim, S. Hong*, et al.*, "Highly Stretchable and Highly Conductive PEDOT:PSS/Ionic Liquid Composite Transparent Electrodes for Solution-Processed Stretchable Electronics," *ACS Applied Materials & Interfaces,* vol. 9, pp. 819-826, 2017.

[49] P. Li, K. Sun, and J. Ouyang, "Stretchable and Conductive polymer films prepared by solution blending," *ACS applied materials & interfaces,* vol. 7, pp. 18415-18423, 2015.

[50] L. Bai, C. G. Elósegui, W. Li, P. Yu, J. Fei, and L. Mao, "Biological Applications of Organic Electrochemical Transistors: Electrochemical Biosensors and Electrophysiology Recording," *Frontiers in Chemistry,* vol. 7, 2019.

[51] H. S. White, G. P. Kittlesen, and M. S. Wrighton, "Chemical derivatization of an array of three gold microelectrodes with polypyrrole: fabrication of a molecule-based transistor," *Journal of the American Chemical Society,* vol. 106, pp. 5375-5377, 1984.

[52] A. Giovannitti, I. P. Maria, D. Hanifi, M. J. Donahue, D. Bryant, K. J. Barth*, et al.*, "The Role of the Side Chain on the Performance of N-type Conjugated Polymers in Aqueous Electrolytes," *Chemistry of Materials,* vol. 30, pp. 2945-2953, 2018.

[53] A. M. Pappa, D. Ohayon, A. Giovannitti, I. P. Maria, A. Savva, I. Uguz*, et al.*, "Direct metabolite detection with an n-type accumulation mode organic electrochemical transistor," *Science Advances,* vol. 4, p. eaat0911, 2018.

[54] C. B. Nielsen, A. Giovannitti, D.-T. Sbircea, E. Bandiello, M. R. Niazi, D. A. Hanifi*, et al.*, "Molecular design of semiconducting polymers for high-performance organic electrochemical transistors," *Journal of the American Chemical Society,* vol. 138, pp. 10252-10259, 2016.

[55] D. A. Bernards and G. G. Malliaras, "Steady-State and Transient Behavior of Organic Electrochemical Transistors," *Advanced Functional Materials,* vol. 17, pp. 3538-3544, 2007.

[56] J. T. Friedlein, R. R. McLeod, and J. Rivnay, "Device physics of organic electrochemical transistors," *Organic Electronics,* vol. 63, pp. 398-414, 2018.

[57] J. Rivnay, S. Inal, A. Salleo, R. M. Owens, M. Berggren, and G. G. Malliaras, "Organic electrochemical transistors," *Nature Reviews Materials,* vol. 3, p. 17086, 2018.

[58] G. D. Spyropoulos, J. Savarin, E. F. Gomez, D. T. Simon, M. Berggren, J. N. Gelinas*, et al.*, "Transcranial Electrical Stimulation and Recording of Brain Activity using Freestanding Plant-Based Conducting Polymer Hydrogel Composites," *Advanced Materials Technologies,* vol. 5, p. 1900652, 2020.

[59] S. Inal, G. G. Malliaras, and J. Rivnay, "Benchmarking organic mixed conductors for transistors," *Nature Communications,* vol. 8, p. 1767, 2017.

[60] D. Khodagholy, J. Rivnay, M. Sessolo, M. Gurfinkel, P. Leleux, L. H. Jimison*, et al.*, "High transconductance organic electrochemical transistors," *Nature Communications,* vol. 4, p. 2133, 2013.

[61] G. C. Faria, D. T. Duong, and A. Salleo, "On the transient response of organic electrochemical transistors," *Organic Electronics,* vol. 45, pp. 215-221, 2017.

[62] E. Zeglio and O. Inganäs, "Active Materials for Organic Electrochemical Transistors," *Advanced Materials,* vol. 30, p. 1800941, 2018.

[63] P. Leleux, J.-M. Badier, J. Rivnay, C. Bénar, T. Hervé, P. Chauvel*, et al.*, "Conducting Polymer Electrodes for Electroencephalography," *Advanced Healthcare Materials,* vol. 3, pp. 490-493, 2014.

[64] S. Carli, M. Bianchi, E. Zucchini, M. Di Lauro, M. Prato, M. Murgia*, et al.*, "Electrodeposited PEDOT:Nafion Composite for Neural Recording and Stimulation," *Advanced Healthcare Materials,* vol. 8, p. 1900765, 2019.

[65] S. K. Sinha, Y. Noh, N. Reljin, G. M. Treich, S. Hajeb-Mohammadalipour, Y. Guo*, et al.*, "Screen-Printed PEDOT:PSS Electrodes on Commercial Finished Textiles for Electrocardiography," *ACS Applied Materials & Interfaces,* vol. 9, pp. 37524-37528, 2017.

[66] Q. Wang, X. Pan, C. Lin, D. Lin, Y. Ni, L. Chen*, et al.*, "Biocompatible, self-wrinkled, antifreezing and stretchable hydrogel-based wearable sensor with PEDOT:sulfonated lignin as conductive materials," *Chemical Engineering Journal,* vol. 370, pp. 1039-1047, 2019.

[67] P. Leleux, C. Johnson, X. Strakosas, J. Rivnay, T. Hervé, R. M. Owens*, et al.*, "Ionic Liquid Gel-Assisted Electrodes for Long-Term Cutaneous Recordings," *Advanced Healthcare Materials,* vol. 3, pp. 1377-1380, 2014.

[68] D. Khodagholy, T. Doublet, P. Quilichini, M. Gurfinkel, P. Leleux, A. Ghestem*, et al.*, "In vivo recordings of brain activity using organic transistors," *Nature Communications,* vol. 4, p. 1575, 2013.

[69] A. Campana, T. Cramer, D. T. Simon, M. Berggren, and F. Biscarini, "Electrocardiographic Recording with Conformable Organic Electrochemical Transistor Fabricated on Resorbable Bioscaffold," *Advanced Materials,* vol. 26, pp. 3874-3878, 2014.

[70] H. Lee, S. Lee, W. Lee, T. Yokota, K. Fukuda, and T. Someya, "Ultrathin Organic Electrochemical Transistor with Nonvolatile and Thin Gel Electrolyte for Long-Term Electrophysiological Monitoring," *Advanced Functional Materials,* vol. 29, p. 1906982, 2019.

[71] J. Wang and F. Zhuge, "Memristive Synapses for Brain-Inspired Computing," *Advanced Materials Technologies,* vol. 4, p. 1800544, 2019.

[72] Y. Park and J.-S. Lee, "Artificial synapses with short-and long-term memory for spiking neural networks based on renewable materials," *ACS nano,* vol. 11, pp. 8962-8969, 2017.

[73] P. Gkoupidenis, N. Schaefer, B. Garlan, and G. G. Malliaras, "Neuromorphic Functions in PEDOT:PSS Organic Electrochemical Transistors," *Advanced Materials,* vol. 27, pp. 7176-7180, 2015.

[74] J. Sun, Y. Fu, and Q. Wan, "Organic synaptic devices for neuromorphic systems," *Journal of Physics D: Applied Physics,* vol. 51, p. 314004, 2018.

[75] S. Carli, M. Di Lauro, M. Bianchi, M. Murgia, A. De Salvo, M. Prato*, et al.*, "Water-Based PEDOT:Nafion Dispersion for Organic Bioelectronics," *ACS Applied Materials & Interfaces,* vol. 12, pp. 29807-29817, 2020.

[76] S. Yamamoto and G. G. Malliaras, "Controlling the Neuromorphic Behavior of Organic Electrochemical Transistors by Blending Mixed and Ion Conductors," *ACS Applied Electronic Materials,* vol. 2, pp. 2224-2228, 2020.

[77] R. Green and M. R. Abidian, "Conducting Polymers for Neural Prosthetic and Neural Interface Applications," *Advanced Materials,* vol. 27, pp. 7620-7637, 2015.

[78] K. A. Ludwig, N. B. Langhals, M. D. Joseph, S. M. Richardson-Burns, J. L. Hendricks, and D. R. Kipke, "Poly(3,4-ethylenedioxythiophene) (PEDOT) polymer coatings facilitate smaller neural recording electrodes," *Journal of Neural Engineering,* vol. 8, p. 014001, 2011.

[79] Y. Qiang, P. Artoni, K. J. Seo, S. Culaclii, V. Hogan, X. Zhao*, et al.*, "Transparent arrays of bilayer-nanomesh microelectrodes for simultaneous electrophysiology and two-photon imaging in the brain," *Science Advances,* vol. 4, p. eaat0626, 2018.

[80] G. Dijk, H. J. Ruigrok, and R. P. O'Connor, "Influence of PEDOT:PSS Coating Thickness on the Performance of Stimulation Electrodes," *Advanced Materials Interfaces,* vol. 7, p. 2000675, 2020.

[81] C. Bodart, N. Rossetti, J. E. Hagler, P. Chevreau, D. Chhin, F. Soavi*, et al.*, "Electropolymerized Poly(3,4-ethylenedioxythiophene) (PEDOT) Coatings for Implantable Deep-Brain-Stimulating Microelectrodes," *ACS Applied Materials & Interfaces,* vol. 11, pp. 17226-17233, 2019.

[82] N. Rossetti, P. Luthra, J. E. Hagler, A. H. Jae Lee, C. Bodart, X. Li*, et al.*, "Poly(3,4-ethylenedioxythiophene) (PEDOT) Coatings for High-Quality Electromyography Recording," *ACS Applied Bio Materials,* vol. 2, pp. 5154-5163, 2019.

[83] Y. Liu, J. Li, S. Song, J. Kang, Y. Tsao, S. Chen*, et al.*, "Morphing electronics enable neuromodulation in growing tissue," *Nature Biotechnology,* vol. 38, pp. 1031-1036, 2020.

[84] A. Williamson, M. Ferro, P. Leleux, E. Ismailova, A. Kaszas, T. Doublet*, et al.*, "Localized Neuron Stimulation with Organic Electrochemical Transistors on Delaminating Depth Probes," *Advanced Materials,* vol. 27, pp. 4405-4410, 2015.

[85] Y. Liu, M. Pharr, and G. A. Salvatore, "Lab-on-Skin: A Review of Flexible and Stretchable Electronics for Wearable Health Monitoring," *ACS nano,* vol. 11, pp. 9614-9635, 2017.

[86] N. Matsuhisa, X. Chen, Z. Bao, and T. Someya, "Materials and structural designs of stretchable conductors," *Chemical Society Reviews,* vol. 48, pp. 2946-2966, 2019.

[87] D. C. Kim, H. J. Shim, W. Lee, J. H. Koo, and D.-H. Kim, "Material-Based Approaches for the Fabrication of Stretchable Electronics," *Advanced Materials,* vol. 32, p. 1902743, 2020.

[88] D.-Y. Khang, J. A. Rogers, and H. H. Lee, "Mechanical Buckling: Mechanics, Metrology, and Stretchable Electronics," *Advanced Functional Materials,* vol. 19, pp. 1526-1536, 2009.

[89] Y. Zhao, A. Kim, G. Wan, and B. C. K. Tee, "Design and applications of stretchable and self-healable conductors for soft electronics," *Nano Convergence,* vol. 6, p. 25, 2019.

[90] T. C. Shyu, P. F. Damasceno, P. M. Dodd, A. Lamoureux, L. Xu, M. Shlian*, et al.*, "A kirigami approach to engineering elasticity in nanocomposites through patterned defects," *Nature Materials,* vol. 14, pp. 785-789, 2015.

[91] L. V. Kayser and D. J. Lipomi, "Stretchable Conductive Polymers and Composites Based on PEDOT and PEDOT:PSS," *Advanced Materials,* vol. 31, p. 1806133, 2019.

[92] D. J. Lipomi, "Stretchable Figures of Merit in Deformable Electronics," *Advanced Materials,* vol. 28, pp. 4180-4183, 2016.

[93] M. Wang, P. Baek, A. Akbarinejad, D. Barker, and J. Travas-Sejdic, "Conjugated polymers and composites for stretchable organic electronics," *Journal of Materials Chemistry C,* vol. 7, pp. 5534-5552, 2019.

[94] K. Sim, Z. Rao, F. Ershad, and C. Yu, "Rubbery Electronics Fully Made of Stretchable Elastomeric Electronic Materials," *Advanced Materials,* vol. 32, p. 1902417, 2020.

[95] J. Kang, J. B. H. Tok, and Z. Bao, "Self-healing soft electronics," *Nature Electronics,* vol. 2, pp. 144-150, 2019.

[96] Y. J. Tan, J. Wu, H. Li, and B. C. K. Tee, "Self-Healing Electronic Materials for a Smart and Sustainable Future," *ACS Applied Materials & Interfaces,* vol. 10, pp. 15331-15345, 2018.

[97] S. Kwon, J. Kim, G. Kim, K. Yu, Y.-R. Jo, B.-J. Kim*, et al.*, "Organic Single-Crystal Semiconductor Films on a Millimeter Domain Scale," *Advanced Materials,* vol. 27, pp. 6870-6877, 2015.

[98] Y. J. Tan, J. Wu, H. Li, and B. C. Tee, "Self-Healing Electronic Materials for a Smart and Sustainable Future," *ACS applied materials & interfaces,* vol. 10, pp. 15331-15345, 2018.

[99] T. Chang, F. Panhwar, and G. Zhao, "Flourishing Self-Healing Surface Materials: Recent Progresses and Challenges," *Advanced Materials Interfaces,* vol. 7, p. 1901959, 2020.

[100] Y. Yang and M. W. Urban, "Self-Healing of Polymers via Supramolecular Chemistry," *Advanced Materials Interfaces,* vol. 5, p. 1800384, 2018.

[101] H. Wang, P. Wang, Y. Feng, J. Liu, J. Wang, M. Hu*, et al.*, "Recent Advances on Self-Healing Materials and Batteries," *ChemElectroChem,* vol. 6, pp. 1605-1622, 2019.

[102] Z. Deng, H. Wang, P. X. Ma, and B. Guo, "Self-healing conductive hydrogels: preparation, properties and applications," *Nanoscale,* vol. 12, pp. 1224-1246, 2020.

[103] M.-M. Song, Y.-M. Wang, X.-Y. Liang, X.-Q. Zhang, S. Zhang, and B.-J. Li, "Functional materials with self-healing properties: a review," *Soft Matter,* vol. 15, pp. 6615-6625, 2019.

[104] S. Zhang and F. Cicoira, "Water-Enabled Healing of Conducting Polymer Films," *Advanced Materials,* vol. 29, p. 1703098, 2017.

[105] X. Xin, J. Yu, N. Gao, Z. Xue, W. Zhang, J. Xu*, et al.*, "Freeze-drying and mechanical redispersion of aqueous PEDOT:PSS," *Journal of Applied Polymer Science,* p. 49774.

[106] Y. Ma, N. Wei, Q. Wang, C. Wu, W. Zeng, Y. Gao*, et al.*, "Ultrathin PEDOT:PSS/rGO Aerogel Providing Tape-Like Self-Healable Electrode for Sensing Space Electric Field with Electrochemical Mechanism," *Advanced Electronic Materials,* vol. 5, p. 1900637, 2019.

[107] L. V. Kayser, M. D. Russell, D. Rodriquez, S. N. Abuhamdieh, C. Dhong, S. Khan*, et al.*, "RAFT Polymerization of an Intrinsically Stretchable Water-Soluble Block Copolymer Scaffold for PEDOT," *Chemistry of Materials,* vol. 30, pp. 4459-4468, 2018.

[108] G. Hirankumar and N. Mehta, "Effect of incorporation of different plasticizers on structural and ion transport properties of PVA-LiClO4 based electrolytes," *Heliyon,* vol. 4, p. e00992, 2018.

[109] J. Y. Oh, S. Kim, H. K. Baik, and U. Jeong, "Conducting polymer dough for deformable electronics," *Advanced Materials,* vol. 28, pp. 4455-4461, 2016.

[110] S. Kee, M. A. Haque, D. Corzo, H. N. Alshareef, and D. Baran, "Self-Healing and Stretchable 3D-Printed Organic Thermoelectrics," *Advanced Functional Materials,* vol. 29, p. 1905426, 2019.

[111] J. Ko, X. Wu, A. Surendran, B. T. Muhammad, and W. L. Leong, "Self-Healable Organic Electrochemical Transistor with High Transconductance, Fast Response, and Long-Term Stability," *ACS Applied Materials & Interfaces,* vol. 12, pp. 33979-33988, 2020.

[112] B. Lu, H. Yuk, S. Lin, N. Jian, K. Qu, J. Xu*, et al.*, "Pure PEDOT:PSS hydrogels," *Nature Communications,* vol. 10, p. 1043, 2019.

[113] D. L. Taylor and M. in het Panhuis, "Self-Healing Hydrogels," *Advanced Materials,* vol. 28, pp. 9060-9093, 2016.

[114] W. Wang, R. Narain, and H. Zeng, "Rational Design of Self-Healing Tough Hydrogels: A Mini Review," *Frontiers in Chemistry,* vol. 6, p. 497, 2018.

[115] Y. Liu and S.-h. Hsu, "Synthesis and Biomedical Applications of Self-healing Hydrogels," *Frontiers in Chemistry,* vol. 6, p. 449, 2018.

[116] Y. Ko, J. Kim, H. Y. Jeong, G. Kwon, D. Kim, M. Ku*, et al.*, "Antibacterial poly (3,4-ethylenedioxythiophene):poly(styrene-sulfonate)/agarose nanocomposite hydrogels with thermo-processability and self-healing," *Carbohydrate Polymers,* vol. 203, pp. 26-34, 2019.

[117] B. Yao, H. Wang, Q. Zhou, M. Wu, M. Zhang, C. Li, *et al.*, "Ultrahigh-Conductivity Polymer Hydrogels with Arbitrary Structures," *Advanced Materials,* vol. 29, p. 1700974, 2017.

[118] S. Zhang, Y. Chen, H. Liu, Z. Wang, H. Ling, C. Wang, *et al.*, "Room-Temperature-Formed PEDOT:PSS Hydrogels Enable Injectable, Soft, and Healable Organic Bioelectronics," *Advanced Materials,* vol. 32, p. 1904752, 2020.

[119] L. Han, X. Lu, M. Wang, D. Gan, W. Deng, K. Wang, *et al.*, "A Mussel-Inspired Conductive, Self-Adhesive, and Self-Healable Tough Hydrogel as Cell Stimulators and Implantable Bioelectronics," *Small,* vol. 13, p. 1601916, 2017.

[120] H. Kamata, Y. Akagi, Y. Kayasuga-Kariya, U.-i. Chung, and T. Sakai, "“Nonswellable” Hydrogel Without Mechanical Hysteresis," *Science,* vol. 343, pp. 873-875, 2014.

[121] S. Cao, X. Tong, K. Dai, and Q. Xu, "A super-stretchable and tough functionalized boron nitride/PEDOT: PSS/poly (N-isopropylacrylamide) hydrogel with self-healing, adhesion, conductive and photothermal activity," *Journal of Materials Chemistry A,* vol. 7, pp. 8204-8209, 2019.

[122] Y. Song, Y. Liu, T. Qi, and G. L. Li, "Towards Dynamic but Supertough Healable Polymers through Biomimetic Hierarchical Hydrogen-Bonding Interactions," *Angewandte Chemie International Edition,* vol. 57, pp. 13838-13842, 2018.

[123] F.-m. Cheng, H.-x. Chen, and H.-d. Li, "Recent advances in tough and self-healing nanocomposite hydrogels for shape morphing and soft actuators," *European Polymer Journal,* vol. 124, p. 109448, 2020.

[124] Z. Jia, Y. Zeng, P. Tang, D. Gan, W. Xing, Y. Hou, *et al.*, "Conductive, Tough, Transparent, and Self-Healing Hydrogels Based on Catechol–Metal Ion Dual Self-Catalysis," *Chemistry of Materials,* vol. 31, pp. 5625-5632, 2019.

[125] F. Luo, T. L. Sun, T. Nakajima, T. Kurokawa, Y. Zhao, K. Sato, *et al.*, "Oppositely Charged Polyelectrolytes Form Tough, Self-Healing, and Rebuildable Hydrogels," *Advanced Materials,* vol. 27, pp. 2722-2727, 2015.

[126] G. Qu, Y. Li, Y. Yu, Y. Huang, W. Zhang, H. Zhang, *et al.*, "Spontaneously Regenerative Tough Hydrogels," *Angewandte Chemie International Edition,* vol. 58, pp. 10951-10955, 2019.

[127] S. Hu, L. Wang, T. Huang, and A. Yu, "A conductive self-healing hydrogel binder for high-performance silicon anodes in lithium-ion batteries," *Journal of Power Sources,* vol. 449, p. 227472, 2020.

[128] Y. Yang, X. Wang, F. Yang, H. Shen, and D. Wu, "A Universal Soaking Strategy to Convert Composite Hydrogels into Extremely Tough and Rapidly Recoverable Double-Network Hydrogels," *Advanced Materials,* vol. 28, pp. 7178-7184, 2016.

[129] H. Chen, Y. Liu, B. Ren, Y. Zhang, J. Ma, L. Xu, *et al.*, "Super Bulk and Interfacial Toughness of Physically Crosslinked Double-Network Hydrogels," *Advanced Functional Materials,* vol. 27, p. 1703086, 2017.

[130] Y. Yang, X. Wang, F. Yang, L. Wang, and D. Wu, "Highly Elastic and Ultratough Hybrid Ionic–Covalent Hydrogels with Tunable Structures and Mechanics," *Advanced Materials,* vol. 30, p. 1707071, 2018.

[131] S. Wang, G. Guo, X. Lu, S. Ji, G. Tan, and L. Gao, "Facile Soaking Strategy Toward Simultaneously Enhanced Conductivity and Toughness of Self-Healing Composite Hydrogels Through Constructing Multiple Noncovalent Interactions," *ACS Applied Materials & Interfaces,* vol. 10, pp. 19133-19142, 2018.

[132] X. Wang, J. Li, H. Song, H. Huang, and J. Gou, "Highly Stretchable and Wearable Strain Sensor Based on Printable Carbon Nanotube Layers/Polydimethylsiloxane Composites with Adjustable Sensitivity," *ACS Applied Materials & Interfaces,* vol. 10, pp. 7371-7380, 2018.

[133] S. Wang, J. Xu, W. Wang, G.-J. N. Wang, R. Rastak, F. Molina-Lopez*, et al.*, "Skin electronics from scalable fabrication of an intrinsically stretchable transistor array," *Nature,* vol. 555, pp. 83-88, 2018.

[134] L. Li, J. Liang, H. Gao, Y. Li, X. Niu, X. Zhu*, et al.*, "A Solid-State Intrinsically Stretchable Polymer Solar Cell," *ACS Applied Materials & Interfaces,* vol. 9, pp. 40523-40532, 2017.

[135] Y. Huang, M. Zhong, F. Shi, X. Liu, Z. Tang, Y. Wang*, et al.*, "An Intrinsically Stretchable and Compressible Supercapacitor Containing a Polyacrylamide Hydrogel Electrolyte," *Angewandte Chemie International Edition,* vol. 56, pp. 9141-9145, 2017.

[136] W. Liu, J. Chen, Z. Chen, K. Liu, G. Zhou, Y. Sun*, et al.*, "Stretchable Lithium-Ion Batteries Enabled by Device-Scaled Wavy Structure and Elastic-Sticky Separator," *Advanced Energy Materials,* vol. 7, p. 1701076, 2017.

[137] H. Sun, M. Vagin, S. Wang, X. Crispin, R. Forchheimer, M. Berggren*, et al.*, "Complementary Logic Circuits Based on High-Performance n-Type Organic Electrochemical Transistors," *Advanced Materials,* vol. 30, p. 1704916, 2018.

[138] G. D. Spyropoulos, J. N. Gelinas, and D. Khodagholy, "Internal ion-gated organic electrochemical transistor: A building block for integrated bioelectronics," *Science Advances,* vol. 5, p. eaau7378, 2019.

[139] D. Mantione, I. del Agua, W. Schaafsma, M. ElMahmoudy, I. Uguz, A. Sanchez-Sanchez*, et al.*, "Low-Temperature Cross-Linking of PEDOT:PSS Films Using Divinylsulfone," *ACS Applied Materials & Interfaces,* vol. 9, pp. 18254-18262, 2017.

[140] S. Zhang, E. Hubis, G. Tomasello, G. Soliveri, P. Kumar, and F. Cicoira, "Patterning of Stretchable Organic Electrochemical Transistors," *Chemistry of Materials,* vol. 29, pp. 3126-3132, 2017.

[141] B. Marchiori, R. Delattre, S. Hannah, S. Blayac, and M. Ramuz, "Laser-patterned metallic interconnections for all stretchable organic electrochemical transistors," *Scientific Reports,* vol. 8, p. 8477, 2018.

[142] N. Matsuhisa, Y. Jiang, Z. Liu, G. Chen, C. Wan, Y. Kim*, et al.*, "High-Transconductance Stretchable Transistors Achieved by Controlled Gold Microcrack Morphology," *Advanced Electronic Materials,* vol. 5, p. 1900347, 2019.

[143] S. Zhang, Y. Li, G. Tomasello, M. Anthonisen, X. Li, M. Mazzeo*, et al.*, "Tuning the Electromechanical Properties of PEDOT:PSS Films for Stretchable Transistors And Pressure Sensors," *Advanced Electronic Materials,* vol. 5, p. 1900191, 2019.

[144] S. P. Lacour, D. Chan, S. Wagner, T. Li, and Z. Suo, "Mechanisms of reversible stretchability of thin metal films on elastomeric substrates," *Applied Physics Letters,* vol. 88, p. 204103, 2006.

[145] J. Xu, S. Wang, G.-J. N. Wang, C. Zhu, S. Luo, L. Jin*, et al.*, "Highly stretchable polymer semiconductor films through the nanoconfinement effect," *Science,* vol. 355, pp. 59-64, 2017.

[146] Y.-Y. Lee, J.-H. Lee, J.-Y. Cho, N.-R. Kim, D.-H. Nam, I.-S. Choi*, et al.*, "Stretching-Induced Growth of PEDOT-Rich Cores: A New Mechanism for Strain-Dependent Resistivity Change in PEDOT:PSS Films," *Advanced Functional Materials,* vol. 23, pp. 4020-4027, 2013.

[147] F. Hassouna, J.-M. Raquez, F. Addiego, P. Dubois, V. Toniazzo, and D. Ruch, "New approach on the development of plasticized polylactide (PLA): Grafting of poly(ethylene glycol) (PEG) via reactive extrusion," *European Polymer Journal,* vol. 47, pp. 2134-2144, 2011.

[148] Z. Kulinski and E. Piorkowska, "Crystallization, structure and properties of plasticized poly(l-lactide)," *Polymer,* vol. 46, pp. 10290-10300, 2005.

[149] K.-m. Choi, M.-C. Choi, D.-H. Han, T.-S. Park, and C.-S. Ha, "Plasticization of poly(lactic acid) (PLA) through chemical grafting of poly(ethylene glycol) (PEG) via in situ reactive blending," *European Polymer Journal,* vol. 49, pp. 2356-2364, 2013.

[150] F. Decataldo, T. Cramer, D. Martelli, I. Gualandi, W. S. Korim, S. T. Yao*, et al.*, "Stretchable Low Impedance Electrodes for Bioelectronic Recording from Small Peripheral Nerves," *Scientific Reports,* vol. 9, p. 10598, 2019.

[151] O. E. Geiculescu, B. B. Hallac, R. V. Rajagopal, S. E. Creager, D. D. DesMarteau, O. Borodin*, et al.*, "The Effect of Low-Molecular-Weight Poly(ethylene glycol) (PEG) Plasticizers on the Transport Properties of Lithium Fluorosulfonimide Ionic Melt Electrolytes," *The Journal of Physical Chemistry B,* vol. 118, pp. 5135-5143, 2014.

[152] S. Sharma, R. W. Johnson, and T. A. Desai, "XPS and AFM analysis of antifouling PEG interfaces for microfabricated silicon biosensors," *Biosensors and Bioelectronics,* vol. 20, pp. 227-239, 2004.

[153] H. Tang, P. Kumar, S. Zhang, Z. Yi, G. D. Crescenzo, C. Santato*, et al.*, "Conducting Polymer Transistors Making Use of Activated Carbon Gate Electrodes," *ACS Applied Materials & Interfaces,* vol. 7, pp. 969-973, 2015.

[154] X. Li, H. Charaya, G. M. Bernard, J. A. W. Elliott, V. K. Michaelis, B. Lee*, et al.*, "Low-Temperature Ionic Conductivity Enhanced by Disrupted Ice Formation in Polyampholyte Hydrogels," *Macromolecules,* vol. 51, pp. 2723-2731, 2018.

[155] W. Zhang, B. Zhao, Z. He, X. Zhao, H. Wang, S. Yang*, et al.*, "High-efficiency ITO-free polymer solar cells using highly conductive PEDOT:PSS/surfactant bilayer transparent anodes," *Energy & Environmental Science,* vol. 6, pp. 1956-1964, 2013.

[156] Y. Mengüç, Y.-L. Park, H. Pei, D. Vogt, P. M. Aubin, E. Winchell*, et al.*, "Wearable soft sensing suit for human gait measurement," *The International Journal of Robotics Research,* vol. 33, pp. 1748-1764, 2014.

[157] J. M. Dechene, "Surface modifications of poly (dimethylsiloxane) for biological application of microfluidic devices," 2010.

[158] G. Schwartz, B. C.-K. Tee, J. Mei, A. L. Appleton, D. H. Kim, H. Wang*, et al.*, "Flexible polymer transistors with high pressure sensitivity for application in electronic skin and health monitoring," *Nature communications,* vol. 4, p. 1859, 2013.

[159] A. Giovannitti, D.-T. Sbircea, S. Inal, C. B. Nielsen, E. Bandiello, D. A. Hanifi*, et al.*, "Controlling the mode of operation of organic transistors through side-chain engineering," *Proceedings of the National Academy of Sciences,* vol. 113, pp. 12017-12022, 2016.

[160] M. W. Urban, D. Davydovich, Y. Yang, T. Demir, Y. Zhang, and L. Casabianca, "Key-and-lock commodity self-healing copolymers," *Science,* vol. 362, pp. 220-225, 2018.

[161] A. Campanella, D. Döhler, and W. H. Binder, "Self-Healing in Supramolecular Polymers," *Macromolecular rapid communications,* p. 1700739, 2018.

[162] P. Baek, N. Aydemir, Y. An, E. W. C. Chan, A. Sokolova, A. Nelson*, et al.*, "Molecularly Engineered Intrinsically Healable and Stretchable Conducting Polymers," *Chemistry of Materials,* vol. 29, pp. 8850-8858, 2017.

[163] Y. Cao, Y. J. Tan, S. Li, W. W. Lee, H. Guo, Y. Cai*, et al.*, "Self-healing electronic skins for aquatic environments," *Nature Electronics,* vol. 2, p. 75, 2019.

[164] B. C. Tee, C. Wang, R. Allen, and Z. Bao, "An electrically and mechanically self-healing composite with pressure-and flexion-sensitive properties for electronic skin applications," *Nature nanotechnology,* vol. 7, p. 825, 2012.

[165] C.-H. Li, C. Wang, C. Keplinger, J.-L. Zuo, L. Jin, Y. Sun*, et al.*, "A highly stretchable autonomous self-healing elastomer," *Nature chemistry,* vol. 8, p. 618, 2016.

[166] Z. Zou, C. Zhu, Y. Li, X. Lei, W. Zhang, and J. Xiao, "Rehealable, fully recyclable, and malleable electronic skin enabled by dynamic covalent thermoset nanocomposite," *Science Advances,* vol. 4, p. eaaq0508, 2018.

[167] Q. Wu, J. Wei, B. Xu, X. Liu, H. Wang, W. Wang*, et al.*, "A robust, highly stretchable supramolecular polymer conductive hydrogel with self-healability and thermo-processability," *Scientific reports,* vol. 7, p. 41566, 2017.

[168] S. Pati, B. P. Singh, and S. Dhakate, "Self-healing Polymer Composites Based on Graphene and Carbon Nanotubes," in *Smart Polymer Nanocomposites*, ed: Springer, 2017, pp. 119-152.

[169] B. C. Tee and J. Ouyang, "Soft electronically functional polymeric composite materials for a flexible and stretchable digital future," *Advanced Materials,* p. 1802560, 2018.

[170] J. Kang, D. Son, O. Vardoulis, J. Mun, N. Matsuhisa, Y. Kim, *et al.*, "Modular and Reconfigurable Stretchable Electronic Systems," *Advanced Materials Technologies,* vol. 4, p. 1800417, 2019.

[171] K. Parida, G. Thangavel, G. Cai, X. Zhou, S. Park, J. Xiong, *et al.*, "Extremely stretchable and self-healing conductor based on thermoplastic elastomer for all-three-dimensional printed triboelectric nanogenerator," *Nature communications,* vol. 10, p. 2158, 2019.

[172] P. Song, H. Qin, H.-L. Gao, H.-P. Cong, and S.-H. Yu, "Self-healing and superstretchable conductors from hierarchical nanowire assemblies," *Nature Communications,* vol. 9, p. 2786, 2018.

[173] Y. Cao, T. G. Morrissey, E. Acome, S. I. Allec, B. M. Wong, C. Keplinger, *et al.*, "A Transparent, Self-Healing, Highly Stretchable Ionic Conductor," *Advanced Materials,* vol. 29, 2017.

[174] Y. Lu, Z. Liu, H. Yan, Q. Peng, R. Wang, M. E. Barkey, *et al.*, "Ultra-Stretchable Conductive Polymer Complex as Strain Sensor with Repeatable Autonomous Self-Healing Ability," *ACS applied materials & interfaces,* 2019.

[175] B. J. Blaiszik, S. L. Kramer, M. E. Grady, D. A. McIlroy, J. S. Moore, N. R. Sottos, *et al.*, "Autonomic restoration of electrical conductivity," *Advanced Materials,* vol. 24, pp. 398-401, 2012.

[176] A. J. Bandodkar, V. Mohan, C. S. López, J. Ramírez, and J. Wang, "Self-Healing Inks for Autonomous Repair of Printable Electrochemical Devices," *Advanced Electronic Materials,* vol. 1, p. 1500289, 2015.

[177] S. A. Odom, S. Chayanupatkul, B. J. Blaiszik, O. Zhao, A. C. Jackson, P. V. Braun, *et al.*, "A self-healing conductive ink," *Advanced Materials,* vol. 24, pp. 2578-2581, 2012.

[178] T. Wang, Y. Zhang, Q. Liu, W. Cheng, X. Wang, L. Pan, *et al.*, "A self-healable, highly stretchable, and solution processable conductive polymer composite for ultrasensitive strain and pressure sensing," *Advanced Functional Materials,* vol. 28, p. 1705551, 2018.

[179] J. Dahlke, S. Zechel, M. D. Hager, and U. S. Schubert, "How to Design a Self-Healing Polymer: General Concepts of Dynamic Covalent Bonds and Their Application for Intrinsic Healable Materials," *Advanced Materials Interfaces,* vol. 5, p. 1800051, 2018.

[180] R. Tamate, K. Hashimoto, T. Horii, M. Hirasawa, X. Li, M. Shibayama, *et al.*, "Self-Healing Micellar Ion Gels Based on Multiple Hydrogen Bonding," *Advanced Materials,* vol. 30, p. 1802792, 2018.

[181] X. Shi, X. Zhou, Y. Zhang, X. Xu, Z. Zhang, P. Liu, *et al.*, "A self-healing and stretchable light-emitting device," *Journal of Materials Chemistry C,* vol. 6, pp. 12774-12780, 2018.

[182] J. Xu, P. Chen, J. Wu, P. Hu, Y. Fu, W. Jiang, *et al.*, "Notch-Insensitive, Ultrastretchable, Efficient Self-Healing Supramolecular Polymers Constructed from Multiphase Active Hydrogen Bonds for Electronic Applications," *Chemistry of Materials,* 2019.

[183] E. J. Markvicka, M. D. Bartlett, X. Huang, and C. Majidi, "An autonomously electrically self-healing liquid metal–elastomer composite for robust soft-matter robotics and electronics," *Nature materials,* vol. 17, p. 618, 2018.

[184] J. Chen, J. Liu, T. Thundat, and H. Zeng, "Polypyrrole-Doped Conductive Supramolecular Elastomer with Stretchability, Rapid Self-Healing, and Adhesive Property for Flexible Electronic Sensors," *ACS applied materials & interfaces,* vol. 11, pp. 18720-18729, 2019.

[185] J. Deng, X. Kuang, R. Liu, W. Ding, A. C. Wang, Y. C. Lai*, et al.*, "Vitrimer Elastomer-Based Jigsaw Puzzle-Like Healable Triboelectric Nanogenerator for Self-Powered Wearable Electronics," *Advanced Materials,* vol. 30, p. 1705918, 2018.

[186] K. Chu, B. G. Song, H. I. Yang, D. M. Kim, C. S. Lee, M. Park*, et al.*, "Smart Passivation Materials with a Liquid Metal Microcapsule as Self-Healing Conductors for Sustainable and Flexible Perovskite Solar Cells," *Advanced Functional Materials,* 2018.

[187] Q. Wang, S. Ling, X. Liang, H. Wang, H. Lu, and Y. Zhang, "Self-Healable Multifunctional Electronic Tattoos Based on Silk and Graphene," *Advanced Functional Materials,* vol. 29, p. 1808695, 2019.

[188] Y. Han, X. Wu, X. Zhang, and C. Lu, "Archimedean Spiral Inspired Conductive Supramolecular Elastomer with Rapid Electrical and Mechanical Self-Healing Capability for Sensor Application," *Advanced Materials Technologies,* vol. 4, p. 1800424, 2019.

[189] K. Parida, J. Xiong, X. Zhou, and P. S. Lee, "Progress on triboelectric nanogenerator with stretchability, self-healability and bio-compatibility," *Nano Energy,* vol. 59, pp. 237-257, 2019.

[190] S. S. Katiyar, V. Kushwah, C. P. Dora, R. Y. Patil, and S. Jain, "Design and Toxicity Evaluation of Novel Fatty Acid-Amino Acid-Based Biocompatible Surfactants," *AAPS PharmSciTech,* vol. 20, p. 186, 2019.

[191] Y. Li, S. Zhang, X. Li, V. R. N. Unnava, and F. Cicoira, "Highly stretchable PEDOT:PSS organic electrochemical transistors achieved via polyethylene glycol addition," *Flexible and Printed Electronics,* vol. 4, p. 044004, 2019.

[192] L. Ouyang, C. Musumeci, M. J. Jafari, T. Ederth, and O. Inganäs, "Imaging the Phase Separation Between PEDOT and Polyelectrolytes During Processing of Highly Conductive PEDOT:PSS Films," *ACS Applied Materials & Interfaces,* vol. 7, pp. 19764-19773, 2015.

[193] Z. Zhu, G. Yang, R. Li, and T. Pan, "Photopatternable PEDOT:PSS/PEG hybrid thin film with moisture stability and sensitivity," *Microsystems & Nanoengineering,* vol. 3, p. 17004, 2017.

[194] T. Ekblad, G. Bergström, T. Ederth, S. L. Conlan, R. Mutton, A. S. Clare*, et al.*, "Poly(ethylene glycol)-Containing Hydrogel Surfaces for Antifouling Applications in Marine and Freshwater Environments," *Biomacromolecules,* vol. 9, pp. 2775-2783, 2008.

[195] C. S. Gudipati, C. M. Greenlief, J. A. Johnson, P. Prayongpan, and K. L. Wooley, "Hyperbranched fluoropolymer and linear poly(ethylene glycol) based amphiphilic crosslinked networks as efficient antifouling coatings: An insight into the surface compositions, topographies, and morphologies," *Journal of Polymer Science Part A: Polymer Chemistry,* vol. 42, pp. 6193-6208, 2004.

[196] M. R. Moraes, A. C. Alves, F. Toptan, M. S. Martins, E. M. F. Vieira, A. J. Paleo*, et al.*, "Glycerol/PEDOT:PSS coated woven fabric as a flexible heating element on textiles," *Journal of Materials Chemistry C,* vol. 5, pp. 3807-3822, 2017.

[197] X. Wang, G. Feng, M. Li, and M. Ge, "Effect of PEDOT: PSS content on structure and properties of PEDOT: PSS/poly (vinyl alcohol) composite fiber," *Polymer Bulletin,* vol. 76, pp. 2097-2111, 2019.

[198] H. S. Mansur, R. L. Oréfice, and A. A. Mansur, "Characterization of poly (vinyl alcohol)/poly (ethylene glycol) hydrogels and PVA-derived hybrids by small-angle X-ray scattering and FTIR spectroscopy," *Polymer,* vol. 45, pp. 7193-7202, 2004.

[199] R. R. Mohamed, R. S. Seoudi, and M. W. Sabaa, "Synthesis and characterization of cross-linked polyethylene glycol/carboxymethyl chitosan hydrogels," *Advances in Polymer Technology,* vol. 34, 2015.

[200] R. B. Barnes and L. G. Bonner, "The Christiansen Filter Effect in the Infrared," *Physical Review,* vol. 49, pp. 732-740, 1936.

[201] M. Hayashi and F. Tournilhac, "Thermal stability enhancement of hydrogen bonded semicrystalline thermoplastics achieved by combination of aramide chemistry and supramolecular chemistry," *Polymer Chemistry,* vol. 8, pp. 461-471, 2017.

[202] Q. Yin, Y. Peng, S. Zhang, F. Zhu, W. Li, and K. Du, "Recyclable heat-resisting polymer poly (ether azaindole ketone)-H+ via hydrogen bonding crosslinking," *Polymer Chemistry,* vol. 9, pp. 1164-1167, 2018.

[203] L. Bießmann, L. P. Kreuzer, T. Widmann, N. Hohn, J.-F. Moulin, and P. Muller-Buschbaum, "Monitoring the Swelling Behavior of PEDOT: PSS Electrodes under High Humidity Conditions," *ACS applied materials & interfaces,* vol. 10, pp. 9865-9872, 2018.

[204] B. Sarkar, M. Jaiswal, and D. K. Satapathy, "Swelling kinetics and electrical charge transport in PEDOT: PSS thin films exposed to water vapor," *Journal of Physics: Condensed Matter,* vol. 30, p. 225101, 2018.

[205] M. ElMahmoudy, S. Inal, A. Charrier, I. Uguz, G. G. Malliaras, and S. Sanaur, "Tailoring the electrochemical and mechanical properties of PEDOT: PSS films for bioelectronics," *Macromolecular Materials and Engineering,* vol. 302, p. 1600497, 2017.

[206] M. D. Bartlett, M. D. Dickey, and C. Majidi, "Self-healing materials for soft-matter machines and electronics," *NPG Asia Materials,* vol. 11, p. 21, 2019.

[207] M. Wu, Y. Li, N. An, and J. Sun, "Applied Voltage and Near-Infrared Light Enable Healing of Superhydrophobicity Loss Caused by Severe Scratches in Conductive Superhydrophobic Films," *Advanced Functional Materials,* vol. 26, pp. 6777-6784, 2016.

[208] Y. Li, S. Chen, M. Wu, and J. Sun, "Polyelectrolyte Multilayers Impart Healability to Highly Electrically Conductive Films," *Advanced Materials,* vol. 24, pp. 4578-4582, 2012.

[209] Y. Li, S. Chen, M. Wu, and J. Sun, "Rapid and Efficient Multiple Healing of Flexible Conductive Films by Near-Infrared Light Irradiation," *ACS Applied Materials & Interfaces,* vol. 6, pp. 16409-16415, 2014.

[210] E. D'Elia, S. Barg, N. Ni, V. G. Rocha, and E. Saiz, "Self-Healing Graphene-Based Composites with Sensing Capabilities," *Advanced Materials,* vol. 27, pp. 4788-4794, 2015.

[211] X. Liu, G. Su, Q. Guo, C. Lu, T. Zhou, C. Zhou*, et al.*, "Hierarchically Structured Self-Healing Sensors with Tunable Positive/Negative Piezoresistivity," *Advanced Functional Materials,* vol. 28, p. 1706658, 2018.

[212] J. Y. Oh, D. Son, T. Katsumata, Y. Lee, Y. Kim, J. Lopez*, et al.*, "Stretchable self-healable semiconducting polymer film for active-matrix strain-sensing array," *Science Advances,* vol. 5, p. eaav3097, 2019.

[213] J. Y. Oh, S. Rondeau-Gagné, Y.-C. Chiu, A. Chortos, F. Lissel, G.-J. N. Wang*, et al.*, "Intrinsically stretchable and healable semiconducting polymer for organic transistors," *Nature,* vol. 539, pp. 411-415, 2016.

[214] M. Ashizawa, Y. Zheng, H. Tran, and Z. Bao, "Intrinsically stretchable conjugated polymer semiconductors in field effect transistors," *Progress in Polymer Science,* vol. 100, p. 101181, 2020.

[215] H. Wang, B. Zhu, W. Jiang, Y. Yang, W. R. Leow, H. Wang*, et al.*, "A Mechanically and Electrically Self-Healing Supercapacitor," *Advanced Materials,* vol. 26, pp. 3638-3643, 2014.

[216] A. J. Bandodkar, R. Nuñez-Flores, W. Jia, and J. Wang, "All-Printed Stretchable Electrochemical Devices," *Advanced Materials,* vol. 27, pp. 3060-3065, 2015.

[217] Y. Li, X. Li, S. Zhang, L. Liu, N. Hamad, S. R. Bobbara*, et al.*, "Autonomic Self-Healing of PEDOT:PSS Achieved Via Polyethylene Glycol Addition," *Advanced Functional Materials,* vol. 30, p. 2002853, 2020.

[218] S. Cao, X. Tong, K. Dai, and Q. Xu, "A super-stretchable and tough functionalized boron nitride/PEDOT:PSS/poly(N-isopropylacrylamide) hydrogel with self-healing, adhesion, conductive and photothermal activity," *Journal of Materials Chemistry A,* vol. 7, pp. 8204-8209, 2019.

[219] C. Duc, A. Vlandas, G. G. Malliaras, and V. Senez, "Wettability of PEDOT:PSS films," *Soft Matter,* vol. 12, pp. 5146-5153, 2016.

[220] Z. Fan, P. Li, D. Du, and J. Ouyang, "Significantly Enhanced Thermoelectric Properties of PEDOT:PSS Films through Sequential Post-Treatments with Common Acids and Bases," *Advanced Energy Materials,* vol. 7, p. 1602116, 2017.

[221] H. Shi, C. Liu, Q. Jiang, and J. Xu, "Effective Approaches to Improve the Electrical Conductivity of PEDOT:PSS: A Review," *Advanced Electronic Materials,* vol. 1, p. 1500017, 2015.

[222] M. N. Gueye, A. Carella, N. Massonnet, E. Yvenou, S. Brenet, J. Faure-Vincent*, et al.*, "Structure and Dopant Engineering in PEDOT Thin Films: Practical Tools for a Dramatic Conductivity Enhancement," *Chemistry of Materials,* vol. 28, pp. 3462-3468, 2016.

[223] F. B. d. Gramont, S. Zhang, G. Tomasello, P. Kumar, A. Sarkissian, and F. Cicoira, "Highly stretchable electrospun conducting polymer nanofibers," *Applied Physics Letters,* vol. 111, p. 093701, 2017.

[224] D. Evans, M. Fabretto, M. Mueller, K. Zuber, R. Short, and P. Murphy, "Structure-directed growth of high conductivity PEDOT from liquid-like oxidant layers during vacuum vapor phase polymerization," *Journal of Materials Chemistry,* vol. 22, pp. 14889-14895, 2012.

[225] A. Håkansson, S. Han, S. Wang, J. Lu, S. Braun, M. Fahlman*, et al.*, "Effect of (3-glycidyloxypropyl)trimethoxysilane (GOPS) on the electrical properties of PEDOT:PSS films," *Journal of Polymer Science Part B: Polymer Physics,* vol. 55, pp. 814-820, 2017.

[226] A. K. Y. Wong and U. J. Krull, "Surface characterization of 3-glycidoxypropyltrimethoxysilane films on silicon-based substrates," *Analytical and Bioanalytical Chemistry,* vol. 383, pp. 187-200, 2005.

[227] V. C. Tung, J. Kim, L. J. Cote, and J. Huang, "Sticky Interconnect for Solution-Processed Tandem Solar Cells," *Journal of the American Chemical Society,* vol. 133, pp. 9262-9265, 2011.

[228] X. Wang, A. K. K. Kyaw, C. Yin, F. Wang, Q. Zhu, T. Tang*, et al.*, "Enhancement of thermoelectric performance of PEDOT:PSS films by post-treatment with a superacid," *RSC Advances,* vol. 8, pp. 18334-18340, 2018.

[229] C. Diacci, J. W. Lee, P. Janson, G. Dufil, G. Méhes, M. Berggren*, et al.*, "Real-Time Monitoring of Glucose Export from Isolated Chloroplasts Using an Organic Electrochemical Transistor," *Advanced Materials Technologies,* vol. 5, p. 1900262, 2020.

[230] W. Lee, S. Kobayashi, M. Nagase, Y. Jimbo, I. Saito, Y. Inoue*, et al.*, "Nonthrombogenic, stretchable, active multielectrode array for electroanatomical mapping," *Science Advances,* vol. 4, p. eaau2426, 2018.

[231] Y.-F. Wang, T. Sekine, Y. Takeda, K. Yokosawa, H. Matsui, D. Kumaki*, et al.*, "Fully Printed PEDOT:PSS-based Temperature Sensor with High Humidity Stability for Wireless Healthcare Monitoring," *Scientific Reports,* vol. 10, p. 2467, 2020.

[232] N. Massonnet, A. Carella, A. de Geyer, J. Faure-Vincent, and J.-P. Simonato, "Metallic behaviour of acid doped highly conductive polymers," *Chemical Science,* vol. 6, pp. 412-417, 2015.

[233] Y. Kim, A. Lund, H. Noh, A. I. Hofmann, M. Craighero, S. Darabi*, et al.*, "Robust PEDOT:PSS Wet-Spun Fibers for Thermoelectric Textiles," *Macromolecular Materials and Engineering,* vol. 305, p. 1900749, 2020.

[234] A. Elschner, S. Kirchmeyer, W. Lovenich, U. Merker, and K. Reuter, *PEDOT: principles and applications of an intrinsically conductive polymer*: CRC press, 2010.

[235] Y. Vlamidis, M. Lanzi, E. Salatelli, I. Gualandi, B. Fraboni, L. Setti*, et al.*, "Electrodeposition of PEDOT perchlorate as an alternative route to PEDOT:PSS for the development of bulk heterojunction solar cells," *Journal of Solid State Electrochemistry,* vol. 19, pp. 1685-1693, 2015.

[236] M. C. Simoes, K. J. Hughes, D. B. Ingham, L. Ma, and M. Pourkashanian, "Estimation of the Thermochemical Radii and Ionic Volumes of Complex Ions," *Inorganic Chemistry,* vol. 56, pp. 7566-7573, 2017.

[237] C.-W. Liew and S. Ramesh, "Comparing triflate and hexafluorophosphate anions of ionic liquids in polymer electrolytes for supercapacitor applications," *Materials,* vol. 7, pp. 4019-4033, 2014.

[238] M. Modarresi, J. F. Franco-Gonzalez, and I. Zozoulenko, "Morphology and ion diffusion in PEDOT:Tos. A coarse grained molecular dynamics simulation," *Physical Chemistry Chemical Physics,* vol. 20, pp. 17188-17198, 2018.

[239] P. Kumar, Z. Yi, S. Zhang, A. Sekar, F. Soavi, and F. Cicoira, "Effect of channel thickness, electrolyte ions, and dissolved oxygen on the performance of organic electrochemical transistors," *Applied Physics Letters,* vol. 107, p. 053303, 2015.

APPENDIX A TUNING THE ELECTROMECHANICAL PROPERTIES OF PEDOT:PSS FILMS FOR STRETCHABLE TRANSISTORS

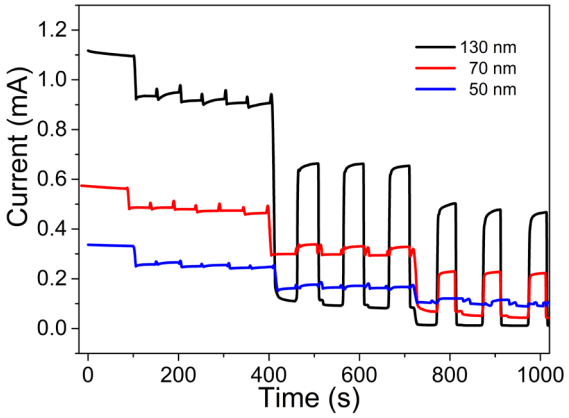

Figure SA1. Current-time measurements for PEDOT:PSS films on PDMS with thickness of 130 nm, 70 nm, and 50 nm at 0%-15%-0%, 0%-30%-0%, 0%-45%-0% strains. Each strain was repeated for 3 cycles. All films were baked are 100 °C for 1 hour.

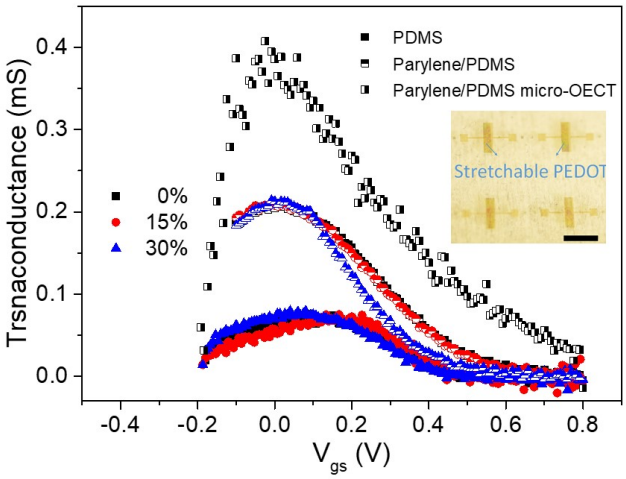

Figure SA2. Transconductance of OECTs on PDMS Parylene/PDMS and micro-OECTs on parylene/PDMS. For OECTs on PDMS Parylene/PDMS the transconductance is evaluated at 0%, 15% and 30% strain. The inset shows the image of 4 micro-OECTs with W/L= 400. The scale bar is 5 mm.

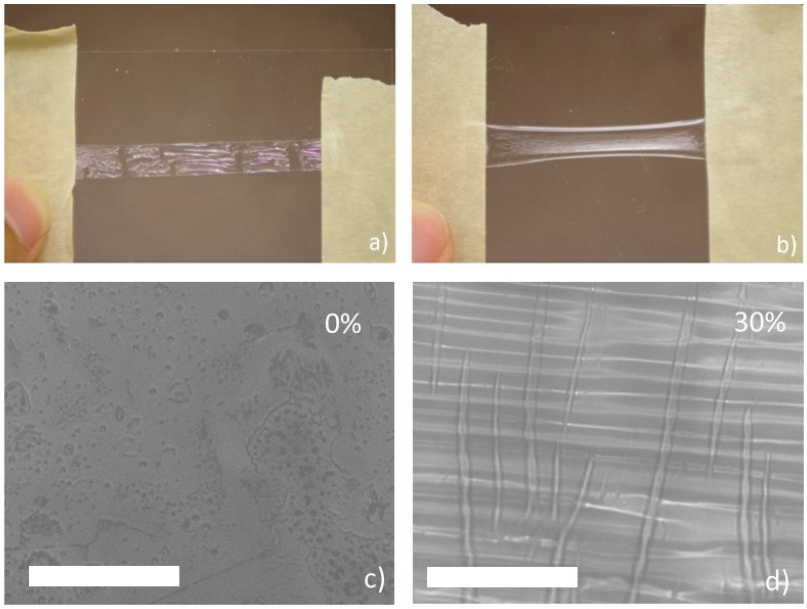

Figure SA3. Optical image of Parylene interlayers on PDMS: a) transferring parylene interlayer onto PDMS via a PET carrier shows cracks at 10% strain; b-d) direct depositing parylene interlayer on PDMS shows only show small microcracks at 30% strain. The scale bar is 50 μm.

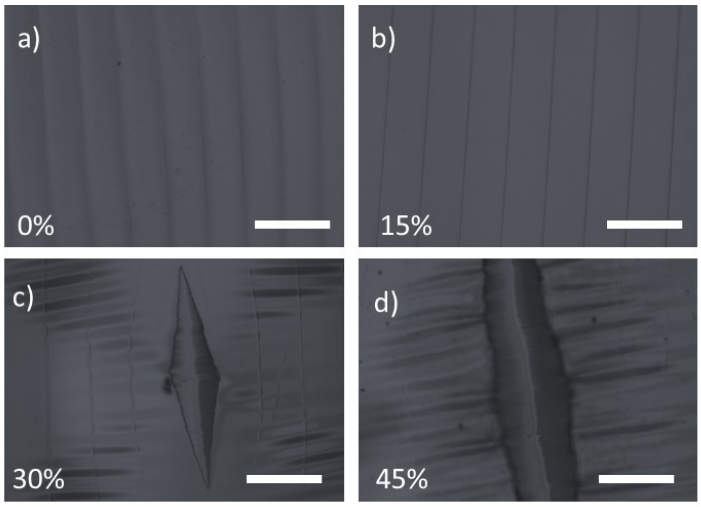

Figure SA4. Optical microscope images of PEDOT:PSS (50 nm, 100 °C baking) on parylene/PDMS at different strains. The wrinkles at 0% strain are formed during the peeling-off process of the film from the glass supporting substrate.

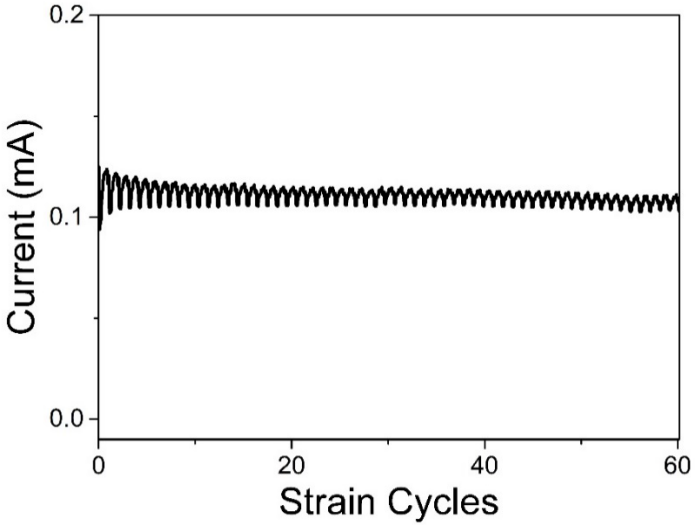

Figure SA5. Current change upon stretching/releasing PEDOT:PSS (50 nm) films on parylene/PDMS between 0% to 30% strain for 60 cycles.

APPENDIX B SUPPORTING INFORMATION OF ARTICLE HIGHLY STRETCHABLE PEDOT:PSS ORGANIC ELECTROCHEMICAL TRANSISTORS ACHIEVED VIA POLYETHYLENE GLYCOL ADDITION

Yang Li[1], Shiming Zhang[2], Xinda Li[1], Venkata Ramana Nitin Unnava[1], Fabio Cicoira[1],*

[1] Department of Chemical Engineering, Polytechnique Montréal, Montreal, Quebec H3C 3A7, Canada

[2] Center for Minimally Invasive Therapeutics, California NanoSystems Institute, University of California, Los Angeles, California 90095, United States

E-mail: fabio.cicoira@polymtl.ca

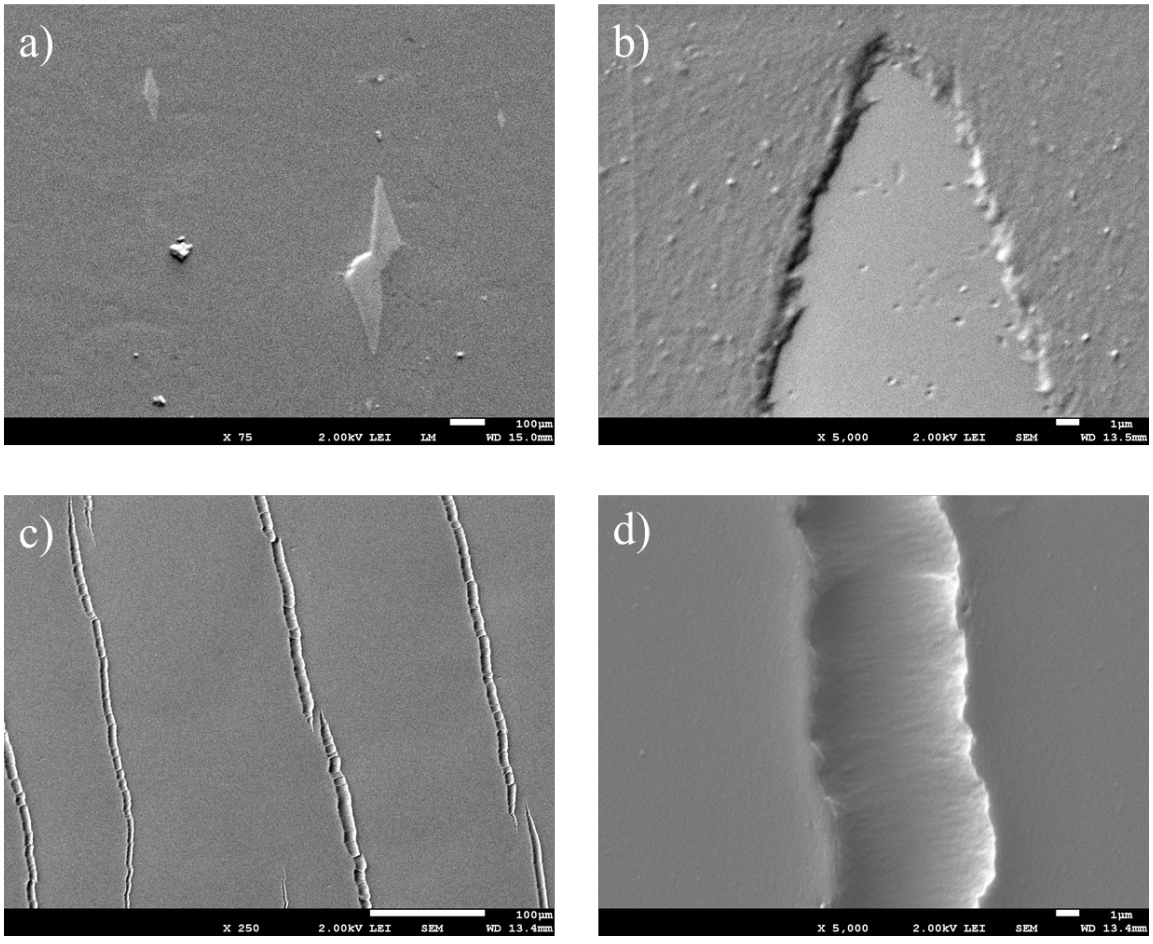

Figure SB1. SEM images of ~300 nm thick PEDOT:PSS/PEG film (a-b) and 50 nm thick PEDOT:PSS film (c-d) on PDMS substrate under 45% strain. All films were baked at 100 °C for 1 hour.

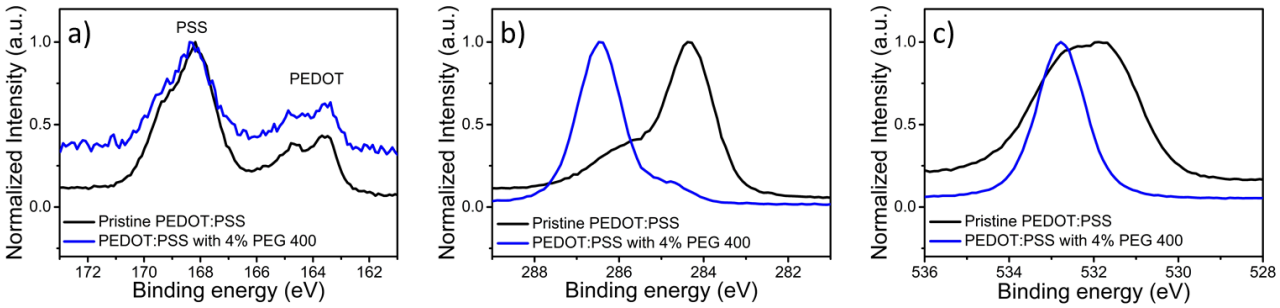

Figure SB2. XPS spectra of (a) S(2p), (b) C(1s) and (c) O(1s) core-level of pristine PEDOT:PSS, and PEDOT:PSS with 4 v/v% PEG 400 addition.

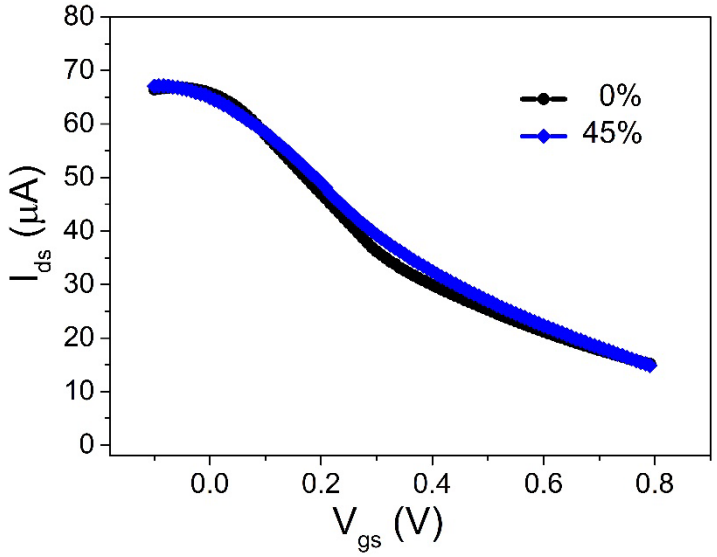

Figure SB3. Transfer characteristics of stretchable OECTs using PEDOT:PSS gate electrode and a polyampholyte hydrogel containing NaCl electrolyte as the gate medium, under 0% and 45% strain. PEDOT:PSS/PEG film is processed from a mixture of PH1000 and 4 v/v% PEG 400, 5 v/v% glycerol and 1 v/v% Capstone FS-30. The films are baked at 100 °C for 1 h. The thickness of the film is 310 nm. The V_{ds} is 0.6 V.

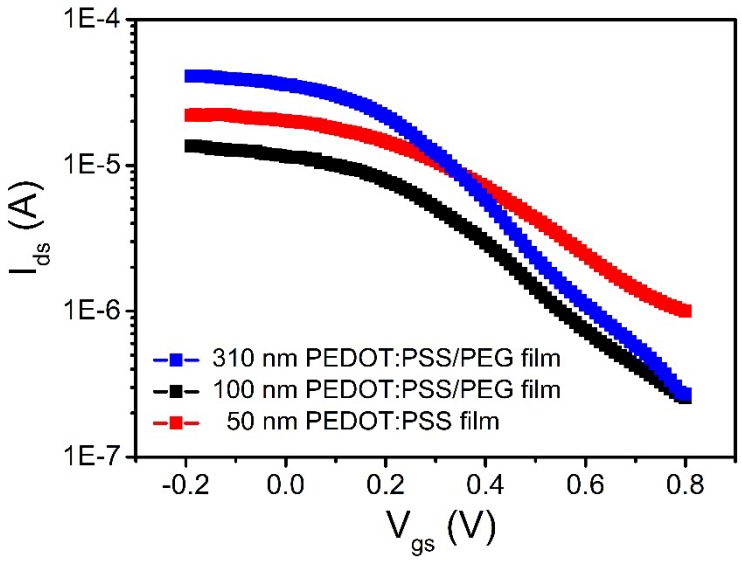

Figure SB4. Transfer characteristics of OECTs using activated carbon gate electrode and 0.1 M NaCl solution as electrolyte. PEDOT:PSS film is processed from a mixture of PH1000, 5 v/v% glycerol and 1 v/v% Capstone FS-30 and PEDOT:PSS/PEG film is processed from a mixture of PH1000 and 4 v/v% PEG 400, 5 v/v% glycerol and 1 v/v% Capstone FS-30. The films are baked at 100 °C for 1 h. The V_{ds} is 0.6 V.

APPENDIX C SUPPORTING INFORMATION OF ARTICLE AUTONOMIC SELF-HEALING OF PEDOT:PSS ACHIEVED VIA POLYETHYLENE GLYCOL ADDITION

Yang Li[1], Xinda Li[1], Shiming Zhang[2], Leslie Liu[1], Natalie Hamad[1], Sanyasi Rao Bobbara[1], Damiano Pasini[3], Fabio Cicoira[1]

[1] Department of Chemical Engineering, Polytechnique Montréal, Montréal, Quebec H3C 3A7, Canada

[2] Center for Minimally Invasive Therapeutics, California NanoSystems Institute, University of California, Los Angeles, California 90095, United States

[3] Department of Mechanical Engineering, McGill University, Montreal, Quebec, H3A0C3, Canada

Email: fabio.cicoira@polymtl.ca.

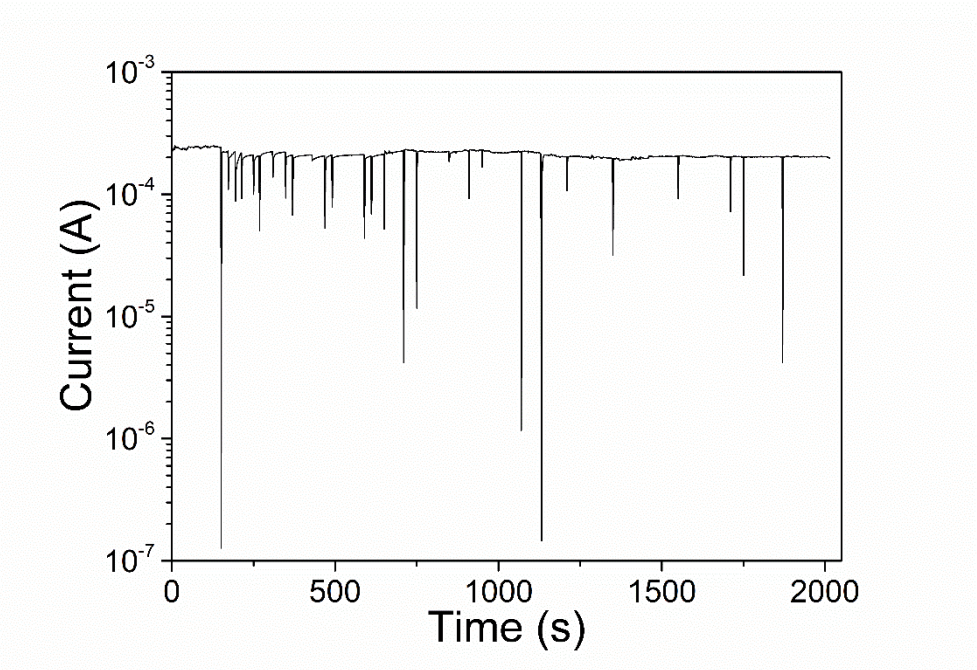

Figure SC1. Current versus time plot of film processed from mixtures containing PEDOT:PSS and 4% PEG-400 after 100 cuts in different regions. The cut was performed every 20 s by Ultrasource Single Edge blade 500205. The voltage applied during the healing test was 0.2 V.

Table SC1: Blades used in this work and cut width measured on pristine PEDOT:PSS film. For each blade, at least ten cuts were made to calculate the average cut width.

Name of Blade	Picture	Cut Size /µm
Gillette 7 O' Clock Super Stainless		15.1±4.1
Gillette Silver Blue		19.6±5.7
Gillette Platinum		14.9±1.0
Shark Super Chrome Blades		44.4±3.2
Astra Superior Platinum Double Edge		16.4±6.1
Feather Hi Stainless Double Edge		19.3±8.7
Derby Extra Super Stainless Double-Edge		11.0±0.3
A2ZSCILAB Blue Wrapper Scalpel Blade # 12		53.4±2.1

A2ZSCILAB Blue Wrapper Scalpel Blade #11		13.5±1.0
A2ZSCILAB Green Wrapper Scalpel Blade #15		27.1±10.1
Slice 10520 Slice Ceramic Craft Blade		66.2±2.4
Ultrasource Single Edge blade 500205		27.8±4.1

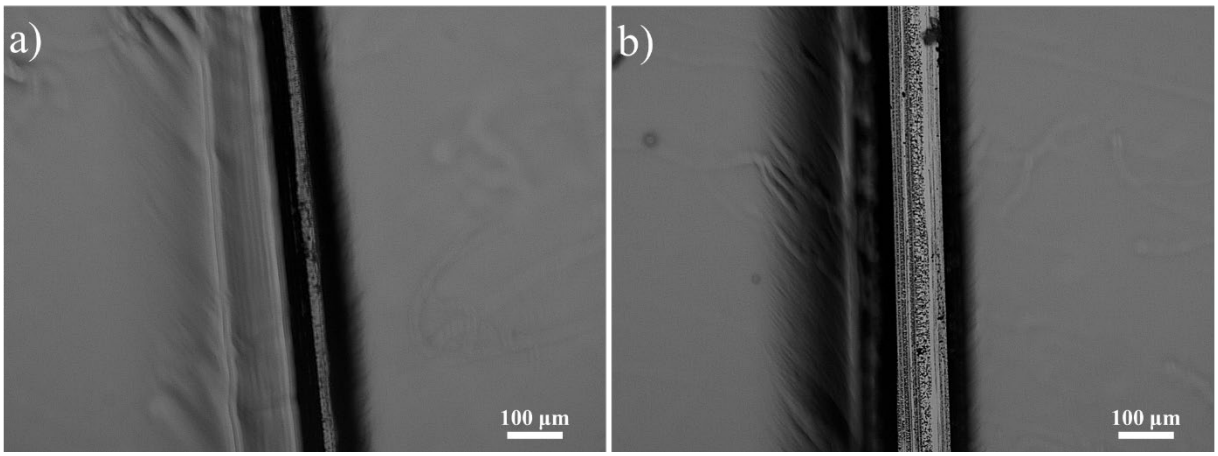

Figure SC2. Optical images of damaged regions of a film processed from mixtures containing PEDOT:PSS and 4% PEG-400 (a) and a pristine PEDOT:PSS film (b) via cutting by the edge of quartz microscope slide.

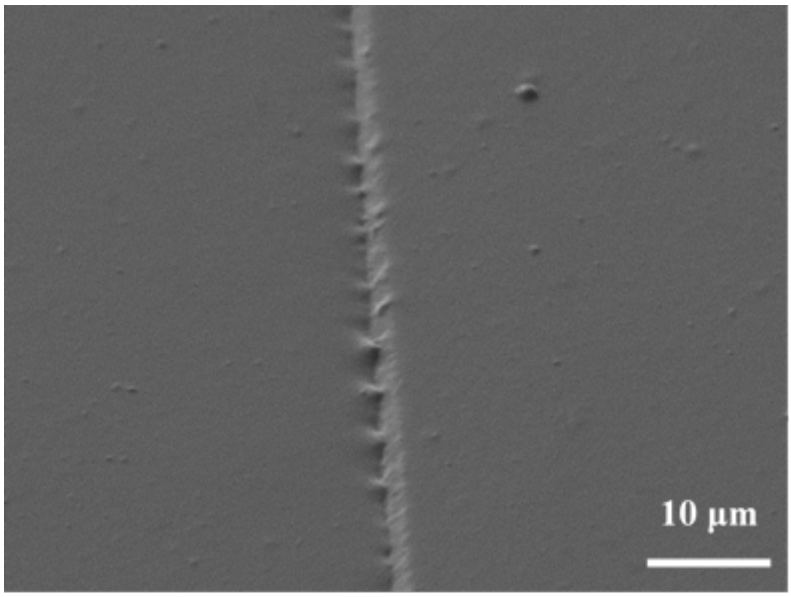

Figure SC3. SEM image of healed region of a film processed from mixtures containing PEDOT:PSS, 5% glycerol and 4% PEG-400.

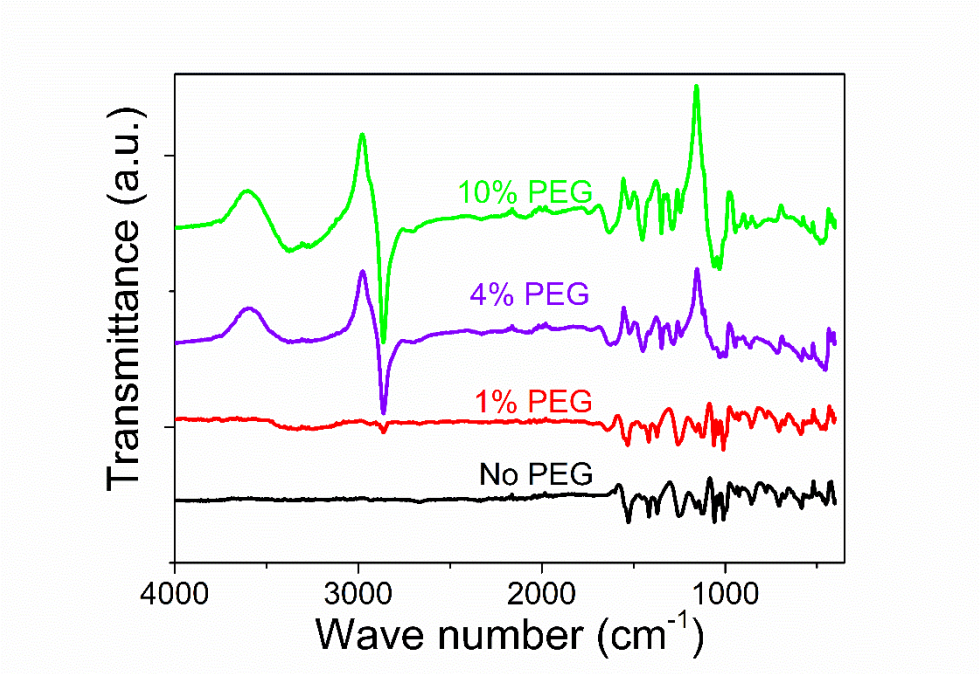

Figure SC4. FTIR spectra of conducting polymer processed from mixtures of PEDOT:PSS and different amounts of PEG-400.

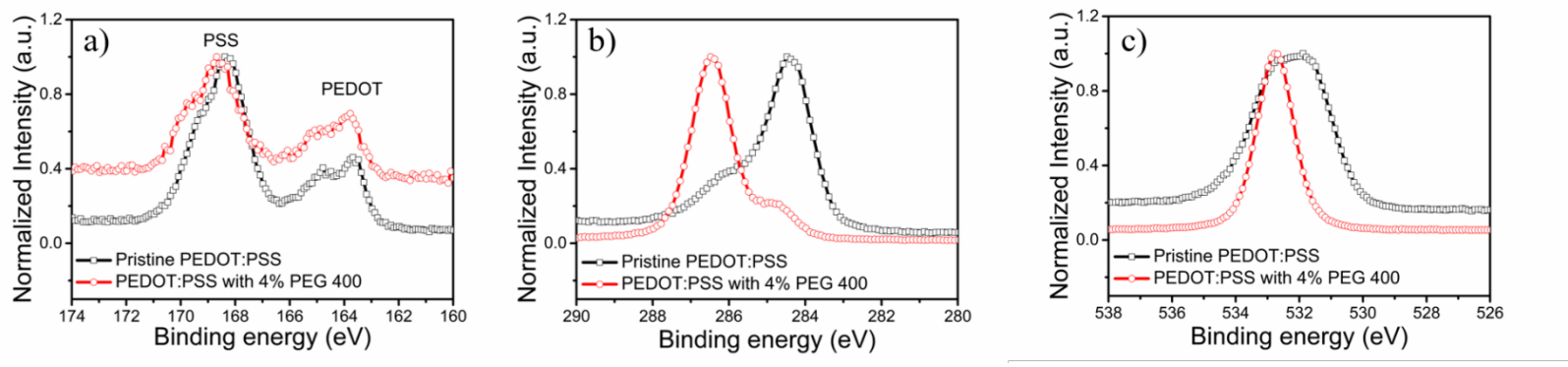

Figure SC5. XPS spectra of S2p (a), C1s (b) and O(1s) (c) core-level of pristine PEDOT:PSS, and PEDOT:PSS/PEG-400-4% film.

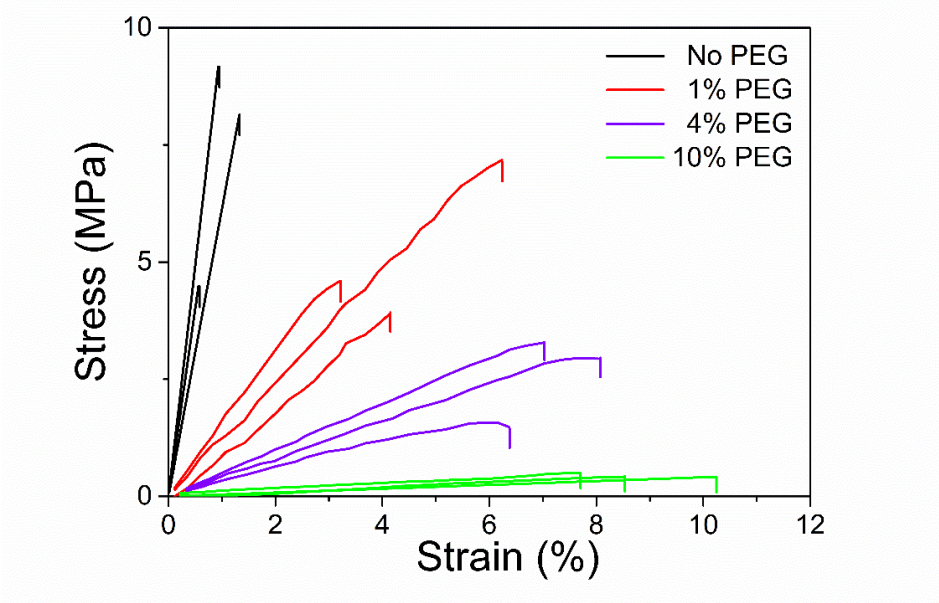

Figure SC6. Stress-strain curves of three films processed from mixtures of PEDOT:PSS and different amounts of PEG-400.

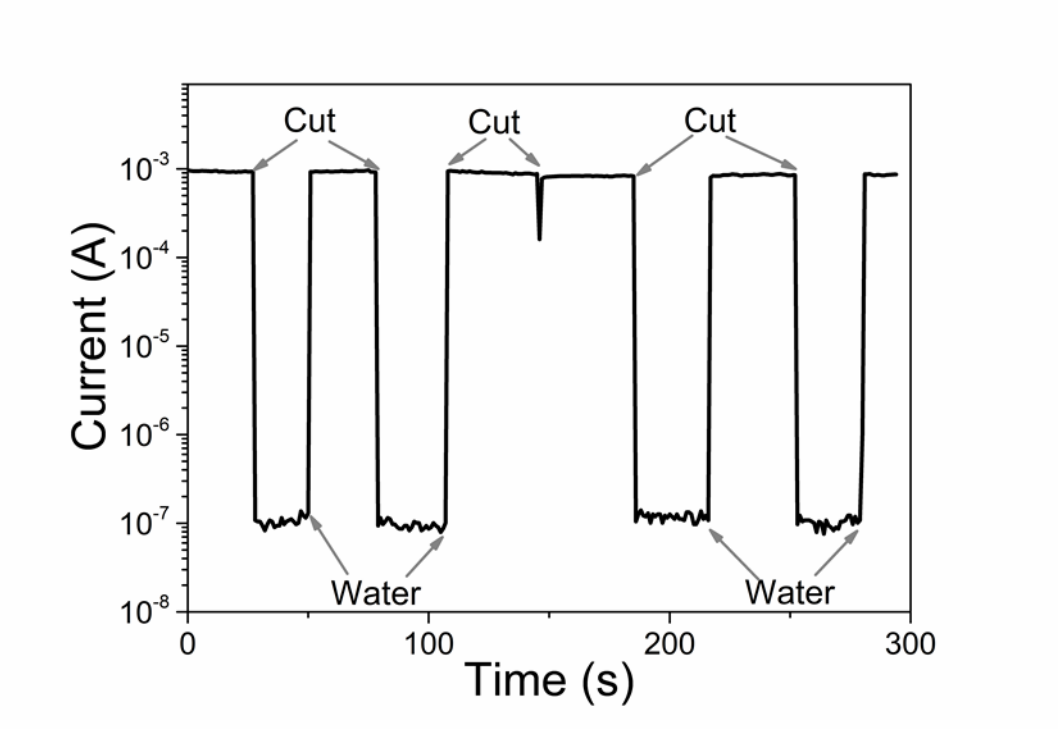

Figure SC7. current versus time plot of a film processed from a mixture containing PEDOT:PSS and 4% PEG-400, rinsed in methanol and soaked in PEG-400 upon several cuts and water healings in different regions. The films were soaked in PEG-400 for 30 min after the methanol treatment. Then PEG was removed by lint-free paper and films were baked at 140 °C for 4 h. The voltage applied during the healing test was 0.2 V.

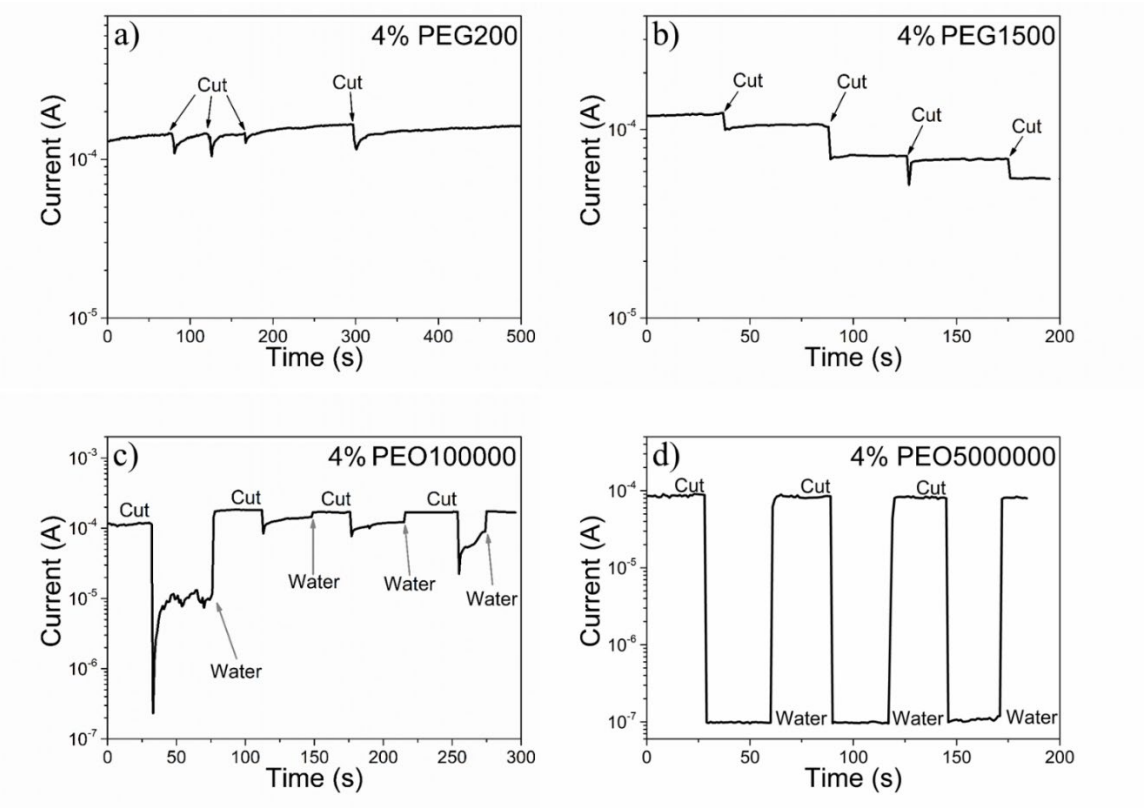

Figure SC8. Current versus time plot of films processed from mixtures containing PEDOT:PSS and 4% PEG-200 (a), 4% PEG-1500 (b), 4% PEO-100000 (c) and 4% PEO-5000000 after several cuts in different regions. The voltage applied during the healing test was 0.2 V.

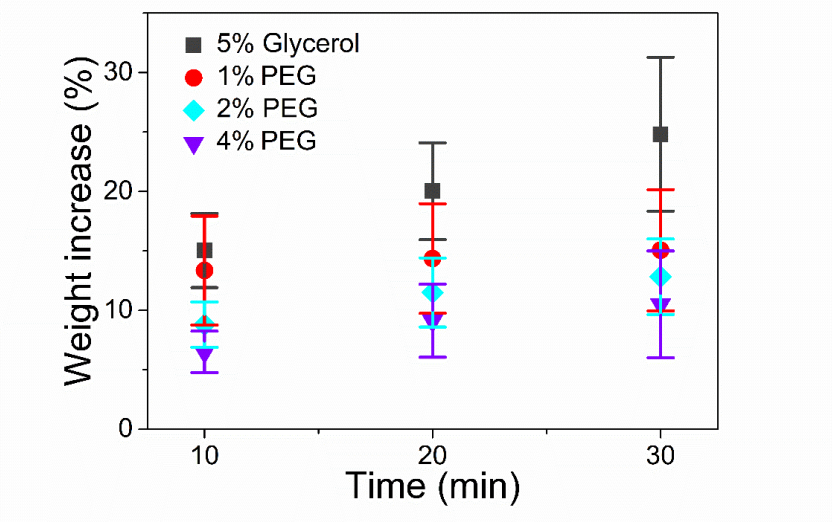

Figure SC9. Weight increase of PEDOT:PSS films containing different amounts of PEG-400 versus exposure time to water vapour into a humidity chamber. The RH is kept constant at 95% during the experiments.

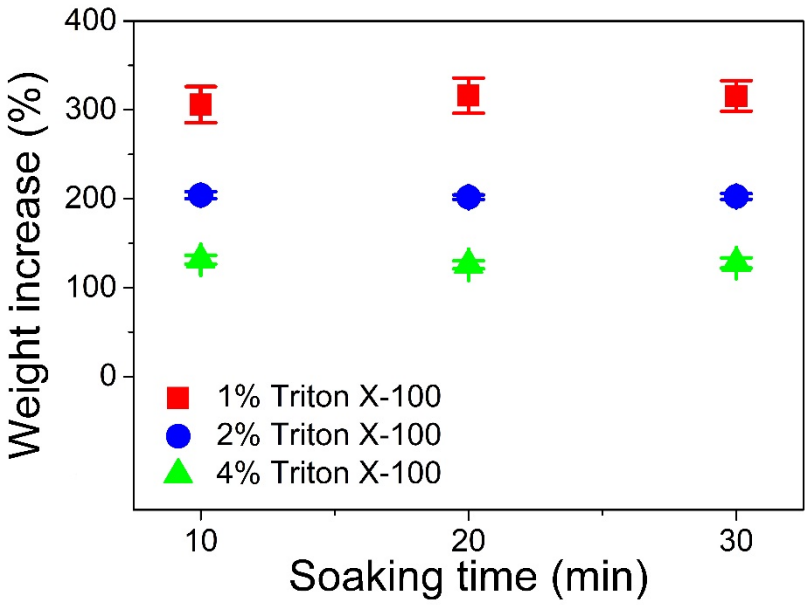

Figure SC10. Weight increase versus water soaking time of PEDOT:PSS films containing different amounts of Triton X-100

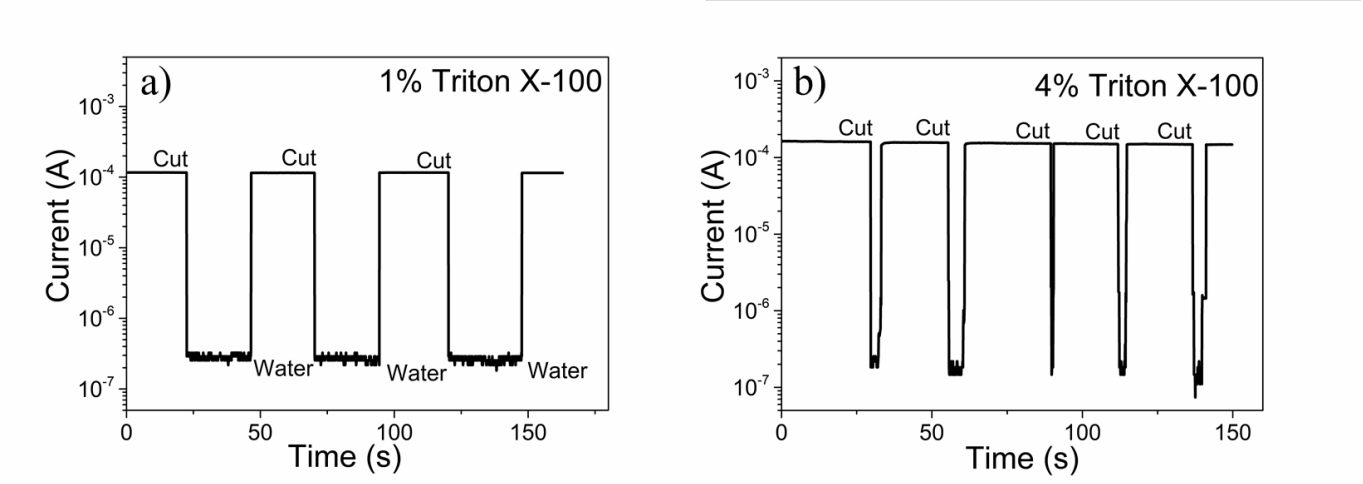

Figure SC11. Current versus time plots of films processed from mixtures containing PEDOT:PSS and 1% (a) and 4% Triton X-100 (b) after several cuts in different regions. The voltage applied during the healing test was 0.2 V.

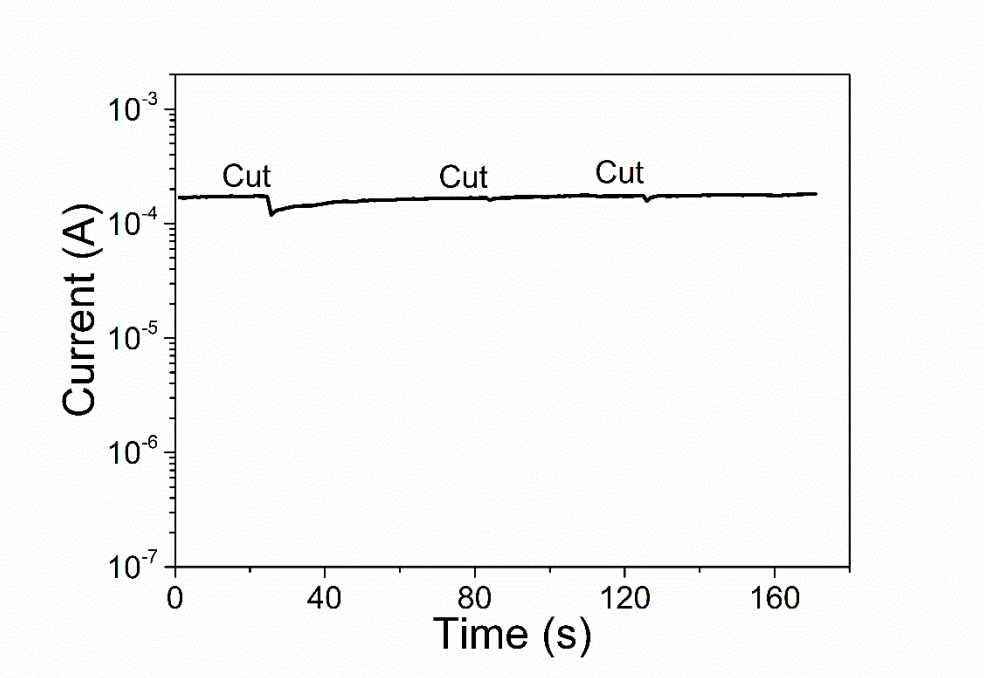

Figure SC12. Current versus time plot of films processed from mixtures containing PEDOT:PSS and 4% PEG after several cuts in different regions. The experiment was carried out in dry conditions inside a N_2-purged glove box after baking the film in situ for 14 h at 140 °C. The voltage applied during the healing test was 0.2 V.

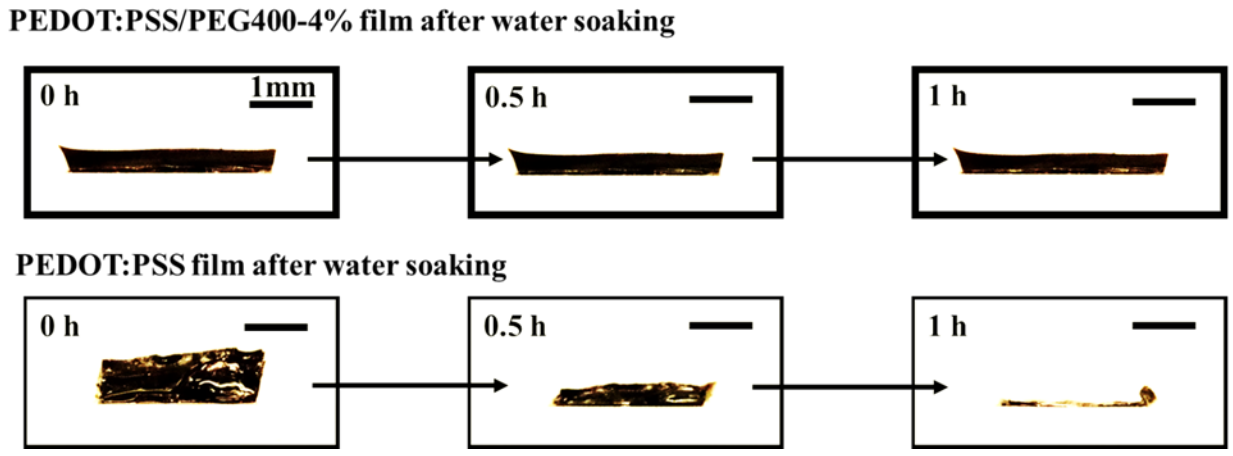

Figure SC13. Optical images of films processed from mixtures containing PEDOT:PSS and 4% PEG and from PEDOT:PSS only, immediately after water soaking and after drying for 30 and 60 minutes.

APPENDIX D SUPPORTING INFORMATION OF ARTICLE TAILORING THE SELF-HEALING PROPERTIES OF CONDUCTING POLYMER FILMS

Yang Li[1], Shiming Zhang[2], Natalie Hamad[1], Kyoungoh Kim[1], Leslie Liu[1], Michael Lerond[1], and Fabio Cicoira[1]

[1] Department of Chemical Engineering, Polytechnique Montréal, Montréal, Québec, H3C3J7, Canada

[2] California NanoSystems Institute, University of California, Los Angeles, California 90095, United Statesartment of Chemical Engineering, Polytechnique Montréal, Montréal, Québec, Canada

E-mail: fabio.cicoira@polymtl.ca

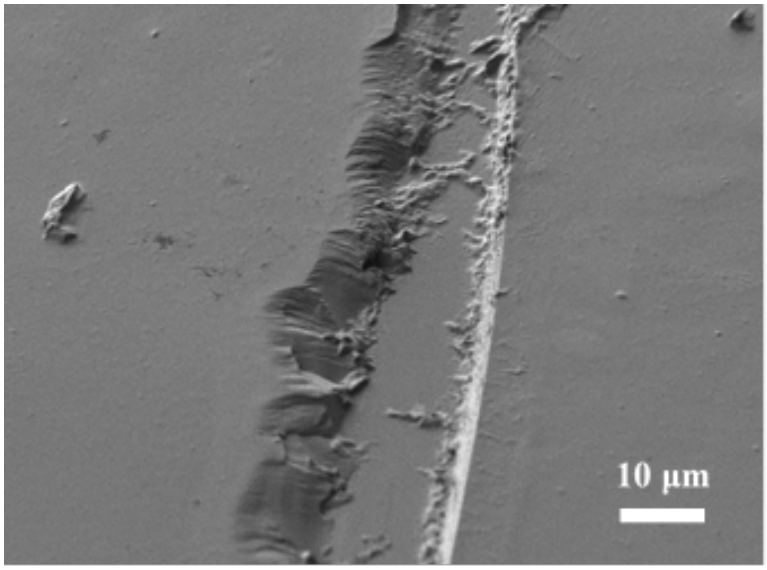

Figure SD1. SEM image of the damaged area of a pristine PEDOT:PSS film after 3 days of H_2SO_4 soaking. The film was cut with a razor blade and DI water was dropped into the damaged area. Then the film was baked at 140 °C for 15 min.

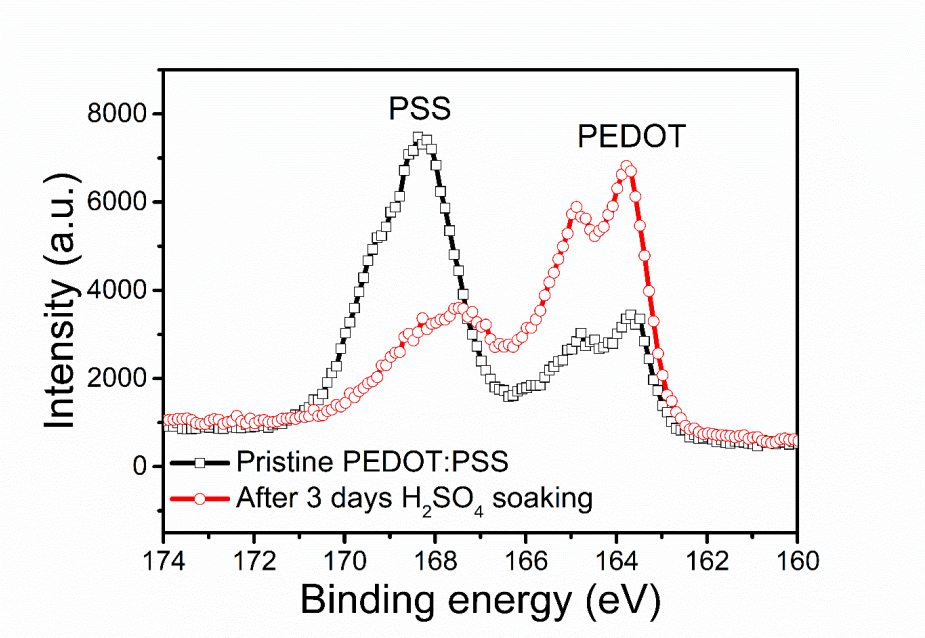

Figure SD2. S(2p) core-level spectra of pristine PEDOT:PSS and PEDOT:PSS film after sulfuric acid post-treatment for 3 days.

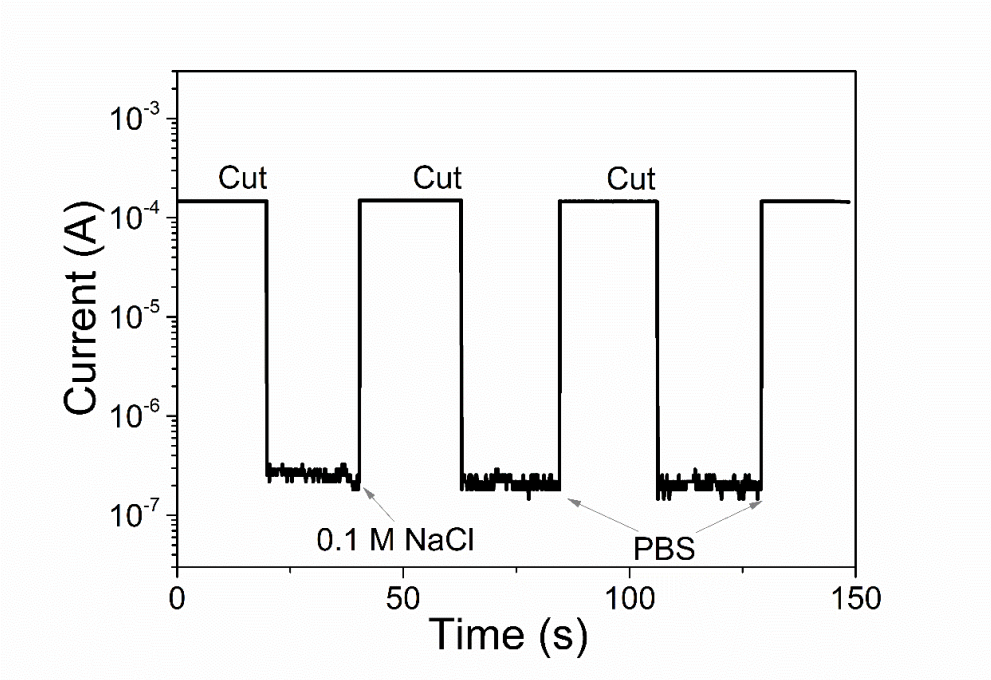

Figure SD3. Current versus time profile of a pristine PEDOT:PSS films after several cuts in different areas of the films. The healing agents used were NaCl and PBS. The thickness of films was ~5 µm.

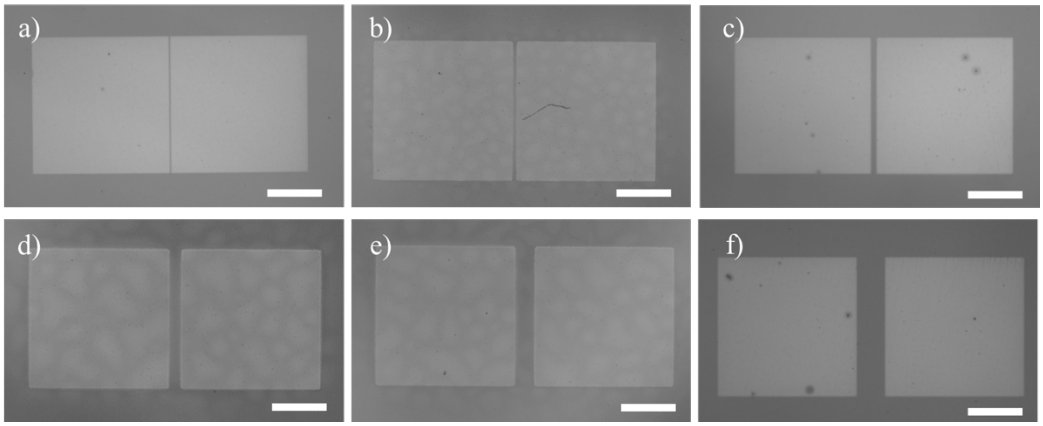

Figure SD4. The optical images of patterned PEDOT:PSS squares on glass with different gap width. The gap width is 5 μm (a), 10 μm (b), 20 μm (c), 50 μm (d), 80 μm (e) and 100 μm (f), respectively. The scale bar is 200 μm.

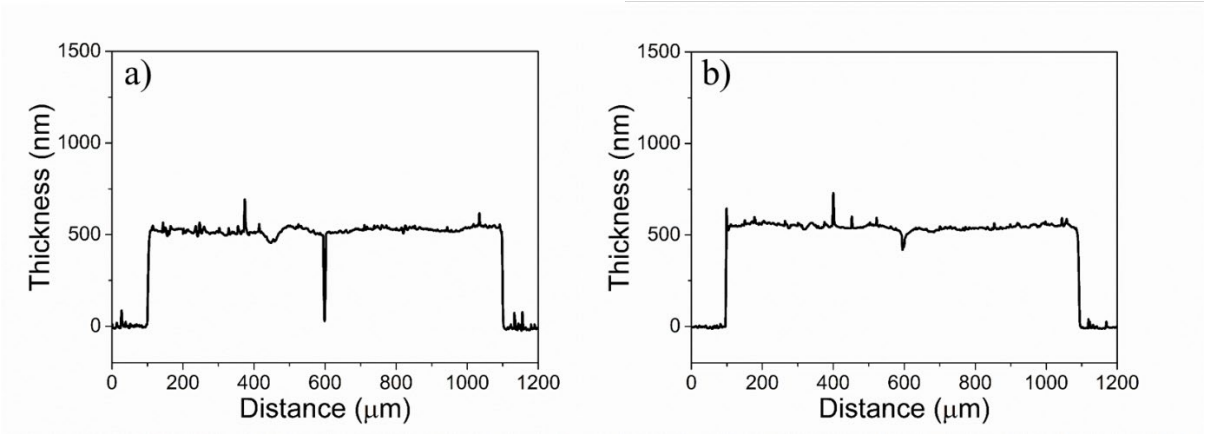

Figure SD5. The thickness variation of patterned PEDOT:PSS squares before (a) and after water drop (b). The gap width is 5 μm. The change of thickness in the middle of squares indicates the "healing".

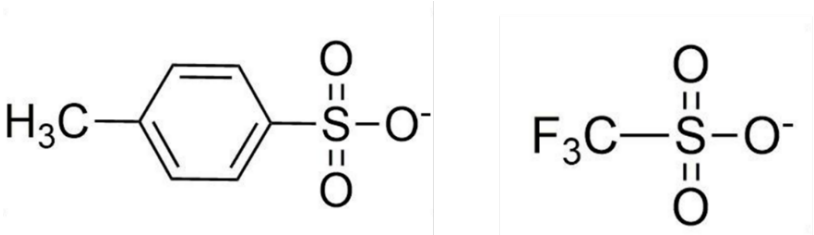

Figure SD6. Chemical structures of para-toluene sulfonate and trifluoromethanesulfonate.

APPENDIX E LIST OF PUBLICATIONS AT POLYTECHNIQUE MONTREAL NOT INCLUDED IN THE THESIS

1. Y. Pan, X. Lu, M. Hayat, F. Yang, C. Liu, **Y. Li**, X. Li, W. Xu, X. Qu, P. Cao. Effect of Sn addition on the high-temperature oxidation behavior of high Nb-containing TiAl alloys. Corros. Sci. 2020, 166, 108449.

2. Q. Tan, P. Li, K. Han, Z. Liu, **Y. Li**, W. Zhao, D. He, F. An, M. Qin, X. Qu. Chemically bubbled hollow Fe_xO nanospheres anchored on 3D N-doped few-layer graphene architecture as a performance-enhanced anode material for potassium-ion batteries. J. Mater. Chem. A. 2019, 7(2), 744.

3. Z. Liu, K. Han, P. Li, W. Wang, D. He, Q. Tan, L. Wang, **Y. Li**, M. Qin, X. Qu. Tuning metallic $Co_{0.85}Se$ quantum dots/carbon hollow polyhedrons with tertiary hierarchical structure for high-performance potassium ion batteries. Nano-Micro Lett. 2019, 11, 96.

4. Y. Pan, X. Lu, A. Volinsky, B. Liu, S. Xiao, C. Zhou, **Y. Li**, M. Chen, X. Qu. Tribological and mechanical properties of copper matrix composites reinforced with carbon nanotube and alumina nanoparticles. Mater. Res. Express. 2019, 6(11), 116524.

5. Y. Pan, S. Xiao, X. Lu, C. Zhou, **Y. Li**, Z. Liu, B. Liu, W. Xu, C. Jia, X. Qu. Fabrication, mechanical properties and electrical conductivity of Al_2O_3 reinforced Cu/CNTs composites. J. Alloys Compd. 2019, 782, 1015.

6. **Y. Li**, F. Cicoira, Conducting polymers based materials and composites for self-healable electronics (In preparation).

APPENDIX F PARTICIPATION TO CONFERENCES

1. **Y. Li**, S. Zhang, and F. Cicoira, Highly stretchable organic electrochemical transistors, Poster, MRS Fall, 2019, Boston.
2. **Y. Li**, S. Zhang, and F. Cicoira, Flexible, stretchable and healable electronics, Oral, 102nd Canadian Chemistry Conference and Exhibition, 2019, Quebec City
3. **Y. Li**, and F. Cicoira, Self-healing property of conducting polymer, Oral, RQMP Spring Annual Meeting, 2018, Montreal.
4. **Y. Li**, S. Zhang, G. Tomasello, M. Anthonisen, P. Grutter, and F. Cicoira, Intrisically stretchable organic electrochemical transistors, Poster, Fall Meeting of the Canadian Section of the ECS, 2018, Montreal
5. **Y. Li**, S. Zhang, and F. Cicoira, Stretchable organic electrochemical transistors, Poster, MRS Fall, 2018, Boston.
6. **Y. Li**, and F. Cicoira, Conducting polymer for stretchable and healable electronics, Oral, MRS Fall, 2018, Boston.

APPENDIX G SCHOLARSHIPS AND AWARDS RECEIVED AT POLYTECHNIQUE MONTREAL

1. Prestige États-Unis scholarship, 2020